Structure and mineralogy of layer silicates: recent perspectives and new trends

Book *in* European Mineralogical Union Notes in Mineralogy · January 2011

DOI: 10.1180/EMU-notes.11.1

4 authors:

Maria franca Brigatti
Università degli Studi di Modena e Reggio Emilia
157 PUBLICATIONS **2,702** CITATIONS
SEE PROFILE

Daniele Malferrari
Università degli Studi di Modena e Reggio Emilia
73 PUBLICATIONS **456** CITATIONS
SEE PROFILE

Angela Laurora
Università degli Studi di Modena e Reggio Emilia
28 PUBLICATIONS **375** CITATIONS
SEE PROFILE

Chiara Elmi
James Madison University
25 PUBLICATIONS **45** CITATIONS
SEE PROFILE

Structure and mineralogy of layer silicates: recent perspectives and new trends

Maria Franca BRIGATTI, Daniele MALFERRARI, Angela LAURORA and Chiara ELMI

Dipartimento di Scienze della Terra, Università di Modena e Reggio Emilia, Largo S. Eufemia 19, I-41121 Modena, Italy
e-mail: mariafranca.brigatti@unimore.it; daniele.malferrari@unimore.it; angela.laurora@unimore.it; chiara.elmi@unimore.it

Because of their many novel and advanced applications, there is increasing interest in layer silicates from the scientific and technical communities. Appropriate application of these minerals requires deep understanding of their properties and of the processes where they are involved. This chapter, by providing fundamental definitions and crystal structural and chemical data pertaining to layer silicates, aims to introduce this field to new researchers and technicians, by describing the fundamental features leading to different behaviours of layer silicates in different natural or technical processes. The subject addressed is vast and so the reader is referred in some cases to work already published. The focus here is on layer silicates for which detailed crystal structures are given in the literature and which are likely to be used in an applied way in the future. Layer-silicate minerals fulfilling these requirements are: (1) kaolin-serpentine group (*e.g.* kaolinite, dickite, nacrite, halloysite, hisingerite, odinite, lizardite, berthierine, amesite, cronstedtite, nepouite, kellyite, fraipontite, brindleyite, guidottiite, bementite, greenalite, caryopilite; minerals of the pyrosmalite series); (2) talc and pyrophyllite groups (*e.g.* pyrophyllite, ferripyrophyllite, willemseite); (3) mica group (*i.e.* some recent advances in crystal chemistry and structure of dioctahedral and trioctahedral micas); (4) smectite group (*e.g.* montmorillonite, saponite, hectorite, sauconite, stevensite, swinefordite); (5) vermiculite group; (6) chlorite group (*e.g.* trioctahedral chlorite such as clinochlore, di,trioctahedral and dioctahedral chlorites such as cookeite and sudoite); and (7) some 2:1 layer silicates involving a discontinuous octahedral sheet and a modulated tetrahedral sheet such as kalifersite, palygorskite and sepiolite; (8) imogolite and allophane.

1. Introduction

There is great interest in the mineralogy, crystallography and potential novel technological applications of layer silicates, especially of those showing nano-sized dimensions, as recently reviewed by Bergaya *et al.* (2006). An increasing number of scientific publications devoted to such subjects is not limited to mineralogical, petrological and geochemical fields, but also includes other disciplines, such as Applied Chemistry, Environmental Sciences, Food and Soil Science, Ceramics, Cultural Heritage, Applied Physics, Engineering, Water Science and Biology. As a result, new possibilities and new priorities have arisen in research on layer silicates. Multi-competence and multidisciplinary approaches need to be supported and well integrated. Knowledge, down to

DOI: 10.1180/EMU-notes.11.1

an atomic level, of the mineral bulk and surface features and of the mineral interaction with its surrounding environment needs to be detailed to a level which allows the formulation of predictive models. The latter need to support better the existing and novel technological applications, which to date are largely based on phenomenological, empirical or trial-and-error approaches.

This chapter attempts to address both priorities: firstly, by introducing the fundamental aspects of layer silicates in terms of their structure and crystal chemistry and how these are related directly to mineral properties and to mineral interactions with the surrounding environment; secondly, by reviewing more recent findings and innovative experimental techniques, especially where they might contribute to novel or future applications, trying, at the same time, to overlap as little as possible, with recent, general purpose reviews on layer silicates (*e.g.* see Moore & Reynolds, 1997; Giese & van Oss, 2002; Mottana *et al.*, 2002a; Fleet, 2003; Meunier, 2005; Bergaya *et al.*, 2006; Deer *et al.*, 2009).

2. Layer silicates: general structural overview

The layer silicates considered in this chapter are commonly characterized by a continuous tetrahedral sheet (Fig. 1a). In the tetrahedral (T) sheet, individual TO_4 tetrahedra are interconnected, by sharing three corners each (*i.e.* the basal oxygen atoms, O_b), to form an infinite two-dimensional 'hexagonal' mesh pattern along the **a** and **b** crystallographic directions. Common tetrahedral cations are Si^{4+}, Al^{3+}, and Fe^{3+}, but Be, B, Ga, and Ge are also documented. The fourth oxygen atom (*i.e.* the apical oxygen atom, O_a) forms a corner of the octahedral coordination unit around the octahedral cations. In the octahedral sheet, each octahedron (M) connects to its neighbouring octahedra by sharing edges. Edge-shared octahedra form sheets of hexagonal or pseudo-hexagonal symmetry (Fig. 1b). Octahedral cations are usually Al^{3+}, Fe^{3+}, Mg^{2+}, Fe^{2+}, but other cations, such as Li^{+}, Mn^{2+}, Co^{2+}, Ni^{2+}, Cu^{2+}, Zn^{2+}, V^{3+}, Cr^{3+}, and Ti^{4+} are also observed. Octahedra show two different topologies, depending on the octahedral oxygen atom (O_o) position (*i.e.* the *cis*- and the *trans*-orientations, Fig. 1b). In the *trans*-orientation (M-*trans*) O_o lies across the octahedral diagonal, whereas in the *cis*-octahedra (M-*cis*) the O_o forms a shared edge between two octahedra. Common anions characterizing the O_o position, which lie near to the centre of each tetrahedral 6-fold ring, are O, OH, F, Cl (Brigatti & Guggenheim, 2002).

A continuous octahedral sheet is generated when the free tetrahedral corners (O_a) of all tetrahedra point to the same side of the sheet (Fig. 2a), thus connecting tetrahedral and octahedral sheets along a plane ideally containing O_o also. In some layer silicates, tetrahedral apices point in opposite directions and link octahedral 'ribbons'. These layer silicates are still characterized by a continuous two-dimensional tetrahedral sheet, but do not show any continuous octahedral sheet (Fig. 2b).

A layer is, by definition, the stacking of tetrahedral and octahedral sheets. Two basic stackings are observed: (1) the 1:1 (or TM), which consists of the repetition of one T and one M sheet along the crystallographic **c** direction; and (2) the 2:1, which consists of one

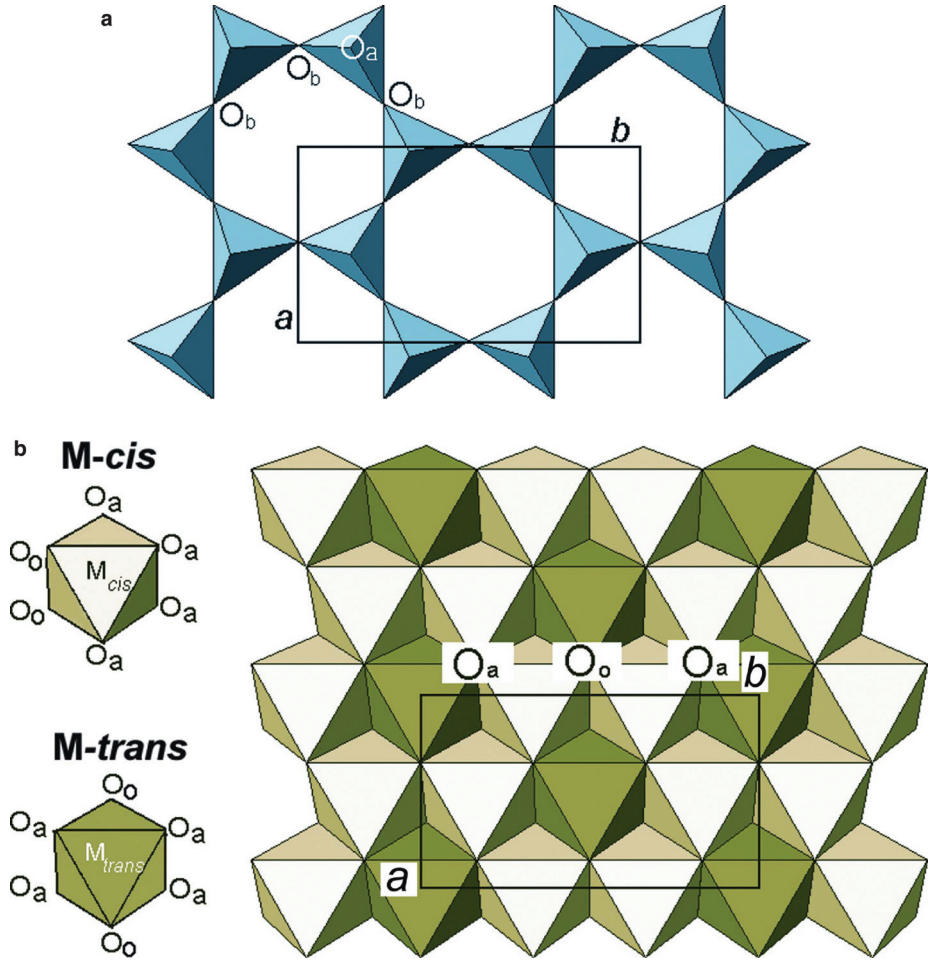

Fig. 1. (***a***) Tetrahedral sheet. O_a and O_b refer to apical and basal oxygen atoms, respectively. *a* and *b* are the unit-cell parameters; (***b***) The octahedral sheet and orientation of the *cis*-octahedron (M-*cis*) and *trans*-octahedron (M-*trans*). In M-*cis* oriented octahedra, two O_o (*i.e.* the octahedral anionic position) lie on an octahedral edge; in M-*trans* oriented octahedra two O_o are placed along the octahedron diagonal. O_a refers to apical oxygen atoms; *a* and *b* are the unit-cell parameters.

M sheet sandwiched between two T sheets (Fig. 2a). Usually, in the 1:1 layer structure, the unit cell includes six M positions (*i.e.* four M-*cis*- and two M-*trans*-oriented octahedra) and four T sites. In the 2:1 layer the unit cell contains six M sites (*i.e.* four M-*cis*- and two M-*trans*-oriented octahedra) and eight T sites. Structures with all the six M sites occupied are defined as trioctahedral. If only four of the six M sites are occupied, the structure is dioctahedral. Sometimes terms such as 'brucite-like' and 'gibbsite-like' are be used instead of trioctahedral and dioctahedral sheets, respectively.

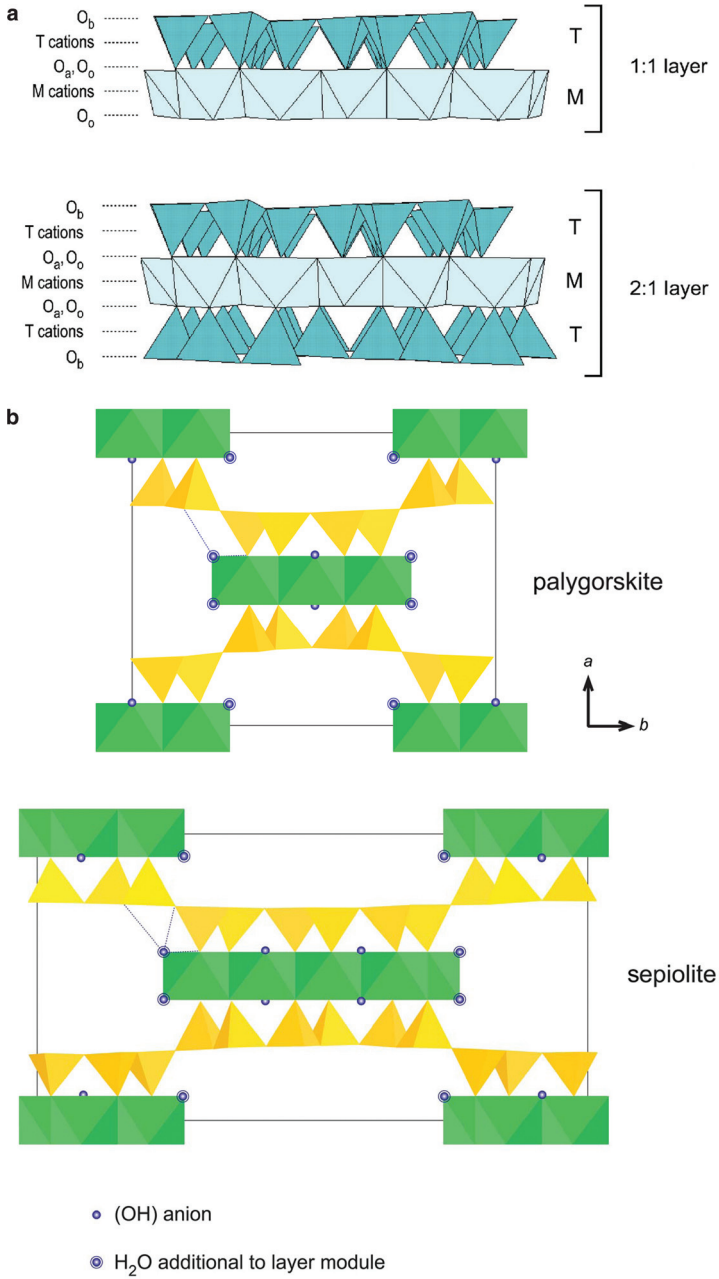

Fig. 2. (***a***) Models of a 1:1 and 2:1 layer structure. O_a, O_b, and O_o refer to tetrahedral basal, tetrahedral apical and octahedral anionic positions, respectively. M and T indicate the octahedral and tetrahedral cations, respectively. (***b***) Modulated layer silicates characterized by a continuous two-dimensional tetrahedral sheet and by a discontinuous octahedral sheet: the schematic structure of palygorskite and sepiolite.

Two adjacent layers are separated by an interlayer space, which can be empty or occupied. The interlayer space can be occupied by cations, hydrated cations, organic material, hydroxide octahedra, and/or hydroxide octahedral sheets. The periodicity along the **c** axis of each 1:1 layer (usually evaluated by the d_{001} reflection) is approximately 7 Å; in the 2:1 layers, it varies from 9.1 to 9.5 Å in talc and pyrophyllite, where the interlayer space is empty; it reaches ~10 Å in micas, which present the interlayer occupied by anhydrous interlayer cations and 14 Å in chlorite, where the interlayer consists of octahedrally coordinated cations. In smectite and vermiculite the periodicity along the crystallographic *c* axis reflects the hydration of the interlayer cations. Generally, in smectite, the intercalation of 0, 1, 2, or 3 planes of H_2O molecules in the interlayer space corresponds to $d_{001} = 10.0–10.2$ Å (dehydrated layers), $d_{001} = 11.6–12.9$ Å (mono-hydrated layers), $d_{001} = 14.9–15.7$ Å (bi-hydrated layers), and $d_{001} = 18.0–19.0$ Å (tri-hydrated layers).

The periodicity along $\mathbf{c}^*$ can vary, depending on polytypic arrangement because of the different number of layers involved in the stacking sequence, and because of different orientations. The theoretical principles of polytypism were reviewed in several works (*e.g.* see Baronnet, 1978; Bailey, 1988a,b; Takeda & Ross, 1995; Ďurovič, 1997, 1999; Nespolo *et al.*, 1997; Nespolo & Ďurovič, 2002) and will not be further discussed in this chapter.

A single layer, in 1:1 layer silicates, shows one negatively charged surface, as consisting entirely of oxygen atoms (O_b) belonging to the T sheet (Fig. 2a), and a positively charged one, when OH groups occupy the O_o position. In 2:1 layer silicates, two-thirds of the octahedral hydroxyl groups are thus replaced by tetrahedral apical oxygen atoms (Fig. 2a), also implying that both surfaces of such a layer are negatively charged, as mostly constituted by tetrahedral O_b.

Allophane and imogolite are commonly referred to in the literature as clay minerals, even though their structural arrangement deviates significantly from that of clays. These minerals are used widely in advanced industrial applications, and share with clay minerals nano-sized dimensions and chemical composition, thus attaining physical properties similar to, or even more pronounced than in clays.

Allophane consists of a 'gibbsite-like' sheet showing hollow spherical morphologies hosting SiO_4 tetrahedra attached to their inner surfaces. Imogolite shows a nano-tube structure. The tubes contain curved gibbsite sheets with silicate groups replacing hydroxyl groups on the inner surface, unlike the outer surfaces which contain $Al(OH)_3$ groups (Fig. 3).

Phyllosilicate layers may present numerous distortions and deviations from the ideal structural arrangement. These structural modifications, which are generally associated with chemical substitutions, could be observed and described in detail only for phyllosilicates with a crystal size suitable for single-crystal X-ray structural refinement. The distortion parameters more often discussed in the literature (mostly for dioctahedral and trioctahedral micas) are: (1) The tetrahedral flattening angle, τ, is derived from: $\tau = \sum_{i=1}^{3} (O_{apical} - T - O_{basal})_i/3$ (Fig. 4a). In an ideal tetrahedron, τ is equal to arcos $(-1/3) \approx 109.47^\circ$. The τ parameter can deviate from its ideal value as a function of the relative position along *c* for the basal oxygen atoms with respect to the tetrahedral

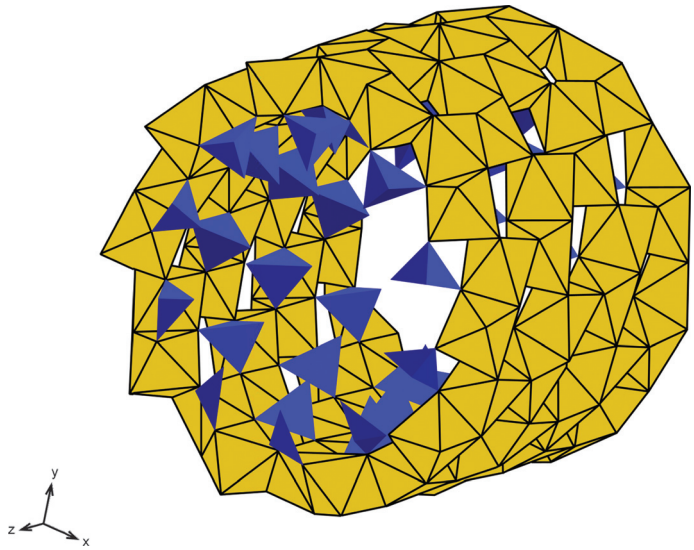

Fig. 3. Model structure of a nano-tube of imogolite.

cation and with respect to the mean basal-edge length and the mean tetrahedral-edge value (Brigatti & Guggenheim, 2002). (2) The tetrahedral rotation angle, α, is defined according to the following formula $\alpha = \frac{\sum_i^6 |120 - \varphi_i|}{12}$ where φ_i is a generic internal angle of the hexagon defined by basal oxygen atoms (Fig. 4b). Brigatti & Guggenheim (2002) demonstrated that α depends mostly on the ratio between the mean octahedral edges defined by O_a oxygen atoms and the distance defined by tetrahedral O_b: $\alpha = \cos^{-1}\left(\frac{\sqrt{3}}{2} \cdot \frac{\langle O_a - O_a \rangle}{\langle O_b - O_b \rangle}\right)$. Brigatti *et al.* (2003), for trioctahedral mica-1*M* with $C2/m$ symmetry, demonstrated that the value of α depends mostly on tetrahedral distortions and that a precise estimation of the α value could thus be obtained from: $\cos(\alpha) = \frac{1}{\sqrt{1+3 \cdot [4 \cdot y(O1) - 1]^2}}$, where y(O1) represent the y atomic coordinate of one of two symmetry-independent O_b. (3) Basal oxygen-plane corrugation, Δz, is calculated from $\Delta z = (zO_{b(max)} - zO_{b(min)}) \times c \times \sin\beta$, where zO_b represents the z atomic coordinates of basal oxygen atoms. (4) The octahedral flattening angle, ψ, expresses the flattening of the octahedral sheet (Fig. 4c) and can be computed from: $\psi = \cos^{-1}\left(\frac{\text{octahedral thickness}}{2 \cdot \langle \text{M–O, OH, F, Cl, S} \rangle}\right)$, where the thickness of octahedral sheet is calculated from oxygen z coordinates of each M octahedron, including O_o. ⟨M-O, OH, F, Cl, S⟩ indicates the mean octahedral distance (Donnay *et al.*, 1964). (v) The ratio between shared and unshared edges, *eu*/*es*, is the ratio between the mean value of unshared and shared octahedral edges and expresses the distortion of each octahedron (Toraya, 1981). (6) The counter rotation angle, ω, defines the counter-rotation of upper and lower octahedral oxygen triads (Newnham, 1961; Appelo, 1978; Lin & Guggenheim,

1983). (7) The effective coordination number of the interlayer cation, ECoN, describes the effective coordination number of the octahedral cation. This parameter was derived for micas by Weiss *et al.* (1992) starting from the equation introduced by Hoppe (1979): $\mathrm{ECoN} = \sum_{j=1}^{j=12} C_j$, where $C_j = \exp[1.0 - (\mathrm{FIR_j}/\mathrm{MEFIR})^6]$, $\mathrm{FIR_j}$ is calculated by dividing the interlayer cation (A) – basal oxygen ($O_{b,j}$) distances by the sum of anion and cation radii and then multiplying them by the cation radii; MEFIR is a weighted mean of FIR, *i.e.* $\mathrm{MEFIR} = \frac{\sum_{j=1}^{j=12} w_j \mathrm{FIR_j}}{\sum_{j=1}^{j=12} w_j}$, $w_j = \exp[1.0 - (\mathrm{FIR_j}/\mathrm{FIR_{min}})^6]$, and $\mathrm{FIR_{min}}$ is the smallest $\mathrm{FIR_j}$ in the interlayer cation coordination. (8) Layer displacement is the displacement between two tetrahedral sheets across the interlayer regions. In 2:1 layer silicates, this parameter is defined as the sum of the intralayer displacement (*i.e.* the distance, ideally $a/3$, between two opposing tetrahedral cations, along the plane normal to c^*) and of interlayer displacement (*i.e.* the distance between the same tetrahedral cation positions along c^*). Both parameters are evaluated from tetrahedral atomic coordinates. (9) The thickness of tetrahedral and octahedral sheets is calculated from oxygen z coordinates of each polyhedron, including the OH group (or else any other anion). The interlayer separation is calculated by considering the tetrahedral basal oxygen z coordinates of adjacent 2:1 layers.

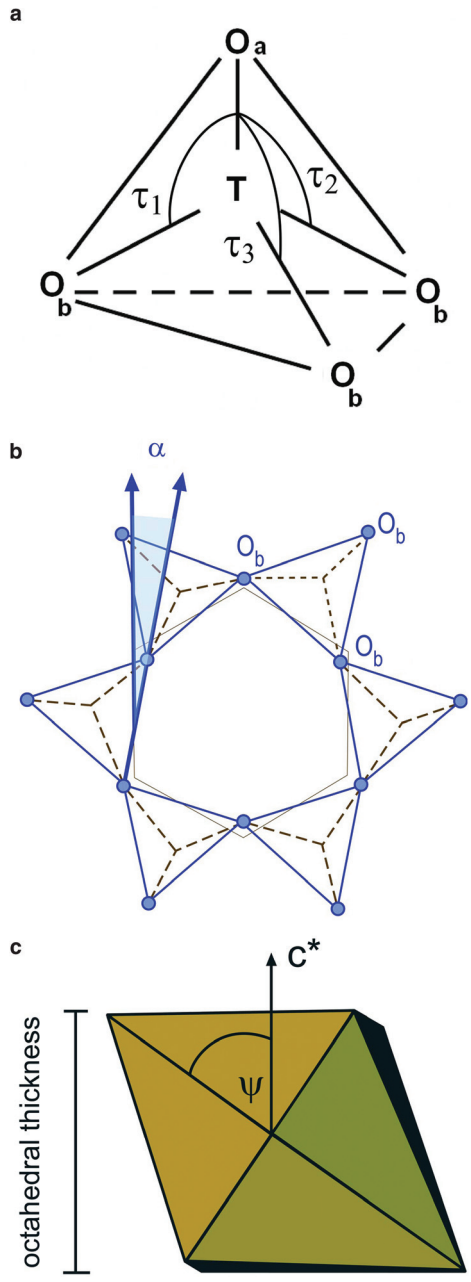

Fig. 4. (***a***) Tetrahedral flattening angle $\tau\left(\tau = \left(\frac{\tau_1 + \tau_2 + \tau_3}{3}\right)\right)$; (***b***) Definition of the tetrahedral rotation angle, α; (***c***) definition of the octahedral flattening angle ψ.

3. Mixed-layer structures and order-disorder in the layer stacking

3.1. Mixed-layer structures

Phyllosilicate crystals can also occur as randomly or regularly alternating layers of two or more phyllosilicate end-member minerals. Mixed-layer phyllosilicates (or interstratified phyllosilicates, or, more generally interstratified clays) are usually considered the metastable intermediate products of a sequence of reactions involving end-member minerals (Merriman & Peacor, 1999).

Mixed-layer phyllosilicates are remarkable examples of order-disorder observed in natural and synthetic lamellar crystals. They consist of the alternation of layers revealing different structures and/or compositions in variable proportions (Lanson, 2011, this volume).

Regular interstratified minerals, often identified with specific mineral names, originate from a strictly regular periodic alternation of different layer types along the *c* axis (*e.g.* ABABAB). Interstratified minerals are mostly constituted by the alternation of 2:1 layers, with the exception of dozyite, which consists of the stacking of 1:1 serpentine layers and of 2:1 chlorite layers. The AIPEA Nomenclature Committee (Bailey, 1981) attributed special names to regular interstratifications of two layer types A and B, only if 'such regularity of alternation is reached so that a well defined series of at least ten 00*l* summation spacings $d_{AB} = d_A + d_B$ is observed; suborders shall be integers and the even and odd suborders shall show very similar diffraction widths. Should any odd 00*l* suborders be missing, calculations shall be provided to demonstrate that their intensities are too small to be observed'.

The coefficient of variation, CV, applied to at least ten 00*l* reflections values should be <0.75. The CV is calculated from: $\mathrm{CV} = \left(100 \times \left[\sum_{i=1}^{n} \frac{(X_i - \bar{X})^2}{(n-1)}\right]^{1/2} \frac{1}{\bar{X}}\right)$ where $X_i = l \times d_{001}$, and $\bar{X} = \sum_{i=1}^{n} \frac{X_i}{n}$) (Bailey, 1981; Reynolds, 1988; Guggenheim *et al.*, 2006).

Examples of regularly interstratified minerals are: (1) aliettite, a regular interstratification between trioctahedral talc and trioctahedral smectite in a 1:1 ratio (Veniale & van der Marel, 1969); (2) brinrobertsite, an ordered, mixed-layered, dioctahedral pyrophyllite-dioctahedral smectite (Dong *et al.*, 2002); (3) corrensite, a regular interstratification of either trioctahedral smectite or trioctahedral vermiculite in a 1:1 ratio with trioctahedral chlorite. Depending on whether trioctahedral smectite or trioctahedral vermiculite is involved, the mineral is termed 'low-charge corrensite' or 'high-charge corrensite', respectively (Lippman, 1954, 1960; Bailey, 1981; Guggenheim *et al.*, 2006); (6) dozyite, a 1:1 regular interstratification of serpentine (amesite) and chlorite (clinochlore) (Bailey *et al.*, 1995); (5) hydrobiotite, a regular 1:1 interstratification of biotite and vermiculite showing a large charge density within the vermiculite interlayer spaces (Bailey, 1989a); (6) kulkeite, a regular interstratification of trioctahedral talc and trioctahedral chlorite in a 1:1 ratio (Abraham *et al.*, 1980; Schreyer *et al.*, 1982); (7) rectorite, a regular interstratification of dioctahedral mica and dioctahedral smectite in a 1:1 ratio

(Caillère *et al.*, 1950; Brown & Weir, 1963; Bailey, 1981); (8) tosudite, a regular interstratification of chlorite and smectite in a 1:1 ratio where the smectite is mostly dioctahedral (Frank-Kamenetskii *et al.*, 1965).

In mixed-layer structures, the different layer types can either alternate randomly or else achieve some sort of ordering (avoiding the existence of pairs of the minor layer type) or segregation (clustering layers of a giving type). If a mineral is constituted by a random interstratification of two components, showing different *c* periodicity values, it is identified by using the name of the components separated by a hyphen, such as, for example, illite-smectite, illite-chlorite, illite-vermiculite and kaolinite-smectite. Some examples are represented by the irregular stacking of (1) illite ($c \approx 10$ Å) and smectite ($c \approx 14$ Å); (2) integral multiples of serpentine ($c \approx 7$ Å) and chlorite ($c \approx 14$ Å); or (3) layers with similar basal spacing, but with different local structure such as the random stacking of *trans*-vacant and *cis*-vacant illite layers (Drits, 1997, 2003).

Recognition of the interstratified character of a sequence and of the disorder in the layer stacking requires the modelling and the precise characterization of the different layer types (*i.e.* structure, composition, thickness), mode of distribution, and thickness distribution of coherent scattering domains.

3.2. Order-disorder of the layer stacking

Many studies were produced to establish the degree of ordering of a given sequence, mostly using models arising from the comparison of calculated and experimental *d* values of basal reflections and/or high-resolution electron microscopy observations.

The Kübler Index is defined as the full width at half-maximum height (FWHM) of the 10 Å X-ray diffraction (XRD) peak of illite-smectite interstratified minerals, measured on the <2 μm size fraction of an air-dried clay sample using Cu$K\alpha$ radiation (Kübler, 1964, 1967, 1984). Despite its widespread use, the Kübler Index remains controversial, mostly because of the numerous factors that affect the standardization and inter-laboratory calibration of its scale. Furthermore, the index is influenced by many parameters such as: (1) the mean size of crystal domains that scatter X-rays coherently (Weber *et al.*, 1976; Dunoyer de Segonzac & Bernoulli, 1976; Árkai & Tóth, 1983; Eberl & Velde, 1989; Drits *et al.*, 1997a); (2) crystallite size (*e.g.* see Eberl & Velde, 1989); (3) lattice strain (Árkai & Tóth, 1983; Árkai *et al.*, 1995, 1996).

The Árkai index (Árkai, 1991; Árkai *et al.*, 1996) is applied to chlorite and, like the Kübler index, involves the quantification of the width at the half-maximum height peaks of chlorite basal reflections. In this case, the index is derived from the 14 Å and 7 Å basal reflections.

The Reichweite index (R) is a simple method to obtain quantitative or semi-quantitative interpretation of the degree of ordering of an interstratified sequence from experimental *d* values of basal reflections. The Reichweite index expresses the probability, for a given layer of type A, that the next layer will be of type B (Drits *et al.*, 1994). This technique mostly applied to illite-smectite, uses graphical simulation of node positions in the reciprocal space along $\mathbf{c}^*$ and/or linear relationships (Guggenheim, 2011, this volume).

Several indices evaluate the kaolinite degree of ordering. These relations are based on changes observed in two specific groups of XRD reflections, namely: (1) the 02*l* and 11*l* sequences, which are sensitive to arbitrary and special interlayer displacements (such as $b/3$); and (2) the 13*l* and 20*l* sequences, which are affected by arbitrary displacements. Following this approach, several parameters could be defined, such as: (1) Hinckley index (HI) (Hinckley, 1963) and Range & Weiss index (QF) (Range & Weiss, 1969); (2) Stoch index (IK) (Stoch, 1974), which is similar to the previous two, but less sensitive to the presence of quartz; (3) Lièrtard index (R2) (Lièrtard, 1977), which, according to Cases *et al.* (1982) is sensitive to presence of arbitrary defects only. Aparicio & Galán (1999), however, suggested that this parameter is also affected by the presence of associated phases (quartz, feldspar, iron and silica gels, illite, smectite and halloysite); (4) EXpert SYstem (EXSY), developed by Plançon & Zacharie (1990), which is based on parameters derived from the second basal reflection and from selected reflections belonging to (0 2 11) and (2 0 13) bands. The first one represents 02*l* and 11*l* reflections in the 2θ range from 19 to 24° and the second one 20*l* and 13*l* reflections in the 2θ range from 35 to 45° (Cu$K\alpha$ radiation); (5) Aparicio-Galán-*Ferrell index (AGFI)* $\left(\text{AGFI} = \frac{(1\bar{1}0 + 11\bar{1}) \text{ peak heights}}{2 \times 020 \text{ peak height}}\right)$, which is determined after applying a peak decomposition procedure by modelling the intensity of reflections in 02*l* and 11*l* sequences. This index seems to be less influenced by peak overlap and by the presence of accessory phases (Aparicio *et al.*, 2006).

Several programs were developed to simulate the diffraction patterns of layered materials showing typical long-tailed diffuse bands. *NEWMOD*™, developed by Reynolds (1985), calculates one-dimensional (oriented) XRD pattern profiles for pure phyllosilicates and for interstratifications of two phyllosilicates. In particular, once the diffraction patterns for each of the two constituent phyllosilicates are calculated, the program can simulate their combination consistently with a given mixture pattern. *NEWMOD*™ can describe effects associated with isomorphous substitutions, ordering of interstratifications, and with the particle size of the minerals present in the sample (for details of the statistical parameters defining the layer stacking of interstratified mineral see Reynolds, 1983; Drits & Tchoubar, 1990; Moore & Reynolds, 1997). Other codes that simulate defective layered structures are *MODXRSD* and *DIFFaX+* (Treacy *et al.*, 1991; Plançon, 2002; Leoni *et al.*, 2004). *MODXRSD* is a valuable tool for the simulation of powder patterns of disordered (both translational and rotational) sheet silicates or even mixed-layer crystals. It can also take into account variable crystal sizes and defects, such as cracks, inner-porosity, bent layers and edge dislocations. The *DIFFaX+* program allows only simulations of SAD (selected-area diffraction) and powder diffraction patterns (X-ray and neutrons). In general, *DIFFaX+* produces simulated powder patterns that can be compared visually to observed ones, thus providing confirmation of the reliability of a structure model.

Calculation of particle size on the diffraction peaks of phyllosilicates using peak broadening and shifts is also possible by means of the MUDMASTER and GALOPER programs. MUDMASTER (Eberl *et al.*, 1996) determines the crystallite size distribution and strain in the crystal direction corresponding to the peak by

Fourier analysis of XRD peak shape. GALOPER (Eberl *et al.*, 1998, 2000) calculates crystal-size distribution that results from crystal growth in open and closed systems using several growth mechanisms.

A good approach to solving the structure of regular mixed-layer structures is the multi-analytical approach, encompassing several experimental techniques, modelling of experimental XRD patterns and high-resolution electron microscopy (Środoń & Eberl, 1984; Drits & Tchoubar, 1990; Baronnet, 1992; Veblen, 1992; Banfield & Bailey, 1996; Drits, 1997; Moore & Reynolds, 1997; Lanson, 2005; Drits *et al.*, 2007; Lanson *et al.* 2009). A good example of the application of this approach is the characterization of brinrobertsite (Dong *et al.*, 2002), using transmission electron microscopy (TEM), energy dispersive (ED) spectral analysis, thermal gravimetric analysis (TGA), and modelling of XRD results (Lanson, 2011, this volume).

The profile-fitting method calculates a complete XRD pattern from a structural model optimized for each clay species present (Drits & Tchoubar, 1990; Drits *et al.*, 1997b; Sakharov *et al.*, 1999). In the multi-specimen method, the optimized structural model should describe all XRD patterns obtained for a given sample following different treatments, such as saturation by different interlayer cations, ethylene-glycol solvation, heating, *etc*., equally well. The multi-specimen method can be applied to mixed layers with more than two layer types whatever the layer stacking sequences are, and there is no *a priori* limitation to the nature of the species identified.

Structural details on irregular structures of mixed-layer crystals may be described in terms of a statistical probability-based model, where parameters define the proportion of structural fragments (in this case, layers) and the pattern of their distribution in the direction of periodicity loss. These parameters may be determined by modelling XRD patterns obtained by scanning in the above direction, seeking the best convergence of the experimental intensities with the intensities calculated by the theory of diffraction from irregular layered structures (Ivanova & Frank-Kamenetskaya, 2001).

Among mixed-layer minerals, the illite-smectite series was the one studied more intensely and, consequently, better detailed (*e.g.* see Altaner & Ylagan, 1997; Dong *et al.*, 1997; Dong, 2005; Lanson *et al.*, 2009). Several studies focused on the intercalation of these minerals with different molecules, mostly to support various applications and technological processes.

4. The *cis*-vacant and the *trans*-vacant octahedral site

Structural and crystal-chemical heterogeneity of layer silicates, especially in dioctahedral species, is affected significantly by the distribution of the octahedral cations and of vacancies in *trans*- and *cis*-oriented sites (Fig. 1b), as demonstrated by an extensive literature mostly concerning 2:1 layer silicates. In the beginning, only dioctahedral 2:1 layer silicates showing the *trans*-site vacant were described. The existence of 2:1 dioctahedral phyllosilicates with one of the *cis*-sites vacant was first reported by Méring & Oberlin (1971). Drits *et al.* (1984) derived unit-cell parameters and atomic coordinates for one-layer monoclinic *cis*-vacant illite; Tsipursky & Drits (1984) indicated that

dioctahedral smectite can be both *cis*-vacant (mostly montmorillonite) and *trans*-vacant (mostly nontronite and beidellite). They also documented many cases showing interstratified *cis*- and *trans*-vacant layers. The major factor driving cation distribution on *cis*- and *trans*-vacant sites was recognized to be the ratio of Si-for-Al substitution. Reynolds (1983) demonstrated that illite in mixed-layer illite-smectite consists either of *trans*-vacant and *cis*-vacant layers or of an interstratification of both layer types. Drits *et al.* (2006) and Drits & Zviagina (2009), starting from powder XRD patterns calculated for different polytypes, consisting of either *trans*- or *cis*-vacant layers, demonstrated that: (1) Fe^{3+}- and Mg-rich dioctahedral species (celadonite, glauconite, Al-celadonite and the majority of phengites) usually present *trans*-vacant octahedra; (2) 1*M*-*cis*-vacant illite, as well as *cis*-vacant layers in the illite fraction of illite-smectite interstratified minerals, can be mostly associated with Fe- and Mg-poor varieties; (3) in illites and illite fundamental particles of illite-smectite consisting of *trans*-vacant and *cis*-vacant layers, *cis*-vacant layers prevail when the Al in octahedral and tetrahedral sites is > 3.10 and > 0.70 atoms per $O_{20}(OH)_4$, respectively; (4) Mg-rich *cis*-vacant smectite shows random distribution of isomorphous octahedral cations, whereas Mg-bearing *trans*-vacant smectite shows dispersed octahedral Mg cations to minimize, as much as possible, the formation of Mg-OH-Mg patterns. The structural characterization of *cis*-vacant and *trans*-vacant 2:1 layer silicates was obtained with different techniques, such as: (1) powder XRD patterns calculated for different polytypes consisting of either *trans*-vacant or *cis*-vacant layers (Zviagina *et al.*, 2007); (2) simulation of experimental XRD patterns corresponding to illite or illite fundamental particles in which *trans*-vacant and *cis*-vacant layers are interstratified (Drits & Zviagina, 2009); (3) semi-quantitative assessment of the relative content of the layer types in interstratified structures (McCarty *et al.*, 2009); (4v) thermal analysis, conveniently exploiting the different dehydroxylation temperatures characterizing *trans*- and *cis*-vacant illite and smectite (Drits *et al.*, 1998; Wolters & Emmerich, 2007); (5) Mössbauer spectroscopy (Shabani *et al.*, 1998; Dainyak *et al.*, 2004, 2009; Dainyak & Drits, 2009). Using Mössbauer spectroscopy evidence, Shabani *et al.* (1998) discovered that $2M_1$ muscovite can present two types of spectra. The first type of muscovite crystals presents a well resolved Fe^{2+} quadrupole doublet, whereas a second type presents a single, broader Fe^{2+} quadrupole doublet. The model used for spectrum fitting, which assumes the occurrence of Fe^{2+} both in *cis*- and *trans*-sites, suggested that spectra of the second type can identify the presence of *cis*-vacant sites in muscovite, whereas spectra of the first type can allow an accurate calculation of the minimum number of *cis*-vacant sites. Dainyak & Drits (2009) considered the local cation arrangement around Fe^{2+} and Fe^{3+} and suggested that the main contribution to first type muscovite is the 2(Fe^{2+}, Mg) Al local cation arrangement around Fe^{2+}, whereas, for second type muscovite, the 3Al and 2AlFe^{3+} local cation arrangements are more important.

5. Layer charge

When the tetrahedral and octahedral sheets are joined in a layer, the resulting layer can be either electrically neutral or negatively charged. Ideally, a layer is electrically neutral

if: (1) the octahedral sheet contains trivalent cations (R^{3+}) at two octahedral sites (usually Al^{3+} or Fe^{3+}), with a vacancy (□) at the third octahedral position [R_2^{3+} □ $(OH)_6$], or else divalent cations (R^{2+}, usually Fe^{2+}, Mg^{2+}, Mn^{2+}) at all the octahedral sites [R_3^{2+} $(OH)_6$]; (2) the tetrahedral sheet contains Si^{4+} in all tetrahedra. However, substitutions within the layer can also produce neutrality (*e.g.* mutual tetrahedral and octahedral substitution producing layer neutrality $^{[iv]}(R_x^{3+}Si_{-x}^{4+})$ $^{[vi]}(R_x^{3+}R_{-x}^{2+})$). Negative layer charge arises from: (1) substitution of lower-charge cations at octahedral sites; (2) substitution of R^{3+} for Si^{4+} in tetrahedral sites; and (3) vacancies. The charge per formula unit, x, is the net negative charge per layer, expressed as a positive number. The net negative layer charge is balanced by the positively charged interlayer material. **Q1**

Layer charge is a fundamental property of 2:1 phyllosilicates. In some minerals this charge is balanced by fixed cations (*e.g.* micas), whereas in others it is balanced by exchangeable cations (*e.g.* smectite and vermiculite), placed in the interlayer position.

Layer charge affects many properties of smectite, such as swelling (Laird, 2006), ion-exchange capacity, ion-exchange selectivity (Maes & Cremers, 1977; Shainberg *et al.*, 1987), and rheological properties (Christidis *et al.*, 2006). A number of independent studies using different analytical methods demonstrated that distribution of layer charge in smectite can vary considerably (Nadeau *et al.*, 1985; Lim & Jackson, 1986; Decarreau *et al.*, 1987; Christidis & Dunham, 1993, 1997; Lagaly, 1994; Mermut, 1994; Christidis, 2001, 2006; Christidis & Eberl, 2003). The layer charge of smectite can be estimated using a variety of analytical methods including: (1) the structural-formula method (Weaver & Pollard, 1973; Grim & Güven, 1978; Bain & Smith, 1987; Newman & Brown, 1987; Laird, 1994, 2006); (2) the alkylammonium method (Lagaly & Weiss, 1975; Lagaly, 1981, 1994); (3) the investigation of XRD traces of K-saturated, ethylene-glycol solvated smectites (Christidis & Eberl, 2003). Additional methods, less frequently used, include: (1) NH^{4+} saturation and examination by infrared (IR) spectroscopy (Petit *et al.*, 2006); and (2) methylene blue absorption and examination by UV spectroscopy (Bujdák, 2006). However, all the methods discussed, aiming at providing an approximation of layer charge value, can be susceptible to deviations, sometimes significant, and can lead to erroneous interpretations if not used properly (Christidis, 2008). More quantitative details for this important topic are addressed extensively by Christidis (2011, this volume).

Layer charge can be located at different places in the layer, as affecting and being affected by isomorphous substitution involving either the tetrahedral or octahedral sheet. This aspect represents another important factor affecting both hydration and cation speciation in the interlayer of hydrated 2:1 layer silicates, such as smectites and vermiculites. In electrically neutral layers, the basal oxygen atoms act as a weak Lewis base (electron donor), forming weak hydrogen bonds with water molecules. When isomorphous substitution occurs, the basal oxygen atoms show an excess negative charge, and their electron-donating capacity increases. Sposito (1984) demonstrated that H-bonding between water molecules and basal oxygen atoms is enhanced by tetrahedral rather than by octahedral sheet substitutions. According to the HSAB (Hard and Soft Acid and Base) theory of Pearson (1963, 1968), the 2:1 silicate layers and the hydrated interlayer cations can be considered as Lewis bases and acids, respectively (Xu & Harsh, 1992). The location of the layer charge determines the strength of the Lewis base: when

the layer charge derives from substitutions mostly at the octahedral sheet, the hydrated 2:1 layer silicate behaves as a soft base, as tetrahedral basal oxygen atoms are affected by a charge imbalance involving the whole layer rather than the tetrahedral sheet directly. On the contrary, when the layer charge derives from substitutions mostly involving the tetrahedral sheet, the hydrated 2:1 layer silicate behaves as a hard base because the layer charge related to tetrahedral substitutions affects the charge of coordinating basal oxygen atoms significantly. In this way, the 2:1 layer charge location affects the layer hydration as well as the cation-sorption process (Brigatti *et al.*, 2004), as hard and soft bases preferentially complex hard acids (cations) and soft acids, respectively. Clay minerals with charge located in the tetrahedral sheet, such as vermiculite, hydrate more strongly than those with charge located mainly in octahedral sheet, such as montmorillonite. Organic cations are thus adsorbed less strongly on the vermiculite surface because of the energy demand in displacing water from the adsorption site.

Residual negative charges can also develop along the edges of clay mineral particles, where Si-O-Si and Al-O-Al bonds are 'broken' and replaced by Si-OH and Al-OH groups (Güven, 1992).

6. The 1:1 layer structure: kaolin-serpentine group

6.1. Kaolin subgroup

Minerals in the kaolin subgroup consist of dioctahedral 1:1 layer structures (Fig. 2a), with general composition $Al_2Si_2O_5(OH)_4$. The layers are kept together by hydrogen bridges between surface hydroxyl groups on the octahedral sheet and basal oxygen atoms on the tetrahedral sheet. Documented polytypes for dehydrated kaolin minerals (Newnham, 1961) are: kaolinite, dickite, nacrite and halloysite-7 Å. These minerals are stacked with different positions of octahedral vacancies in successive layers (Fig. 5). Kaolinite is known to be the more abundant polytype, while dickite, nacrite and halloysite-7 Å are less common. Halloysite-10 Å, general stoichiometry $Al_2Si_2O_5(OH)_4 \cdot 2H_20$, also belongs to kaolin subgroup and presents water molecules between two adjacent TO layers. The intercalated water is bonded weakly and can be removed readily and irreversibly.

Zvyagin (1954) investigated the polytypic arrangement of kaolinite, demonstrating 1-, 2- or 3-layer structures. Different polytypes of the kaolinite group could then be defined depending on the location of the vacant cavity (Bookin *et al.*, 1989; Adams, 1983; Thompson & Withers, 1987; Bish & Von Dreele, 1989; Smrčok *et al.*, 1990; Bish, 1993).

The composition of the kaolin group minerals is characterized by a predominance of Al^{3+} in octahedral sites. Isomorphous substitution of Mg^{2+}, Fe^{3+}, Ti^{4+}, and V^{3+} for Al^{3+} can also occur.

The kaolinite stacking sequence consists of identical layers with an interlayer shift of $2a/3$. Dickite and nacrite show two-layer stacking sequence where the vacant site of the octahedral sheet alternates between two distinct sites (Brindley & Brown, 1980; Zheng & Bailey, 1994). Bailey (1963) demonstrated that both kaolinite and dickite are based on

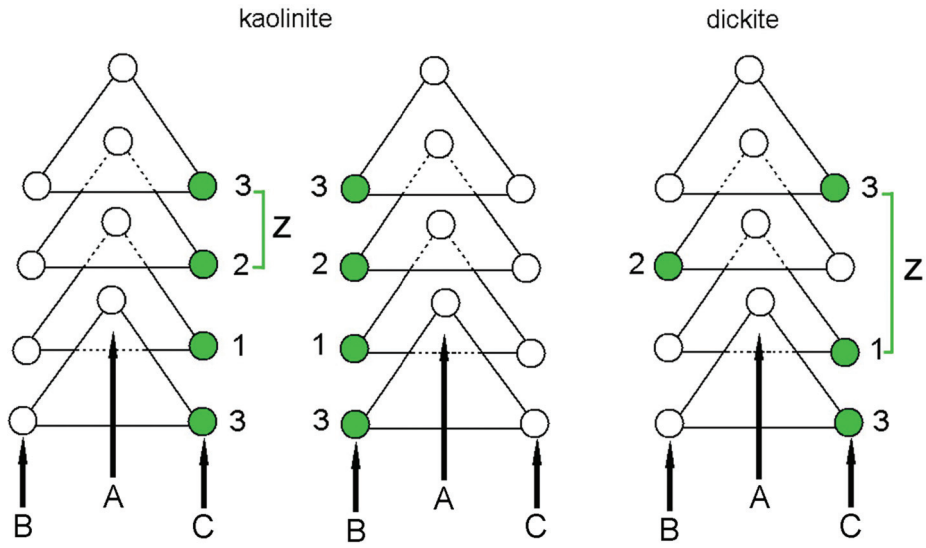

Fig. 5. Projection on the (001) plane of the octahedral sites in kaolinite and dickite showing the possible placement of the vacant octahedral site (filled circles) (modified after Bailey, 1963).

a 1*M* stacking sequence of layers. In the 1*M* structure there are three octahedral sites, denoted as A, B, or C (Fig. 5). In well-crystallized kaolinite each layer is identical and shows an octahedral site C (or B) vacant. In dickite the vacant site alternates between C and B in successive layers to create a two-layer structure. The sequence of layers in nacrite agrees with standard 6*R* polytype.

6.1.1. Kaolinite

Experiments aimed at investigating the kaolinite structure have reported conflicting results for space group and hydroxyl bond lengths and orientations. Explanations for such discrepancies have been discussed in the literature; the differences may be related to impurities in samples, temperature, preferential orientation of the crystallites and difficulties with structure refinement.

The first attempts, aiming at a definition of the kaolinite structure, date back to 1930, when Pauling, starting from models based on idealized polyhedra, provided a basic description. Later, several studies were devoted to the definition of the space group for this mineral (Gruner, 1932a; Hendricks, 1938; Brindley & Robinson, 1945, 1946). Gruner (1932a) indicated, for kaolinite, a monoclinic *Cc* symmetry with $d_{001} =$ 14.3 Å, corresponding to a two-layer structure. Brindley & Robinson (1945, 1946) recognized many reflections in the powder pattern that could not be indexed correctly on the basis of a monoclinic structure, and suggested a lowering of layer to the triclinic symmetry. This evidence was also confirmed by Zvyagin (1960), who suggested a rotation of SiO_4 tetrahedra, and by several other authors (*e.g.* see Brindley &

Nakaira, 1958; Drits & Kashaev, 1960; Suitch & Young, 1983; Thompson & Withers, 1987; Bish & Von Dreele, 1989; Rocha & Pedrosa De Jesus, 1994). In particular, Suitch & Young (1983) and Young & Hewat (1988) reported the appropriate space group for kaolinite as $P1$ and Bish (1993) reported unit-cell parameters (at 1.5 K) as: $a = 5.1535(3)$, $b = 8.9419(5)$, $c = 7.3906(4)$ Å, $\alpha = 91.926(2)$, $\beta = 105.046(2)$, $\gamma = 89.797(2)^\circ$ (space group $C1$). Furthermore, Rocha & Pedrosa De Jesus (1994) demonstrated the existence of two different octahedral coordinations for Al.

Ab initio energy-minimization method (Hobbs *et al.*, 1997; Castro & Martins, 2005), low-temperature neutron powder diffraction (Bish, 1993), refinement of the structure from single- crystal synchrotron data (Neder *et al.*, 1999) and molecular-dynamics simulations based on first-principles calculations within density functional theory (Sato *et al.*, 2004) further contributed in detailing and clarifying kaolinite structure, in particular by underlining that: (1) the average length of apical Si–O bonds (1.59 Å) is nearly equal to that characterizing basal Si–O bonds (1.60 Å) (Bish, 1993); (2) in *C*-site polytype (Fig. 5a), Al-OH bonds (1.84 Å) are shorter than Al-O bonds observed elsewhere in kaolinite (1.90–2.04 Å) (Sato *et al.*, 2004); (3) low-temperature conditions mostly affect the interlayer separation, but not significantly tetrahedral and octahedral parameters.

The positions and orientations of OH groups have been investigated using different approaches. Raman and IR vibrational spectra (Farmer, 1974; Prost *et al.*, 1989; Johnston *et al.*, 1990; Frost, 1995; Frost & Van der Gaast, 1997; Shoval *et al.*, 1999, 2002; Farmer, 1998, 2000; Balan *et al.*, 2001) show four bands. The band at 3619 cm^{-1} is related to the stretching of the inner OH groups whereas the broad band observed at 3695 cm^{-1} is related to in-phase stretching mode of inner-surface OH groups. This band is shifted to a slightly lower frequency in the Raman spectrum (3679 cm^{-1}). The two other bands at 3651 and 3669 cm^{-1} are related to the two out-of-phase stretching modes of inner-surface OH groups.

Suitch & Young (1983) and Young & Hewat (1988) refined H-atom positions using neutron powder diffraction data, assuming a $P1$ space group. H-atom positions were determined also by Rietveld X-ray powder refinement (Adams, 1983), and by a Rietveld refinement of neutron powder diffraction data collected at low temperature in the space group $C1$ (Bish, 1993). This latter study revealed that the inner OH group is in the plane of the layers, and the inner-surface OH groups form angles in the range 60–73° with the (001) plane. Benco *et al.* (2001a,b) explained interlayer H bonding in kaolinite from *ab initio* molecular-dynamic simulations of a hypothetical isolated layer after identifying four distinct OH groups, in $P1$ symmetry. Of these four, two (OH3 and OH4) form weak H bonds with H...O distances of between 1.8 and 2.6 Å, and the other two (OH1 and OH2) are not involved in H bonding. Similar results were obtained by modelling IR spectra (Balan *et al.*, 2001, 2010) (Fig. 6).

White *et al.* (2009), using a density functional modelling approach, confirmed that kaolinite, at temperature values close to 0 K presents the inner OH groups nearly parallel (5.057°) and the inner-surface OH groups nearly perpendicular (78.272°, 84.585°, 68.582°) to the *a,b* plane. OH bond lengths vary between 0.970 and 0.974 Å.

The crystal-structure refinement of a deuterated kaolinite (Akiba *et al.*, 1997) suggested that the three inner OD vectors point towards the tetrahedral sheet, forming

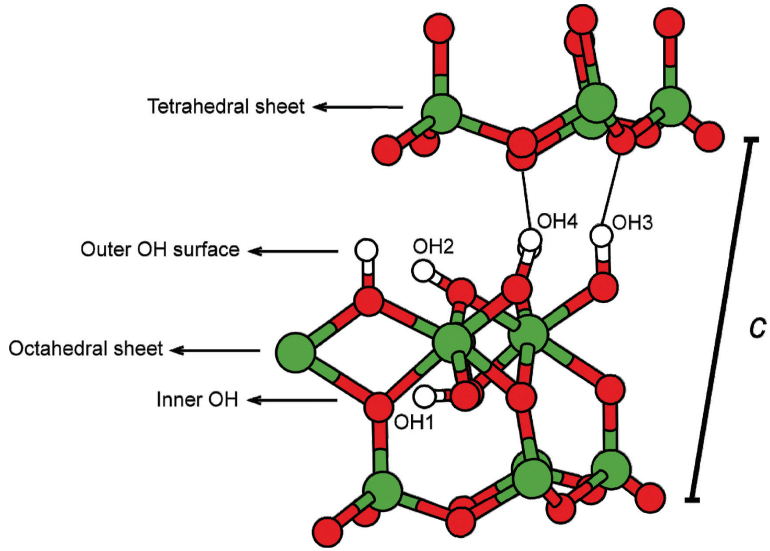

Fig. 6. Different OH orientations on the octahedral surface of kaolinite (modified after Benco *et al.*, 2001a).

H bonding with basal oxygen atoms of the adjacent kaolinite layer. One of the three vectors, however, differs from the other two in terms of bond angle, thus suggesting a different orientation of the bond.

Many other contributions have addressed the structure modifications of kaolinite following temperature/pressure variation (*e.g.* see Prost *et al.*, 1989; Mercier & Le Page, 2008, 2009; Mercier *et al.*, 2010; Welch & Crichton, 2010) or mechanical stress (*e.g.* Reynolds & Bish, 2002). Reynolds & Bish (2002) demonstrated that ordered kaolinite subjected to mechanical grinding presents an increase in disorder that could be modelled as a physical mixture of low- and high-defect material. Mercier & Le Page (2008, 2009) and Mercier *et al.* (2010) calculated enthalpies and cell volumes under pressure with models optimized for *ab initio* density functional theory calculations and identified new interlayer translations for kaolinite, (*i.e.* $-a/3$ and $(a+b)/3$), thus defining a new family of kaolin polytypes generating moderate pressure. Both translations place each silicon atom of each 1:1 layer on top of an OH group from the layer below, resulting in a triangular dipyramidal fivefold coordination for all silicon atoms. These authors also indicated that kaolinite and dickite are the lowest-energy models at zero temperature and pressure (Mercier & Le Page, 2008). Welch & Crichton (2010) observed two-phase transitions in kaolinite. The ambient phase (kaolinite I) transforms reversibly into kaolinite II at 3.7 GPa, whereas kaolinite II transforms irreversibly into kaolinite III at 7.8 GPa.

Smirnov & Bougeard (1999) applied molecular dynamics to investigate the structure and short-time dynamics of interlayer water molecules of the 'hydrated kaolinite', *i.e.* halloysite with layer spacing of 8.5 and 10.0 Å. The structure of interlayer water is characterized by density profiles of the oxygen and hydrogen atoms of water molecules along the direction perpendicular to the surface of the clay layer. This direction (**p**) is the

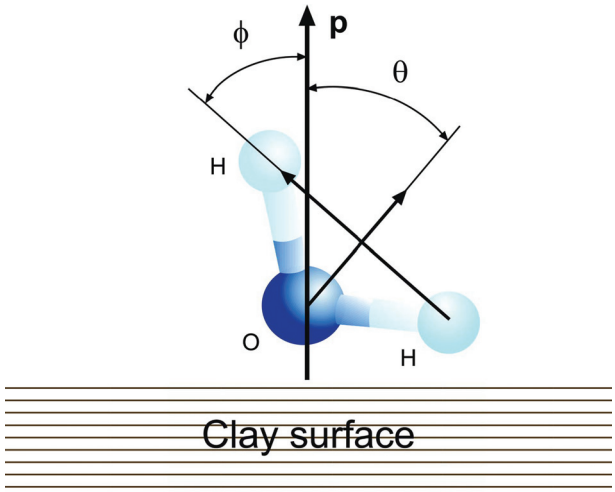

Fig. 7. Orientation of adsorbed water molecules with respect to the surface of kaolinite. **p** is the vector product of the **a** and **b** crystallographic axes vectors (**p** [**a b**]). The θ angle represents the orientations of the molecular dipole and the φ angle represents the HH interatomic vector with respect to the **p** axis. The definition is after Smirnov & Bougeard (1999).

vector product of the **a** and **b** crystallographic axis vectors (**p** [**a b**]). Figure 7 also demonstrates the orientations of the water dipole (θ angle) and the HH interatomic vector (φ angle) with respect to the **p** axis. These authors identified two types of adsorbed water molecules, which are characterized by different orientations with respect to the surface of the clay layer (Fig. 7). Adsorbed molecules of the first type are oriented with the **H**–**H** vector parallel to the surface and with water dipole inclined by 30° to the surface normal; molecules of the second type show **H**–**H** vectors and water dipole perpendicular to the surface and the surface normal, respectively. Such water molecules are located on surfaces of both tetrahedral and octahedral sheets. The increase in interlayer spacing and in the number of interlayer water molecules leads to the formation of a sheet consisting of associated water (Tarý *et al.*, 1999). This sheet is weakly bonded to OH groups in the octahedral sheet and more strongly to molecules adsorbed on the surface of the tetrahedral sheet.

Many theoretical studies have investigated the influence of kaolinite structural features on its ability to adsorb given molecules (*e.g.* see Michalková & Tunega, 2007; Vasconcelos *et al.*, 2007). For example, molecular-dynamics simulation demonstrated that the adsorption of cations and anions on kaolinite surfaces is controlled by the mineral surface charge, thus accounting for preferential adsorption of cations and anions on the basal tetrahedral surface and on the basal octahedral surface, respectively (Vasconcelos *et al.*, 2007).

Possible substitution of Al in octahedral sites and Si in tetrahedral sites was investigated by extended X-ray absorption fine structure (EXAFS), X-ray absorption near edge spectroscopy (XANES), electron paramagnetic resonance (EPR), magic angle spinning nuclear magnetic resonance (MAS-NMR) and Mössbauer spectroscopies (Bonnin *et al.*, 1982; Schroeder & Pruett, 1996; Gualtieri *et al.*, 2000; Balan *et al.*, 2001; He *et al.*, 2003). Those studies have contributed to the following conclusions: (1) Al atoms cannot be easily substituted in both tetrahedral and octahedral sites, and (2) some cations such as Fe, often noted in chemical analyses, are related to associated phases

(Bonnin *et al.*, 1982). Other contributions have suggested that well ordered kaolinite contains only [6]-fold coordinated Fe^{3+} (Balan *et al.*, 1999) whereas disordered kaolinite can also present Fe^{3+} substitutions in tetrahedral sites (Gualtieri *et al.*, 2000) (Mottana & Aldega, 2011, this volume).

The structural order in kaolin minerals is usually defined in terms of a series of either extended (*e.g.* stacking faults) or localized (*e.g.* due to impurities) faults (Bookin *et al.*, 1989; Plançon *et al.*, 1989; Zvyagin & Drits, 1996). Ordered and disordered kaolinites differ significantly in terms of diffraction patterns. The former shows sharp and narrow peaks, while the latter is characterized by less well defined, broad and asymmetrical peaks. A quantitative assessment of the degree of structural order in kaolinite can be derived from powder XRD (see paragraph 3.2); IR spectroscopy (Schroeder, 2002) and thermal analysis (*e.g.* see Balek & Murat, 1996).

Stacking disorder in kaolinite was recently investigated by means of electron microscopy by Kogure *et al.* (2010), also demonstrating that the degree of stacking disorder is variable among individual grains. Stacking faults are mainly produced by disorder of alternating $-a/3$ and $-a/3 + b/3$ layer displacements. Furthermore, stacking faults can be isolated and can form different kind of interstratification of two kinds of multilayer blocks, showing regular $a/3$ and $-a/3 + b/3$ layer displacements.

6.1.2. Dickite

(Unit-cell parameters at 12 K: $a = 5.1474(6)$, $b = 8.9386(10)$, $c = 14.390(2)$ Å and $\beta = 96.483(1)^\circ$, space group: *Cc*, Bish & Johnston, 1993.) The basic description of the dickite structure was provided by Gruner (1932b). The first refinement of the structure, except for the definition of hydrogen atom positions, was undertaken in the space group *Cc*, using single-crystal X-ray data, by Newnham & Brindley (1956, 1957). These studies and the subsequent results from Newnham (1961) showed that dickite exhibits significant distortions from the ideal kaolinite-type layer, including the rotation of SiO_4 tetrahedra and distortion of the octahedral sheet. The structural similarity of the dickite and kaolinite layers was first suggested by Brindley & Nakahira (1958) and confirmed later by Bailey (1963) in the space group *Cc*.

Structure refinements, achieved by single-crystal XRD measurements, were reported by Giese & Datta (1973), Adams & Hewat (1981), Suitch & Young (1983), Sen Gupta *et al.* (1984), Joswig & Drits (1986), and Dera *et al.* (2003). Bish & Johnston (1993) suggested that the inner OH group is approximately parallel to the (001) plane, inclined at just 1.3° to the tetrahedral sheet. The study of OH-group orientation was also addressed by IR (Farmer, 1974; Prost *et al.*, 1989; Johnston *et al.*, 1990; Bish & Johnston, 1993; Shoval *et al.*, 2001) and Raman spectroscopies (Johnston *et al.*, 1998; Shoval *et al.*, 2001), as well as by molecular-dynamics simulations. Balan *et al.* (2005) applied quantum mechanical calculations in the framework of density functional theory to explain experimental spectra of dickite. They concluded that: (1) the band observed at 3622 cm^{-1} may be related to the inner OH stretching; (2) the high-frequency bands, observed in IR spectra at 3711 cm^{-1} (3708 cm^{-1} in Raman spectra) and at 3655 cm^{-1} (3642 cm^{-1} in Raman spectra) correspond to transverse and longitudinal

in-phase motion mode and are attributed to the two outer OH groups. Johnston *et al.* (2002) carried out a single-crystal Raman study of dickite at pressures up to 6.5 GPa using a diamond-anvil cell. They found a dramatic shift in the ν(OH) bands at $\sim$2.2 GPa, indicating a significant change in the local environment of the interlayer OH groups. The lattice mode region showed only minor changes as a function of pressure, suggesting that the individual 1:1 layers did not change significantly with pressure. The spectra also showed that the phase transition is reversible.

Benco *et al.* (2001a) investigated the orientation of OH vectors by *ab initio* molecular dynamics and total-energy calculations and suggested that the inner OH and one inner-surface OH are oriented horizontally, while the other two OH are involved in interlayer bonding. On the contrary, Sato *et al.* (2004), starting from molecular-dynamics simulations based on first-principles calculations, concluded that the inner-surface OH groups are oriented perpendicular to (001) and form interlayer hydrogen bonding.

6.1.3. Nacrite

(Unit-cell parameters: $a = 8.910(3)$, $b = 5.144(2)$, $c = 14.593(3)$ Å, $\beta = 100.50(3)^\circ$, space group: *Cc*; Zhukhlistov, 2008.)

The first crystal-structure refinement of nacrite was reported by Hendricks (1939) who suggested the space group *Cc* for this mineral. The structure is made up of six stacking layers, closely approaching rhombohedral symmetry with a pseudo-space group *R*3*c*. The refinement of the nacrite structure by XRD analysis (Blount *et al.*, 1969) and electron diffraction analysis (Zvyagin *et al.*, 1972) confirmed that the ideal structure of nacrite is based on 6*R* stacking sequence of TM layers, simulating an *R*3*c* symmetry. However, the pattern of vacant octahedral sites reduces the symmetry to *Cc* symmetry. Successive refinement of the nacrite structure with the use of single-crystal precession (Zheng & Bailey, 1994) allowed the determination of the hydrogen atoms and of the OH groups' position in the difference electron density syntheses. It was shown that the O–H interatomic distances is $\sim$0.8 Å and that the angles of inclination of the OH vectors with respect to the layer plane are $\sim 60^\circ$ for the outer OH groups, and $\sim -20^\circ$ for the inner OH group.

Zhukhlistov (2008) refined the nacrite-2M_2 structure from the oblique-texture electron diffraction patterns in the space group *Cc*. Zhukhlistov (2008) suggested that: (1) the octahedra are oblate and their bases are rotated so that a ditrigonal pattern originates in the normal projection onto the *ab* plane; (2) octahedral shared edges are shorter with respect to other octahedral edges, and the OH–OH edge is the shortest among all the shared edges; (3) the Al cations are displaced towards the outer OH surface of the octahedral sheet; (4) the tetrahedra are slightly elongated and α is 7.8°; (5) the O–H interatomic distances and the angles of inclination of the O–H bond with respect to (001) are equal to 0.97 Å and -18.3° for the inner OH group and 0.92, 0.85, 0.93 Å, 60.8, 67.8, 58.4° for the outer OH groups; (6) the electrostatic potential distributions of the hydrogen atoms of the inner OH group and one of the outer OH groups located close to the pseudo-symmetry plane *m* of the layer are characterized by anisotropy, thus suggesting a statistical distribution of these hydrogen atoms.

Ben Haj Amara *et al.* (1997, 1998) described the structure of hydrated and dehydrated nacrite. The hydrated form is characterized by a basal distance of 8.42 Å, containing one water molecule per $Si_2Al_2O_5(OH)_4$ in the interlayer space. The interlayer water molecule is placed above the vacant octahedral site of the layer and is embedded in the ditrigonal cavity of the tetrahedral sheet of the upper layer.

6.1.4. Halloysite

(Unit-cell parameters: $a = 5.1$, $b = 8.9$, $c = 7.57$ Å, $\beta = 100^\circ$, space group: *Cm* (dehydrated form); $a = 5.20$, $b = 8.92$ $c = 10.25$ Å, $\beta = 100^\circ$, space group: *Cm* (hydrated form), Mehmel, 1935.) Halloysite was firstly studied by Berthier (1826). Hofmann *et al.* (1934) proposed the presence of H_2O molecules in its interlayer space, giving the general formula $Si_2Al_2O_5(OH)_4 \cdot 2H_2O$ (Fig. 8). Hydrated halloysite presents layer periodicity close to 10 Å and is referred to as halloysite-10Å (Brindley & Robinson, 1948). The interlayer water in halloysite can be removed easily, giving a dehydrated form with layer periodicity close to 7.2 Å (Bailey, 1989b). The symmetry of these crystals is either monoclinic ($C2/m$, $C21/c$ or *Cc* space groups were reported) or triclinic (Bates *et al.*, 1950; Honjo *et al.*, 1954; de Souza Santos *et al.*, 1965; Zvyagin, 1967). Kohyama *et al.* (1978) suggested a two-layer monoclinic structure with *Cc* space group for both halloysite-10 Å and halloysite-7 Å; unit-cell parameters are $a \approx 5.14$, $b \approx 8.90$, $c \approx 14.9$ Å, $\beta \approx 101.9^\circ$ for the anhydrous form. The insertion of water molecules strongly influences the c parameter, which is increased to $c \approx 20.4$ Å for fully hydrated halloysite. The particles of halloysite can show different morphologies, such as spheres, tubes, plates (*e.g.* see Zvyagin *et al.*, 1966; Churchman & Theng, 1984; García *et al.*, 2009). The tubular halloysite is an attractive material from a technological

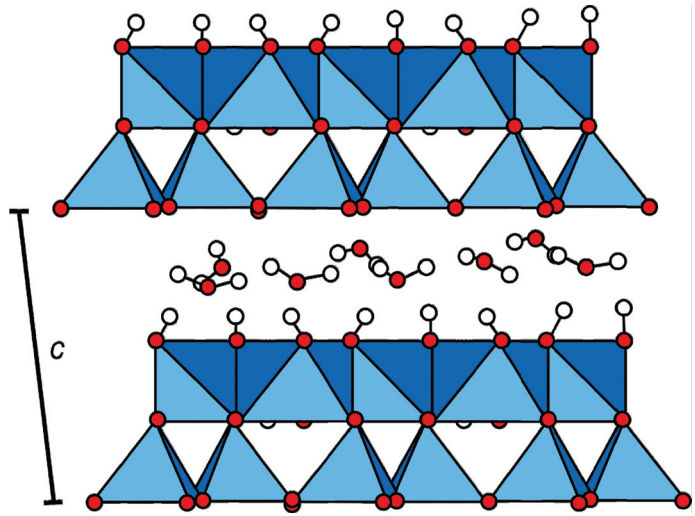

Fig. 8. Layer periodicity in halloysite-10 Å.

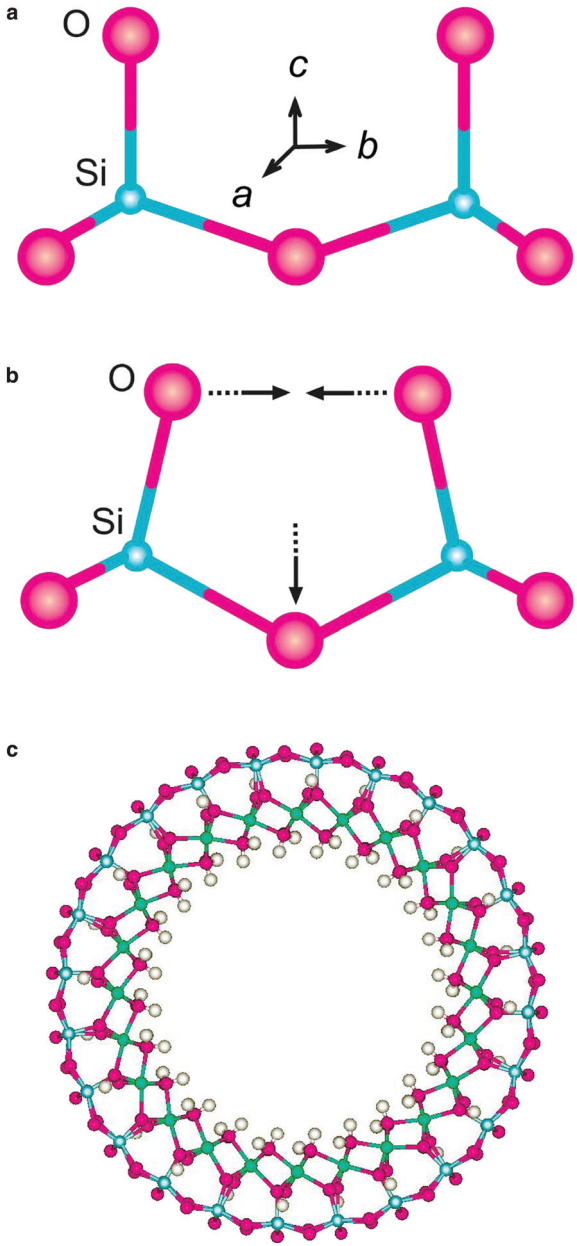

Fig. 9. The rolling mechanism in halloysite. (***a***) Halloysite planar tetrahedral sheet; (***b***) halloysite curved tetrahedral sheet. The distance between apical oxygen atoms in the curved sheet is reduced by decreasing Si–O–Si angle; (***c***) example of a halloysite nanotube (modified after Singh, 1996).

viewpoint, due to its availability and to the vast range of applications, including some showing remarkable biological relevance. Bailey (1989b) assumed that tubular halloysite is generated by a rolling mechanism promoted by Si–Si Coulomb repulsion in the Si plane. Singh (1996) suggested that the rolling mechanism is favoured, from a Si–Si repulsion perspective, in comparison to tetrahedral rotation at a given similar amount of misfit between tetrahedral and octahedral sheets (Fig. 9).

Tubular halloysite is a viable nanocage for biologically active molecules due to the empty space inside the nanotube, allowing entrance of molecules of specific sizes. Halloysite has been used as a support for immobilization of catalyst molecules such as metal complexes and for the controlled release of anticorrosion agents, herbicides and fungicides. It exhibits interesting features and offers a wide range of potential applications, such as entrapping hydrophilic and lipophilic active agents, acting as an enzymatic nanoscale reactor, closely controlling the release rate of drugs and other medical treatments

in humans or animals, and improving mechanical performance of cements and polymers. A detailed review of the vast literature devoted to the application of this mineral is outside the scope of this chapter. Interested readers are directed to a recent review on this topic by Joussein *et al.* (2005).

6.1.5. Hisingerite

Hisingerite [$Fe_2^{3+}Si_2O_5(OH)_4 \cdot 2H_2O$] was originally described by Hisinger (1810) as an amorphous phase and, more recently, as an interstratified montmorillonite/chlorite (Lindqvist & Jansson, 1962) and as a poorly crystallized form of either Fe-rich saponite (*e.g.* see Whelan & Goldich, 1961; Brigatti, 1981) or nontronite (*e.g.* see Gruner, 1935; Sudo & Nakamura, 1952; Kohyama & Sudo, 1975; Mackenzie & Berezowski, 1980; Manceau *et al.*, 1995). Eggleton & Tilley (1998), based on TEM results, demonstrated for hisingerite a fabric of concentric spheres, with diameters of ~140 Å and ~7 Å thick layers as walls. High-resolution images of these walls suggested a structure similar to that of spherical halloysite, thus leading to the conclusion that hisingerite is a ferric-iron member of the kaolin subgroup.

6.2. Odinite subgroup

The odinite structure, ideal composition $(Fe^{3+},Fe^{2+},Mg,Al,Ti,Mn^{2+})_{2.5}(Si,Al)_2O_5(OH)_4$, is based on a 1:1 layer, which is intermediate between dioctahedral and trioctahedral. The polytypic arrangement of this phase, which shows fine grain size and poor crystallinity, is mostly monoclinic (1*M*, space group *Cm*) and sometimes trigonal (or hexagonal) (1*T*) (Bailey, 1988b).

6.3. Serpentine subgroup

Minerals of the serpentine subgroup are commonly hydrous Mg-rich trioctahedral 1:1 phyllosilicates. Al and Fe^{3+} can substitute for Si in tetrahedral sites. Mg in octahedral sites can be substituted by Fe^{2+}, Fe^{3+}, Al, Cr, Ni and Mn^{2+}. They can present an extremely wide range of structural modifications, mainly to compensate for the geometrical misfit between the lateral dimensions of tetrahedral and octahedral sheets. Lizardite presents a flat structure, chrysotile is characterized by cylindrical or spiral tubes; antigorite shows a modulated wave-like shape (*e.g.* see Wicks & O'Hanley, 1988; Bailey, 1988a).

Like lizardite [$Mg_3Si_2O_5(OH)_4$], the trioctahedral 1:1 minerals berthierine [$(Fe^{2+},Al)_3(Si,Al)_2O_5(OH)_4$], amesite [$(Mg,Al)_3(Si,Al)_2O_5(OH)_4$], cronstedtite [$(Fe_2^{2+}Fe^{3+})(Si,Fe^{3+})O_5(OH)_4$], nepouite [$(Ni,Mg)_3Si_2O_5(OH)_4$], kellyite [$(Mn^{2+},Mg,Al)_3(Si,Al)_2O_5(OH)_4$], fraipontite [$(Zn,Cu,Al)_3(Si,Al)_2O_5(OH)_4$], brindleyite [$(Ni_2Al)(SiAl)O_5(OH)_4$], and guidottiite [$(Mn_2^{2+}Fe^{3+})(SiFe^{3+})O_5(OH)_4$] present a planar structure. Like antigorite (general formula [$Mg_3Si_2O_5(OH)_4$]), bementite [$Mn_7^{2+}Si_6O_{15}(OH)_8$] shows a modulated layer structure, whereas greenalite [$(Fe^{2+},Fe^{3+})_{<3}Si_2O_5(OH)_4$], caryopilite [$(Mn^{2+},Mg)_3Si_2O_5(OH)_4$], and minerals of the pyrosmalite series (general formula [$(Mn^{2+},Fe)_8Si_6O_{15}(OH,Cl)_{10}$), such as friedelite [$Mn_8^{2+}Si_6O_{15}(OH,Cl)_{10}$], mcgillite [$(Mn^{2+},Fe^{2+})_8Si_6O_{15}(OH)_8Cl_2$], schallerite [$(Mn^{2+}Fe^{2+})_{16}Si_{12}As_3^{3+}O_{36}(OH)_{17}$], and nelenite [$(Mn^{2+},Fe^{2+})_{16}Si_{12}As_3^{3+}O_{36}(OH)_{17}$]), show islands of tetrahedral sheets (Mandarino & Back, 2004; Wahle *et al.*, 2010).

The serpentine subgroup also includes polygonal serpentine (*e.g.* see Middleton & Whittaker, 1976; Baronnet *et al.*, 1994; Baronnet & Devouard, 2005), and polyhedral serpentines (Baronnet *et al.*, 2007; Andreani *et al.*, 2008). Polygonal serpentines consist of fibres each showing 15 or 30 arranged sectors (Baronnet & Devouard, 2005); polyhedral serpentines comprise spheroids consisting of 92 or 176 lizardite crystals, each one defining a triangular facet of the spheroid (Baronnet *et al.*, 2007; Cressey *et al.*, 2010).

Because of small crystal dimensions and a low level of structural order, crystal-structure data are limited for most of these minerals. A short crystal-structure overview will thus be restricted to samples with 'applications' possibilities and a crystalline order enabling structural investigation.

6.3.1. Mg-rich species

Lizardite (Fig. 10). High quality three-dimensional structural studies for lizardite (Mellini, 1982; Mellini & Zanazzi, 1987, 1989; Mellini & Viti, 1994; Gregorkiewitz *et al.*, 1996; Zhukhlistov, 2007; Mellini *et al.*, 2010; Laurora *et al.*, 2011) were reported mostly for the 1*T* and $2H_1$ polytypes in the space groups *P*31*m* (unit cell

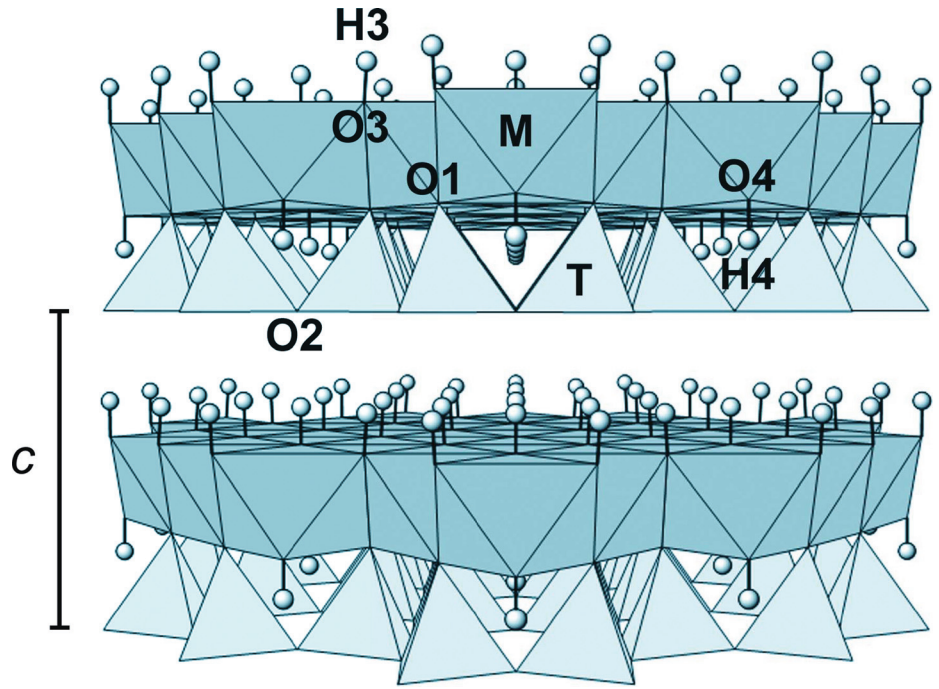

Fig. 10. Crystal structure of lizardite-1T. Tetrahedral sites (T), tetrahedral oxygen atoms (O1, O2), octahedral sites (M), (O1) oxygen atom is shared between tetrahedral and octahedral sheet; octahedral oxygen atoms (O3, O4), and hydrogen atoms (H3, H4) related to O3 and O4 oxygen atoms.

parameters: $a = 5.332(3)$, $c = 7.233(4)$ Å, Mellini, 1982), and $P6_3cm$ (unit cell parameters $a = 5.\ 318(4)$, $c = 14.541(7)$ Å, Mellini & Zanazzi, 1987), respectively. Brigatti *et al.* (1997) examined the $2H_2$ form of Al-rich lizardite (intermediate between lizardite and amesite) in the space group $P6_3$. Previous studies have documented the effects of octahedral substitution on crystal structure, thus demonstrating that: (1) the substitution of trivalent cations in octahedral and tetrahedral sites promotes thermal stability (Caruso & Chernosky, 1979) and crystal order (Mellini & Viti, 1994); (2) homovalent Fe-for-Mg substitution produces a decrease in the octahedral site distortion and an increase in the *c* unit-cell parameter (Laurora *et al.*, 2011). Laurora *et al.* (2011) also suggested that the whole-rock composition affects lizardite crystal chemistry and structure, which are sensitive to the overprint of secondary, metasomatic events. Hydrogen positions were located on the *Fo* map and then refined (Mellini, 1982; Laurora *et al.*, 2011). Hydrogen bonding is not observed for the hydrogen atom placed at the centre of the tetrahedral hexagonal ring, unlike other hydrogen atoms which help to keep adjacent layers connected.

The effect of pressure on the structure of $1T$ lizardite was investigated by Mellini & Zanazzi (1989). Guggenheim & Zhan (1998) reported a high-temperature study on both $1T$ and $2H_1$ lizardite crystals. Geometrical changes induced by cation substitutions and details of the hydrogen bond were also studied by means of *ab initio* quantum chemistry calculations (Benco, 1997; Benco & Smrčok, 1998; Scholtzová *et al.*, 2000; Scholtzová & Smrčok, 2005; Auzuende *et al.*, 2006). All these studies suggested that: (1) cation substitutions account for geometrical changes in tetrahedral sheets, whereas octahedral sheets are almost unaffected; (2) substituted tetrahedra are tilted and their basal oxygen atoms are pushed below the plane defined from basal vertices of unsubstituted tetrahedra; (3) the hydrogen bond in lizardite consists of dipole to ion interaction with a total energy of 28.121 kJ mol^{-1}; (4) lizardite, as suggested by analysing the variation in cell dimensions following pressure increase, is stiffer in directions parallel to the layer than in the **c** direction, normal to the layer; (5) the cohesive energy between two successive layers along **c** is 0.33 eV (*i.e.* 0.11 eV per OH bond).

The internal dimensions of a 1:1 layer are remarkably less affected by chemical substitutions and by pressure or temperature increase, than interlayer thickness, which varies significantly with composition (Chernoski, 1975) or with pressure increase (Mellini & Zanazzi, 1989). As the interlayer thickness increases, the ditrigonalization of the tetrahedral sheet, which, depending on orientation, can be expressed either by a positive or negative angle, decreases. In the $1T$ polytype, the ditrigonal ring distortion changes from -1.5° to $\sim 0^\circ$ when the temperature changes from 20 to 480°C. In the $2H_1$ polytype, this structural parameter changes from 1.8°, at room temperature, to 1.3° at 300°C and remains unchanged up to 475°C. In the $2H_1$ polytype, the O–O distance, referring to the interlayer O–H. . .O bond, increases linearly from 3.08 to 3.15 Å as the temperature increases from 20 to 475°C. On the contrary, in the $1T$ polytype, this distance remains nearly constant up to 360°C. Above this temperature, the O–O distance increases slightly, thus apparently suggesting weaker hydrogen bonding for the $2H_1$ polytype than for the $1T$ polytype (Guggenheim & Zhan, 1998).

Antigorite (unit-cell parameters: $a = 43.505(6)$, $b = 9.251(1)$, $c = 7.263(1)$ Å, $\beta = 91.32(1)$, space group Pm for the $m = 17$ polysome, Capitani & Mellini, 2004; $a = 81.66(1)$, $b = 9.255(5)$, $c = 7.261(5)$ Å, $\beta = 91.409(5)$ space group $C2/m$ for the $m = 16$ polysome, Capitani & Mellini, 2006).

Antigorite is a 1:1 layer silicate characterized by a modulated crystal structure. This mineral, because of its chemical composition and structural arrangement, belongs to the serpentine subgroup, without being considered a serpentine polymorph *sensu stricto*, due to the evident $Mg(OH)_2$ depletion, as indicated by the formula $^{vi}M^{v}_{3m-3}T_{2m}O_{5m}(OH)_{4m-6}$ (where M = Mg, Fe, Ni, Al; T = Si, Al; m = number of unique tetrahedra spanning a wavelength along the **a** axis) (Capitani & Mellini, 2004).

The antigorite polysomatic series (Spinnler, 1985; Ferraris *et al.*, 1986) was investigated by XRD (*e.g.* see Aruja, 1945; Kunze, 1956, 1958, 1961; Capitani & Mellini, 2004, 2006) and TEM (*e.g.* see Zussman *et al.*, 1957; Yada, 1979; Spinnler, 1985; Uehara & Shirozu, 1985; Mellini *et al.*, 1987; Wu *et al.*, 1989; Otten, 1993; Viti & Mellini, 1996; Uehara, 1998; Dódony *et al.*, 2002; Grobéty, 2003; Dódony & Buseck, 2004; Capitani & Mellini, 2005). The antigorite structure consists of positional modulations of the curved 1:1 silicate layer along the **a** direction (Fig. 11a). Although the structural continuity of both the tetrahedral and octahedral sheets is maintained, the modulation is due to the periodic reversal of the layer polarity (and of silicate tetrahedra), thus generating a wave-like effect, where each individual half wave is characterized by the same orientation of silicate tetrahedra. If m is even, two consecutive half waves are equal in dimension. Whe m is odd, one ('short half wave') is made from $(m/2) - 0.5$ tetrahedra, whereas the following one ('long half wave') consists of $(m/2) + 0.5$ tetrahedra. Most antigorite specimens are monoclinic, space groups $C2/m$ and Pm, for m even and odd, respectively (Capitani & Mellini, 2004, 2006). Two distinct reversals along the **a** direction are always observed across six-membered rings, where four contiguous tetrahedra point down and the two remaining tetrahedra point up, and *vice versa*. If the structural pattern for the first reversal is accepted, the second reversal is described with two different models. The first model assumes eight-membered rings (8-reversals) with four neighbouring tetrahedra pointing up and four neighbouring tetrahedra pointing down, which alternate along the **b** direction with four-membered rings (4-reversals) with two neighbouring tetrahedra pointing up and the other two tetrahedra pointing down, or *vice versa* (Wu *et al.*, 1989; Otten, 1993; Uehara & Kamata, 1994; Uehara, 1998; Grobéty, 2003, Capitani & Mellini, 2004, 2006; Capitani *et al.*, 2009). This pattern was first supported by HRTEM imaging (Wu *et al.*, 1989; Otten, 1993; Uehara & Kamata, 1994; Uehara, 1998; Grobéty, 2003), and, later confirmed by 3D refinement of X-ray data from the $m = 16$ (Capitani & Mellini, 2004) and $m = 17$ (Capitani & Mellini, 2006, 2008) polysomes.

Another structural model assumes 6-reversals (Dodòny *et al.*, 2002, 2006). Theoretical approaches based on density functional theory indicate that the structural model by Capitani & Mellini (2004) is energetically more favoured (Capitani *et al.*, 2009).

Chrysotile. A preliminary structure determination for chrysotile dates back to a study by Pauling (1930) who suggested for this commonly fibrous mineral, a curved hollow morphology, because of the need to fit tetrahedral and octahedral sheets. Further

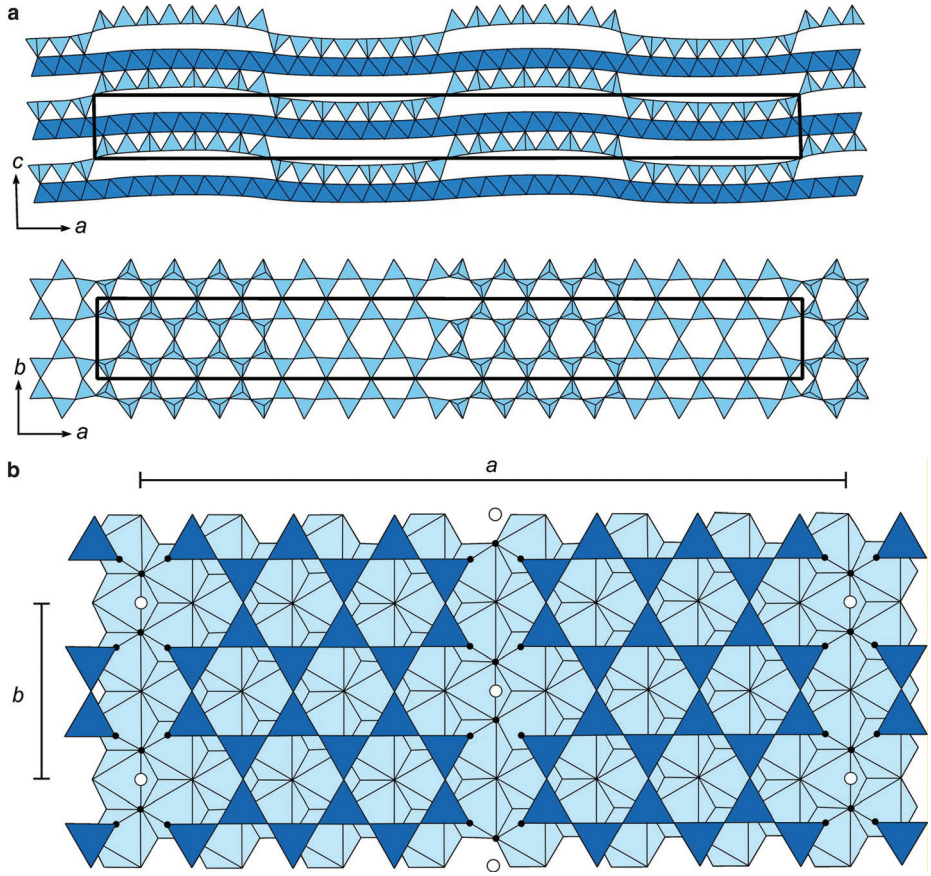

Fig. 11. (***a***, ***b***) The antigorite polysome ($m = 16$). (***a***) [010] projection, (***b***) [001] projection of the modulated tetrahedral sheet (modified after Capitani & Mellini, 2006); (***c***) [001] projection of carlosturanite. Small filled circles represent OH groups, open circles refer to water molecules (modified after Mellini *et al.*, 1985).

studies were promoted in the 1950s by Whittaker, starting from XRD data (Whittaker, 1953, 1956a, 1956b, 1956c) and, later on, by Yada (1971), using high-resolution TEM. The latter author also defined three types of chrysotile: clinochrysotile, orthochrysotile and parachrysotile. Clinochrysotile shows, when its cylindrical structure is ideally developed into a plane, a two-layer monoclinic unit cell, where no rotation is observed among layers and where the *x* axis is parallel to the cylindrical axis. Unlike clinochrysotile, orthochrysotile shows an orthorhombic two-layer unit cell with 180 degrees rotation among the layers. Parachrysotile differs then from orthochrysotile as the *y*, instead of the *x* axis, is parallel to the cylindrical axis.

The technological application of chrysotile has decreased significantly over recent decades, substituted in traditional applications, by materials more compatible with human health and safety requirements. In recent times, however, the interest in the

synthetic rather than the natural mineral has increased because of the interesting technological properties associated with the nanotube structure. This mineral shows various morphologies: hollow and full cylinders, tube-in-tube cylinders, conically wrapped fibres, cone-in-cone shaped concentric structures, spiral and multi-spiral (Yada, 1971).

Amesite (unit-cell parameters: $a = 5.319(2)$, $b = 9.208(3)$, $c = 14.060(5)$ Å, $\alpha = 90.01(3)$, $\beta = 90.27(3)$, $\gamma = 89.96(3)^\circ$, space group: $C1$; Hall & Bailey, 1979).

Several studies have been devoted to the structure determination of amesite (*e.g.* see Brindley *et al.*, 1951; Steinfink & Brunton, 1956; Steadman & Nuttall, 1962; Hall & Bailey, 1979; Anderson & Bailey, 1981). All these studies agree in suggesting a two-layer polytype for this mineral and hexagonal or pseudohexagonal symmetry. Wiewióra *et al.* (1991) identified an uncommon amesite showing a triclinic symmetry and ordering of cations in both tetrahedral and octahedral sites [unit cell parameters: $a = 5.31(1)$, $b = 9.212(2)$, $c = 14.401(7)$ Å, $\alpha = 102.11(3)$, $\beta = 90.2(1)$, $\gamma = 90.1(1)^\circ$]. Two stacking modes were recognized for amesite layers: the first shows a 180° rotation with no shift of adjacent layers, whereas the second shows a 180° rotation combined with a translation of $-b/3$.

Carlosturanite (Fig. 11b) shows a modulated structure (Compagnoni *et al.*, 1985), with the following general formula: $M_{21}[T_{12}O_{28}(OH)_4](OH)_{30}\cdot H_2O$ where M is predominantly Mg^{2+} with small amounts of Fe^{3+}, Mn^{2+}, Ti^{4+}, Cr^{3+}, and T is Si^{4+} or Al^{3+} and unit-cell parameters: $a = 36.70(3)$, $b = 9.41(2)$, $c = 7.291(5)$ Å, $\beta = 101.1(1)$, space group: Cm. Carlosturanite is poorer in Si and richer in H_2O than the common serpentine-group phases (Compagnoni *et al.*, 1985; Belluso & Ferraris, 1991). On the basis of its chemical properties and results of a detailed structural investigation, supported by high-resolution TEM, Mellini *et al.* (1985) proposed a structural model based on the interruption of the tetrahedral sheet (T_2O_5) and on the introduction of vacancies at tetrahedral sites along rows parallel to the direction of TO chains. In this model, the octahedral sheet of the serpentine structure is preserved, whereas $\frac{1}{7}$ of the $[Si_2O_7]^{6-}$ tetrahedral groups is replaced by $[(OH)_6H_2O]^{6-}$ groups, bonding to only one Si ion. The resulting layer of tetrahedra is thus formed from triple chains of tetrahedra bound to each other by means of H_2O molecules. Starting from a carlosturanite structural arrangement, Mellini *et al.* (1985) introduced the inophite family name to indicate a polysomatic series resulting from combination of serpentine S modules with composition $M_3T_2O_5(OH)_4$ (M = octahedral cations, T = tetrahedral cations) and X modules with composition $M_6T_2O_3(OH)_{14}\cdot H_2O$.

6.3.2. Fe-rich species

Cronstedtite. Kogure *et al.* (2001) discovered a great variety of polytypes in cronstedtite, *i.e.* all polytypes of groups A, C and D defined by Bailey (1969). Three-dimensional crystal-structure refinements for this mineral were provided by several authors and more recently determined or re-determined for polytype $1T$, space group $P31m$ [$a = 5.512(1)$, $c = 7.106(1)$ Å], for $3T$ polytype, space group: $P3_1$ [$a = 5.497(2)$, $c = 21.355(7)$ Å] and for $2H_2$ polytype, space group $P6_3$ [$a = 5.500(1)$, $c = 14.163(2)$ Å] (Smrčok *et al.*, 1994; Hybler *et al.*, 2000; Hybler *et al.*, 2002; Ďurovič *et al.*, 2004; Hybler,

2006). All polytypes show a full Fe octahedral occupancy, while differing for tetrahedral Si/Fe occupancy and/or ordering. In the 1*T* polytype, the Si/Fe ratio is ~3:1 (Hybler *et al.*, 2000). In the $2H_2$ polytype there is an Fe tetrahedral ordering, which is missing in the 3*T* polytype (Smrčok *et al.*, 1994).

Berthierine. The mineral, poorly crystallized, is commonly considered to be typical of marine sediments, probably because of its frequent occurrence in marine-oolitic ironstone formations (Brindley, 1982). However, non-marine occurrences have also been documented. The mineral is frequently associated (or interlayered) with Fe-rich chlorites, as demonstrated by electron diffraction studies (Jiang *et al.*, 1992). Berthierine is commonly a one-layer structure, showing semi-random stacking.

Greenalite. The structure of greenalite (Guggenheim & Eggleton, 1998) consists of octahedrally coordinated Fe and of continuous trioctahedral sheets. Six-member rings of tetrahedra link together to form triangular islands, made up of four or five tetrahedra and coordinating one octahedral sheet. The number of tetrahedra, constituting each island, varies constantly, according to a pattern assuring a limited, short-range order, but missing any long-range ordering, because of domain-boundary linkages and domain positioning. This structural modulation gives a chemical formula, deviating considerably from the stoichiometry characterizing serpentine minerals. In greenalite, Fe atoms are divalent and surrounded by six Fe atoms at 3.21–3.22 Å, consistently with edge-sharing Fe octahedra (Manceau *et al.*, 1995).

6.3.3. Mn-rich species

Kellyite is considered to be the Mn analogue of amesite. Peacor *et al.* (1974) identified two main polytypes: a six-layer rhombohedral phase and a two-layer hexagonal phase (space group *P*6).

Guidottiite is the Mn analogue of cronstedtite (Wahle *et al.*, 2010). This mineral, only recently described, presents the coexistence of $2H_1$ and $2H_2$ polytypes, together with areas dominated by disordered layer stacking. The single-crystal structure refinement suggests that the $2H_2$ polytype is hexagonal, space group $P6_3$ with $a = 5.5472(3)$, $c = 14.293(2)$ Å. Substitution of Fe^{3+} for Si occurs in tetrahedral sites.

Bementite. The description of bementite structure, a modulated phyllosilicate, was addressed by several authors (*e.g.* see Kato, 1963; Kato & Takeuchi, 1980), who suggested an orthorhombic symmetry (space group, $P222_1$). Heinrich *et al.* (1994) described the bementite structure in space group $P2_1/c$, with $a = 14.838(2)$, $b = 17.584(2)$, $c = 14.700(2)$ Å, $\beta = 95.54(2)^\circ$, as consisting of two hexagonal sheets of Mn octahedra, which are alternately rotated by 22° in the *ab* plane. These octahedral sheets are interlayered by a continuous tetrahedral sheet containing pairs of six-membered rings interconnected with five- and seven-membered rings (Fig. 12). Inverted tetrahedra form strips showing the same orientation (up or down) parallel to the **a** direction. Linked pairs of six-membered rings are rotated, with respect to pairs across the strip boundaries, by 22° to allow coordination with adjacent octahedral sheets. The bementite topology is closely related to that of armbrusterite $K_5Na_6Mn^{3+}Mn^{2+}_{14}[Si_9O_{22}]_4(OH)_{10} \cdot 4H_2O$, space group $C2/m$, with $a = 17.333(2)$, $b = 23.539(3)$, $c = 13.4895(17)$ Å, $\beta = 115.069(9)^\circ$. The structure of armbrusterite is

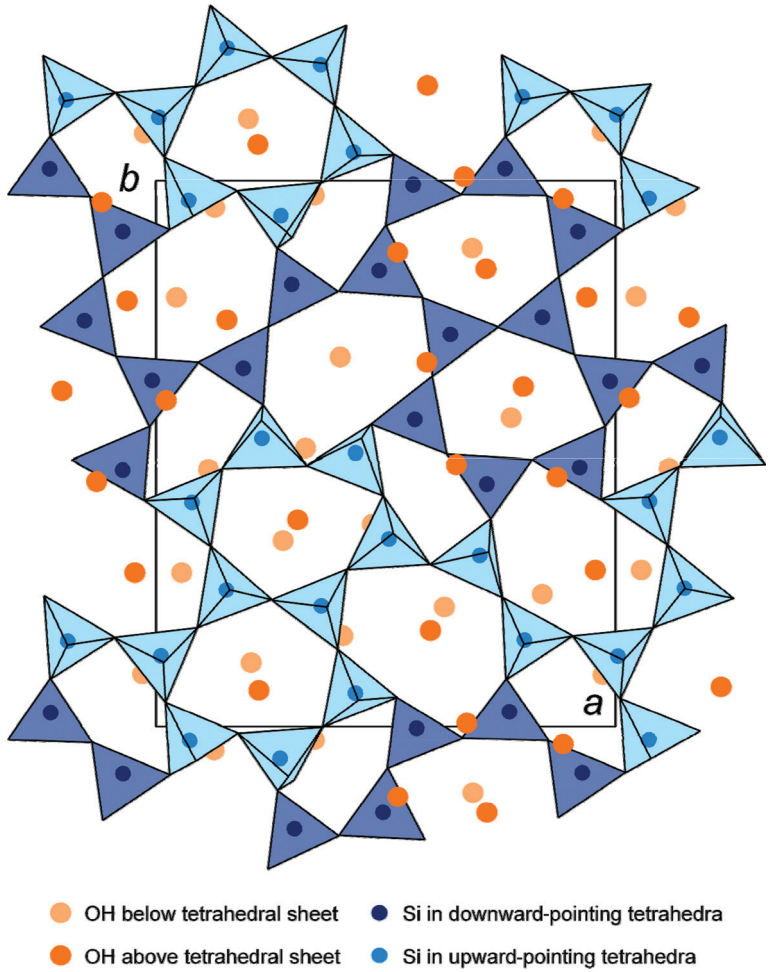

Fig. 12. Projection of bementite tetrahedral sheet on the *ab* plane. The tetrahedral sheet is sandwiched between two Mn octahedral sheets, alternately rotated by 22° in the *ab* plane (modified after Heinrich *et al.*, 1994).

based on double silicate sheets consisting of [5]-, [6]-, [7]- and [8]-membered tetrahedral rings. The sheets are linked by octahedral sheets formed by Na and Mn octahedral. K is located between two silicate sheets and links H_2O molecules (Yakovenchuk *et al.*, 2007).

Pyrosmalite group. Pyrosmalite is the name given to a relatively rare series of Fe-Mn silicates, usually containing some chlorine also. Mn-rich members of the series are more common. The name friedelite is reserved for the pure Mn end-member (Vaughan, 1986; Ozawa *et al.*, 1983). Friedelite, mcgillite and nelenite show 1*M* structure (space group $C2/m$). The basic X-ray reflections characterizing the monoclinic structure are sharp in

mcgillite and diffuse in friedelite, which may thus be considered as the disordered equivalent of mcgillite.

Caryopilite structure is similar to that of greenalite, while differing from this the latter because of a predominant Mn octahedral population.

6.3.4. Ni-rich species

Nepouite generally gives poorer XRD patterns than lizardite and is recognized by 7.2–7.3 Å basal spacing. The stacking of the layers is highly disordered. The large Ni content is indicated by the intense, dark green colour (Brindley & Wan, 1975). Manceau & Calas (1986) and O'Day *et al.* (1994), using EXAFS, suggested that Ni atoms, in Ni-rich serpentine species, cluster in octahedral domains with the Ni–O distance ranging from 2.03 to 2.08 Å and Ni–Ni distances ranging from 3.05 to 3.07 Å.

Fraipontite. Although several natural occurrences are reported, studies on fraipontite are mostly related to synthetic phases due to its considerable industrial and commercial interest (as a smoke suppressant, honeycomb forms for adsorbents and deodorants, in paint, in air-purification filters, as an odour adsorbent, in the treatment of waste gases, and as a blood coagulant for treatment of waste blood) (Kloprogge *et al.*, 2001). The mineral, poorly crystallized, presents a basal reflection at 7.44 Å.

Brindleyite is closely related in structure and stacking sequence to berthierine and occurs as mixtures of the groups A and group C polytypes, as defined by Bailey (1969). The mineral is also characterized by a disordered cation arrangement (Maksimovic & Bish, 1978).

7. 2:1 layer structures

7.1. Talc and pyrophyllite group

Talc is a 2:1 layered, trioctahedral Mg silicate mineral; its ideal structural formula is $Mg_3Si_4O_{10}(OH)_2$. A small amount of water may also be present. Pyrophyllite is also a 2:1 layered hydrous silicate mineral. Its layer structure is dioctahedral and Al is located in the larger octahedron; its ideal structural formula is $Al_2Si_4O_{10}(OH)_2$ and, like talc, can include a small amount of water (Fig. 2a). The chemical composition of talc and pyrophyllite can vary depending on their geological history and parent-rock association. The ideal layer structure of talc and pyrophyllite is electrically neutral, and contiguous TOT layers are connected by van der Waals interactions, thus significantly impacting physical (and mechanical) properties of both minerals. Both minerals are very soft: talc is the softest mineral on the Mohs hardness scale at 1, and pyrophyllite is at 1 to 2 on that scale of 1–10.

7.1.1. Pyrophyllite and ferripyrophyllite

The three-dimensional crystal structure refinement of pyrophyllite [space group $C\bar{1}$ with $a = 5.160(2)$, $b = 8.966(3)$, $c = 9.347(6)$ Å, $\alpha = 9l.18(4)$, $\beta = 100.46(4)$, $\gamma = 89.64(3)$, Lee & Guggenheim, 1981] suggests that the tetrahedral $\langle T–O \rangle$ distance

(1.618 Å) is consistent with the lack of significant Al^{3+}-for-Si^{4+} substitutions and that the octahedral $\langle M-O\rangle$ distance (1.912 Å) matches well with complete Al occupancy. The pyrophyllite layer presents a tetrahedral rotation of $\sim 10^{\circ}$ and a strong corrugation of the basal oxygen-atom plane. Polytypism in pyrophyllite was addressed by several authors (see Evans & Guggenheim, 1988 for a review). Two dominant sequences were identified: a two-layer monoclinic, and a one-layer triclinic, sometime coexisting in the same sample. A significant number of theoretical studies was also devoted to pyrophyllite, in particular suggesting that Mg^{2+}-for-Al^{3+} substitutions tend to be distributed in the octahedral sheet, whereas Fe^{3+}-for-Al^{3+} substitutions tend to be clustered (Sainz-Diaz *et al.*, 2002).

Ferripyrophyllite, $Fe_2^{3+}Si_4O_{10}(OH)_2$, is isostructural with the 2*M* modification of pyrophyllite and presents virtually no substitutions in either the tetrahedral or octahedral sheet, which are thus occupied exclusively by Si and Fe^{3+}, respectively. Ferripyrophyllite was first recognized by Chukhrov *et al.* (1979), who identified a ferric analogue of pyrophyllite in a precipitate from a low-temperature hydrothermal solution. After powder XRD measurements, these authors reported a monoclinic unit cell with $a = 5.26$, $b = 9.10$, $c = 19.1$ Å, and $\beta = 95.30^{\circ}$.

Ferriphyrophyllite can be considered as the Fe end-member of the series (Fe, Al)$_2$Si$_4$O$_{10}$(OH)$_2$. Coey *et al.* (1984) were the first to investigate the cation distribution in the layer by means of Mössbauer spectroscopy, in order to clear out divergent and conflicting interpretations of the spectra for ferric 2:1 layer minerals. Their experimental data demonstrated a Mössbauer spectrum at 4.2K, consisting of a single, resolved magnetic pattern with hyperfine field ($B_{hf} = 51.8$ T). The relatively high Néel temperature, compared to other dioctahedral ferric phyllosilicates, further demonstrated that Fe^{3+} cations tend to be ordered on M2 sites.

7.1.2. Talc and talc-like minerals

Pioneering studies described talc structure as monoclinic ($C2/c$ space group, Gruner, 1934a,b). More recently, the talc structure has been described as triclinic (space group $C\bar{1}$, Rayner & Brown, 1973), or as pseudomonoclinic (space group *Cc*), or else in the $C\bar{1}$ space group with $a = 5.290(3)$, $b = 9.173(5)$, $c = 9.460(3)$ Å, and $\alpha = 90.46(5)$, $\beta = 98.68(5)$, $\gamma = 90.09(5)^{\circ}$ (Perdikatsis & Burzlaff, 1981). The talc layer presents a nearly planar basal oxygen surface and the tetrahedral rotation at 3.6°. The cation distribution in the talc structure was described recently (Petit *et al.*, 2004; Martin *et al.*, 2006), following results obtained from Fourier-transform infrared (FTIR), Mössbauer and MAS-NMR spectroscopies. These studies quantified Fe^{2+}- (or Al^{3+}-) for-Mg substitution and the F content from the 2νOH region and suggested that Fe^{2+} (or Al^{3+}) substitutes randomly for Mg in octahedral sites. Detailed images of the talc basal oxygen plane at the molecular scale were recently obtained by atomic force microscopy (AFM) (Ferrage *et al.*, 2006), indicating for talc a flat surface and well defined tetrahedral rings, deviating little from hexagonal symmetry.

Different polytypic sequences of TOT layers were discussed by Weiss & Ďurovič (1984), who found 10 non-equivalent polytypes, where only seven of these can be distinguished by XRD.

Willemseite $(Ni,Mg)_3Si_4O_{10}(OH)_2$ is the Ni-bearing analogue of talc. Willemseite is a secondary mineral in a Ni-bearing layered igneous sill, and it is characterized by a fine-grained and massive structure, by a perfect {001} cleavage, and by a Mohs hardness scale equal to 2. De Waal (1970), who first suggested the name willemseite, indicated that willemseite is monoclinic (space group Cc or $C2/c$) with $a = 5.316(2)$, $b = 9.149(3)$, $c = 18\ 994(6)$ Å, and $\beta = 99.96(6)^\circ$.

Ni should only be observed in octahedral coordination, as a substitute for Mg; nevertheless, Tejedor-Tejedor *et al.* (1983) demonstrated the presence of tetrahedral Ni by comparing the Ni/Si atomic ratio in extremely well crystallized willemseite, to its theoretical stoichiometry.

As demonstrated by Koshimizu *et al.* (1981), after measurements on various hydrothermally synthesized terms of the talc–willemseite series, the Ni contents could be derived both from the intensities of the absorption band in the OH-stretching region, and from the temperature value of the DTA endothermic effect related to dehydroxylation reaction. In particular, the greater the Ni^{2+}/Mg^{2+} ratio, the greater are both the intensity of the absorption band in the OH-stretching region and the temperature value at which the dehydroxylation reaction occurs.

Several investigations, based mainly on spectroscopic data (*e.g.* optical spectroscopy, IR spectroscopy, X-ray absorption spectroscopy (XAS), *etc.*), agree well, considering Ni as bivalent (Brindley *et al.*, 1979; Manceau *et al.*, 1984, 1985), without determining any appreciable distortion of the coordinating polyhedron when Ni substitutes for Mg (Manceau *et al.*, 1985). In addition, XAS measurements indicate that Ni atoms are segregated into domains inside the octahedral sheet, with an average size of at least 30 Å. However, experimental data could not exclude even the existence of octahedral sheets completely occupied by Ni (Manceau & Calas, 1986).

7.2. The mica group: some recent advances on crystal chemistry and structure of dioctahedral and trioctahedral micas

The crystal chemistry and structure of dioctahedral and trioctahedral micas were reviewed recently by Brigatti & Guggenheim (2002). A complete description of the complex interrelationships between chemical composition and structure in micas is not given here, therefore. A short discussion of the main aspects of mica crystal chemistry and of some new trends and results is given however.

Although the basic structure of a mica layer is well known, the accurate crystal-chemical description of micas is often a challenge because of: (1) the large number of cationic and anionic substitutions; (2) the presence of the same element in different structural sites; (3) different oxidation states for metals; (4) light elements not detected by electron microprobe analysis; (5) structural vacancies; and (6) cation ordering. Recent advances in mica crystal chemistry are mostly attributed to: (1) the determination of light elements, Fe speciation, hydrogen content (Scordari *et al.*, 2006; Mesto *et al.*, 2006; Scordari *et al.*, 2008; Di Vincenzo *et al.*, 2006; Gianfagna *et al.*, 2007; Matarrese *et al.*, 2008); (2) detailed structural evidence based on both X-ray and neutron diffractions at room and given temperature and pressure conditions

(Zanazzi & Pavese, 2002; Ferraris & Ivaldi, 2002; Pavese *et al.*, 2003; Comodi *et al.*, 2004; Welch *et al.*, 2004; Welch & Crichton, 2005; Curetti *et al.*, 2006; Dobson *et al.*, 2007; Zanazzi *et al.*, 2007a,b; Pavese *et al.*, 2007; Gemmi *et al.*, 2008; Ventruti *et al.*, 2009; Gatta *et al.*, 2009); (3) spectroscopic determinations on both powder and single crystals, *e.g*. IR (Scordari *et al.*, 2006; Beran, 2002; Chon *et al.*, 2006; Ferrage *et al.*, 2006; Boukili *et al.*, 2003; Busigny *et al.*, 2004; Asimow *et al.*, 2006; Mookherjee *et al.*, 2002; Piccinini *et al.*, 2006a,b), Raman (Rinaudo *et al.*, 2004; Comodi *et al.*, 2006), Mössbauer (Rancourt *et al.*, 2001; Dyar, 2002; Evans *et al.*, 2005; Redhammer *et al.*, 2005; Dyar *et al.*, 2008; Mercier *et al.*, 2006; Zazzi *et al.*, 2006), XAFS (Mottana *et al.*, 2002b; Cibin *et al.*, 2005, 2006, 2008; Dyar *et al.*, 2002a,b), XPS (Schingaro *et al.*, 2005), and NMR (Fechtelkord *et al.*, 2003a,b; Lee & Stebbins, 2003).

The study of polytypism, twinning, microstructures, intergrowths of different stacking sequences and zonation was recently further developed both experimentally (Dobson *et al.*, 2007; Ferraris *et al.*, 2000, 2005; Giorgetti *et al.*, 2000; Di Vincenzo *et al.*, 2003; Kogure, 2002; Kogure *et al.*, 2005, 2006; Kogure & Kameda, 2008; Viti *et al.*, 2004; Sugimori *et al.*, 2008) and theoretically (Nespolo & Ďurovič, 2002; Nespolo *et al.*, 2004). Theoretical models allow the description of cation ordering from structure determinations and spectroscopic data (Brigatti *et al.*, 2003, 2005, 2008a,b), from Monte-Carlo simulation (Palin & Dove, 2004; Palin *et al.*, 2004) and from MEM approaches (Merli *et al.*, 2009). The literature cited reveals widespread attention to micas, and the abundance of recent and relevant results means that they cannot be summarized here. Aspects which may bring together some features of mica crystal chemistry with those of 2:1 layer clay minerals, will be detailed only instead.

2:1 clay minerals sometimes show an octahedral occupancy that appears to be intermediate between dioctahedral and trioctahedral species. This crystal-chemical feature may either be attributed to an interlayering of dioctahedral- and trioctahedral-like layers or to a cation-exchange mechanism involving a vacant octahedral cavity. Usually the latter is placed in the *trans*-site for micas, whereas it can be both in the *trans*- or in the *cis*-site for 2:1 illite, as suggested by Drits *et al.* (1984), who also predicted and outlined the powder XRD features of illites with *trans*-vacant and *cis*-vacant sites and structures where there is a statistical distribution of cations over all three sites (simulating a trioctahedral arrangement).

As mentioned, current experimental constraints prevent a final conclusion on most clay minerals, but in some cases for micas, a single-crystal structure solution is viable. The octahedral sheet of ideal muscovite consists of two Al-occupied octahedral *cis*-sites and one octahedral vacancy in the *trans*-site. Structural refinements on a great number of dioctahedral micas show a residual occupancy at the *trans*-site and Fe- or Mg-for-Al substitutions, connecting muscovite and celadonite end-members. Brigatti *et al.* (2005) demonstrated that the residual occupancy observed for the *trans*-octahedral site is related to octahedral Al substitution by assessing a direct relationship between the probability of finding a cation other than Al in octahedral coordination and the probability of finding a *trans*-octahedral site being occupied. This evidence seems to suggest that the residual occupancy at the *trans*-octahedral site should be interpreted as the substitution of a trioctahedral cell, mostly composed of divalent and monovalent

cations, for a dioctahedral cell, rather than simply as the substitution of a monovalent or divalent cation for a vacancy. In micas, however, this substitution mechanism does not appear to be complete.

In other words, all the dioctahedral micas refined so far show an octahedral Al content greater than 1.4 atoms per formula unit (a.p.f.u.) calculated on $O_{10}(OH)_2$. Moreover, the maximum Al content in trioctahedral micas is <1 a.p.f.u., to reach ~1.1 a.p.f.u. in Li-rich micas. Therefore a composition gap in the range 1.1–1.4 a.p.f.u. seems to persist.

This behaviour may be attributed to crystal-chemical features and in particular to the requirements deriving from the matching of octahedral to tetrahedral sheets.

A discriminating feature between micas and most 2:1 clays is related to interlayer occupancy. The interlayer site in micas is usually fully occupied either by monovalent cations (mostly K) in true micas, or by divalent cations in brittle micas. On the contrary, the interlayer of most clay minerals is not fully occupied and is sometimes hydrated. Mica from some metamorphic environments may constitute an exception, as both chemical analyses and structure refinements seem to suggest that the interlayer site is not fully occupied (interlayer occupancy ≤ 0.90 a.p.f.u.), consequently presenting low interlayer charge. This feature is consistent either with $^{[XII]}(K,Na)^{+}_{-1}$ $^{[XII]}(H_3O)^{+}$ substitution or with $^{[XII]}(K, Na)^{+}_{-1}$ $\square$ substitution. Reaching a final conclusion on this issue is **Q1** extremely challenging, mostly because of the limited number of crystal-structure refinements for micas from metamorphic environments. Metamorphic micas, for which structural refinements are available, show that when the value of the interlayer occupancy decreases, the size of the interlayer site increases. This result is consistent with interlayer vacancies or with the substitution mechanism $^{[XII]}(K, Na)^{+}_{-1}$ $^{[XII]}(H_3O)^{+}$, or both. Furthermore, the tetrahedral flattening angle, τ, increases with interlayer occupancy and, unlike most micas described in the literature, it decreases with increasing Si content (Brigatti *et al.*, 2008b). These data are consistent with a reduced interlayer charge, thus suggesting the existence of interlayer vacancies in metamorphic micas.

7.3. The smectite group

In the smectite-group minerals, isomorphic substitutions in either tetrahedral or octahedral sites induce a permanent negative layer charge (between −0.1 and −0.6 per half unit cell), which is compensated by the presence of hydrated cations in the interlayer.

The octahedral sheet in smectite group minerals may either be mainly occupied by trivalent cations (dioctahedral smectites) or divalent cations (trioctahedral smectites).

The general formula is:

$$\left(M^{+}_{(x+y+2z+3w)}, M^{2+}_{\frac{(x+y+2z+3w)}{2}}\right) \times n\mathrm{H_2O}(R^{3+}_{2-(y+z+w)}R^{2+}_{y}R^{+}_{z}V_{w})(\mathrm{Si}^{4+}_{4-x}R^{3+}_{x})\mathrm{O}_{10}(\mathrm{OH})_2$$

for dioctahedral smectites and:

$$\left(M^{+}_{(x-y+z-2\mathrm{w})}, M^{2+}_{\frac{(x-y+z-2w)}{2}}\right) \times n\mathrm{H_2O}(R^{2+}_{3-(y+z+w)}R^{3+}_{y}R^{+}_{z}V_{w})(\mathrm{Si}^{4+}_{4-x}R^{3+}_{x})\mathrm{O}_{10}(\mathrm{OH})_2$$

for trioctahedral species, where *x, y* and *z* indicate the layer charge resulting from substitutions in tetrahedral and octahedral sites, respectively; R^+, R^{2+}, and R^{3+} refer to a generic monovalent, divalent and trivalent octahedral cation; M^+ and M^{2+} refer to a generic monovalent and divalent interlayer cation; *V* indicates a vacancy.

A wide range of cations can occupy tetrahedral, octahedral and interlayer positions. Commonly Si^{4+}, Al^{3+} and Fe^{3+} are found in tetrahedral sites. Al^{3+}, Fe^{3+}, Fe^{2+}, Mg^{2+}, Ni^{2+}, Zn^{2+} and Li^+ generally occupy octahedral sites.

Most of the technological uses of smectite are related to reactions taking place in the interlayer space where cations such as Na^+, K^+, Ca^{2+} and Mg^{2+}, which balance the negative 2:1 layer charge, are commonly hydrated and exchangeable.

The ability of smectites to incorporate interlayer H_2O molecules and the subsequent change in basal spacing was studied extensively for several decades (MacEwan & Wilson, 1980; Sposito & Prost, 1982; Newman, 1987; McBride, 1989; Güven, 1992; Brown *et al.*, 1995; Moore & Reynolds, 1997; Laird, 2006; Ferrage *et al.*, 2005a,b, 2007, 2010 should be consulted for more details). The hydration properties of smectites are seen to be controlled by several factors, such as the type of interlayer cation and the amount and location of layer charge. Crystalline swelling is controlled by the balance between the repulsive forces, following from 2:1 layer interactions, and the attractive forces between hydrated interlayer cations and the negatively charged surface of Si–O layers (Norrish, 1954; van Olphen, 1965; Kittrick, 1969a,b; Laird, 1996, 1999, 2006).

The observation of (00*l*) basal reflections on XRD patterns demonstrated that 2:1 layer periodicity along $\mathbf{c}^*$ can swell from ~10.0 to 19.0 Å depending on the intercalation of layers of water molecules between individual 2:1 layers (*i.e.* in the interlayer positions). Pioneering XRD studies of smectite hydration analysed the position of (00*l*) basal reflections as a function of relative humidity, and revealed a stepwise expansion, where the different steps correspond to the intercalation of 0, 1, 2 or 3 planes of H_2O molecules in the interlayer (Moore & Reynolds, 1997). Different layer types were thus defined for smectite: dehydrated (d_{001}: 9.7–10.2 Å), monohydrated (d_{001}: 11.6–12.9 Å), bihydrated (d_{001}: 14.9–15.7 Å), and trihydrated (d_{001}: 18.0–19.0 Å). Structural heterogeneities in layer charge location and/or in its value most often lead to the coexistence of different domains within smectite crystals (Ferrage *et al.*, 2005a,b). These heterogeneities are revealed by comparing XRD patterns recorded on the same smectite sample under contrasting relative humidity conditions (Ferrage *et al.*, 2005a).

Laird (2006) suggested that the expandability of 2:1 phyllosilicates, saturated with alkali and alkaline earth cations in aqueous systems, is controlled by six different factors: (1) the crystalline swelling (deriving from the balance between electrostatic-attraction and hydration-repulsion forces); (2) the double-layer swelling (occurring when an electrostatic repulsion force develops between positively charged diffuse portions of double smectite layers overlapping in an aqueous suspension); (3) the formation and break-up of smectite layer-clusters; (4) cation demixing (depending by the nature of exchangeable cations); (5) the co-volume swelling (an entropy-driven process caused by restrictions on the rotational freedom of suspended smectite particles); and (6) Brownian swelling (resulting from random thermal motion of suspended smectite particles). The

crystalline swelling occurs within each smectite layer and depends strongly on smectite layer charge: double-layer swelling, co-volume swelling, or Brownian swelling occur between two different smectite particles and are less affected by smectite layer charge. However, because layer charge influences the size and stability of smectite particles, layer charge may show an indirect effect also on double-layer and co-volume swelling. In mixed cation-smectite systems, layer charge significantly affects cation exchange selectivity and thus the relative proportions and distributions of the various cations in the interlayer and in exchange sites on external crystal surfaces. Demixing of cations, where, for example, Na preferentially concentrates in certain interlayers, significantly impacts on break-up and formation of smectite particles and thus on swelling.

In monohydrated smectite, interlayer cations are considered to be located in the mid-plane of the interlayer, together with H_2O molecules for one layer. For bi-hydrated layers, interlayer cations are also commonly assumed to be located in the mid-plane of the interlayer. In addition, it is usually assumed that two planes of H_2O molecules, each bearing 0.69 H_2O per $O_{20}(OH)_4$, are located at 0.35 and 1.06 Å from the cation along the $\mathbf{c}^*$ axis, whereas a third plane (1.20 H_2O per $O_{20}(OH)_4$) is located further away from the central interlayer cation at 1.20 Å along the $\mathbf{c}^*$ axis (Moore & Reynolds, 1997). For bi-hydrated smectites, Ferrage *et al.* (2005a,b, 2010) proposed an alternative configuration for H_2O molecules in the interlayer, gaining a better fit with XRD spectrum in the high-angle region. This model considers a unique plane of H_2O molecules located, along the $\mathbf{c}^*$ axis, on either side of the central interlayer cation. The layer hydration depends heavily on layer charge: as layer charge increases, the number of interlayer cations, and thus the total hydration, increases. Structural variations related to the transition from different hydration states were addressed by Ferrage *et al.* (2007). They suggested that the transition from bi- to mono-hydrated layers produced the maximum structural heterogeneity, with strong interlayer thickness fluctuation (in individual layers), and the presence of several elementary mixed-layer structures. In contrast, the transition from mono-hydrated to dehydrated layers occurs homogeneously within layers. The decrease in thickness of the bi-hydrated layer with dehydration is thus controlled by a mechanism of two-dimensional diffusion of water molecules through the interlayer space. Variation in the thickness of mono-hydrated layers is produced by localized layer collapse, following the restoration of the interlayer cation hydration shell (Ferrage *et al.*, 2007).

Saponite, ideally $(M_x^+ \cdot nH_2O)Mg_3^{2+}(Si_{4-x}^{4+}Al_x^{3+})O_{10}(OH)_2$, is a trioctahedral smectite, where the layer charge derives mostly from Al-for-Si tetrahedral substitutions. Octahedral Fe^{3+}- and Fe^{2+}-for-Mg substitutions are also possible, and several saponite with different Mg/Fe_{total} ratios are described in literature (*e.g.* see Güven, 1988). The interlayer is usually occupied by Ca, Na and K; basal spacing in air-dried species can vary from 13.5 up to 16.8 Å, where the higher limit applies to glycolated samples. The first crystallographic and structural modelling investigations were by Suquet *et al.* (1975, 1977) on a monoclinic, *C*-centered, Na-saturated saponite with a tetrahedral charge of 0.46 and unit-cell parameters $a = 5.333$, $b = 9.233$, $c = 15.42$ Å, $\beta = 96.66^\circ$.

Nowadays, most of the applied and theoretical research on saponite refer to synthetic samples. In particular, due to the great potential applications of this mineral, much

research has focused on the hydration properties and interlayer organization of water and cations, to better understand the reactivity of smectites toward water in natural media. Several experimental and computational investigations (*e.g.* see Coombes *et al.*, 2003) were carried out to model the disorder of interlayer H_2O molecules. Ferrage *et al.* (2010) integrated the positional disorder to model the fine interlayer structure of saponite and its evolution until dehydration, using low- and high-charge synthetic Na-saturated saponites. Modelling was achieved by collecting XRD patterns along a water-vapour-desorption isotherm and fitting with two randomly interstratified mixed-layer structures down to $\sim 65\%$ relative humidity. The XRD profile modelling can detail aspects of the structural evolution of synthetic saponites upon dehydration. Profile modelling can only be achieved, however, by assuming positional disorder of water molecules around one or two positions for mono- or bihydrated layers, respectively. Furthermore, the modelling procedure allows the discrimination of different types of H_2O molecules (*i.e.* crystalline water and pore-space network) present in saponite.

Hectorite, ideally $(M_y^+ \cdot n H_2O)(Mg_{3-y}^{2+}Li_y)Si_4^{4+}O_{10}(OH)_2$, is characterized by Li^+-for-Mg^+ and F^- for $(OH)^-$ substitutions in the octahedral sheet. Basal spacing, measured on an oriented Na-saturated clay film, gives a periodicity of 12.4 Å (McAtee & Lamkin, 1978). Only a few structure refinements are reported in literature. Recently, Breu *et al.* (2003) identified a monoclinic cell (space group $C2/m$) with unit-cell parameters $a = 5.2401$, $b = 9.0942$, $c = 10.7971$ Å and $\beta = 99.21^\circ$, for a Cs-saturated sample with formula $Cs_{0.601}(Mg_{2.398}Li_{0.602})Si_4O_{10}F_2$. Seidl & Breu (2005) provided a single-crystal structure refinement of a synthetic Cs-saturated hectorite intercalated with tetramethylammonium (TMA), determining a monoclinic cell (space group $C2/m$) and unit-cell parameters: $a = 5.2735(11)$, $b = 9.1165(14)$, $c = 13.5609(35)$, and $\beta = 97.693(3)^\circ$. As in saponite, several investigations were focused on preparing and characterizing synthetic samples (*e.g.* see Sun *et al.*, 2008), and on modelling both water diffusion and stacking disorder in relation to the interlayer cation (Breu *et al.*, 2003; Malikova *et al.*, 2007). In particular, Malikova *et al.* (2007), by means of a quasi-elastic neutron scattering technique on a synthetic Na-hectorite, documented a water-diffusion coefficient of $\sim 1.5 \times 10^{-10}$ m^2 s^{-1} and 4.5×10^{-10} m^2 s^{-1} for the monohydrated and bihydrated states, respectively.

Sauconite, ideally $(M_x^+ \cdot n H_2O)Zn_3^{2+}(Si_{4-x}^{4+}Al_x^{3+})O_{10}(OH)_2$, is a Zn-bearing smectite with octahedral Zn cations ranging from 1.48 to 2.89 a.p.f.u. and with the total octahedral occupancy varying from 2.70 to 3.06 a.p.f.u., thus suggesting that layer charge is dependent on tetrahedral substitution (Güven, 1988). Interlayer cations are commonly Ca, Na and K. Ross (1946) reported a monoclinic cell (space group $C2/m$) and unit-cell parameters $a = 5.34$, $b = 9.32$, $c = 15.8$ Å, and $\beta = 95^\circ$ for sauconite. Another detailed investigation, also including several determinations at non-ambient temperature conditions is that by Faust (1951). Thermal analyses reported a marked exothermic effect at $\sim 810^\circ$C, closely related to the amount of Fe present in the mineral: the greater the Fe content, the lower the temperature of the exothermic reaction. This effect might be related to the formation of a Zn-spinel. Thermal analyses of saponite samples did not show any higher temperature exothermic reaction, which could be masked by a double endothermic reaction between 832 and 978°C (Faust, 1951).

Stevensite, ideally $(Na,Ca/2)_{0.3}Mg_3Si_4O_{10}(OH)_2$, is a trioctahedral smectite that derives its layer charge from both octahedral vacancies and Li-for-Mg substitution (Faust & Murata, 1953; Faust *et al.*, 1959; Ianovici *et al.*, 1990). It is a typical alteration product of sepiolite, and it is frequently observed to be interstratified with not-expanding talc-like minerals (*e.g.* see Martin de Vidales *et al.*, 1991).

Swinefordite, ideally $[(Ca,Na)_{0.3}(Li,Mg)_2(Si,Al)_4O_{10}(OH,F)_2{\cdot}nH_2O]$, is a Li-bearing smectite. Initially it was assumed to show intermediate dioctahedral features (Tien *et al.*, 1975). Further investigations, however, taking the CEC into account also, in order to calculate the chemical formula, demonstrated octahedral occupancy similar to that characteristic of trioctahedral smectites. Only a few data about this mineral have been reported in literature, and a review was provided by Güven (1988).

7.4. The vermiculite group

Vermiculite presents hydrated interlayer cations that compensate the negative layer charge in a range from 0.6 to 0.9 a.p.f.u., *i.e.* greater than observed in smectite.

Vermiculite is generally trioctahedral and the layer charge is usually related to Al-for-Si substitution in tetrahedral sites. The structure of natural vermiculite is known from the pioneering investigations of Gruner (1934b) who proposed, using powder XRD data, a monoclinic Cc or $C2/c$ cell. Later, this assumption was confirmed by Hendricks & Jefferson (1938), using single-crystal diffraction data. Water molecules and exchangeable cations were later demonstrated to occupy well defined sites within the interlayer space (Mathieson & Walker, 1954; Mathieson, 1958). Shirozu & Bailey (1966), after studying a 2-layer ordered vermiculite ($c = 28.89$ Å), suggested that the shift between successive 2:1 layers is always $-a/3$ along the x axis and alternates between $+b/3$ and $-b/3$ along the y axis. Vermiculites can present different layer-stacking sequences (de la Calle *et al.*, 1975a,b, 1978, 1985) depending on the nature of the interlayer cation and of the H_2O content. In fact the nature of the interlayer cation and the relative position of adjacent silicate layers influences the organization of the interlayer water molecules which generally show an ordered arrangement. Argüelles *et al.* (2010) obtained information on both the atomic positions and occupancies of exchangeable cations and water molecules in the interlayer space of vermiculite comparing experimental powder XRD patterns with those calculated by the program package *DIFFaX+*. Their results matched the conclusions of de la Calle *et al.* (1988) well and confirmed the suggestion that vermiculite is a semi-ordered crystalline material characterized by the existence of a large density of defects due to random $\pm b/3$ translations along the [010] direction.

The crystal structure of vermiculite modified after exchange with several different molecules has been investigated extensively. Some studies considered vermiculite intercalated with organic cations, such as tetramethylammonium, teramethylphosphonium (Vahedi-Faridi & Guggenheim, 1997, 1999) and polyvinyl acetate (Martynková *et al.*, 2007).

The arrangement and mobility of water molecules in one- and two-layer hydrates of vermiculite saturated with alkaline and alkali-earth cations was addressed by several

authors (*e.g.* see Slade *et al.*, 1985; de la Calle *et al.*, 1984; Beyer & Von Reichenbach, 2001; Sanz *et al.*, 2006). Sanz *et al.* (2006) indicated two different orientations for water molecules, depending on the hydration state and on the sites occupied by interlayer cations. In one-layer-hydrated Na-vermiculite, two water molecules, coordinated to Na ions, are symmetrically disposed with respect to the vermiculite layers and the **H**–**H** vectors of water molecules are parallel to the **c*** axis. In the case of one-layer hydrated Li- and Ba-vermiculites, water molecules, present at a rate of three or six per cation, respectively, are arranged in an asymmetric way, forming only one H bond with one of the adjacent layers. In this case, the angle between the **H**–**H** vector and the **c*** axis is close to 38°. Furthermore, as the amount of water increases, hydrogen bond interactions between water molecules increase at the expense of water-silicate interactions. This effect favours water mobility.

Some simulation studies were devoted to the characterization of treated and untreated vermiculite. Monte Carlo simulation was applied to verify the interlayer molecular water structure in monolayer hydrated Na-vermiculite by Skipper *et al.* (1995). They found that water molecules in the interlayer are affected significantly by the magnitude and distribution of layer charge. As layer charge increases, water molecules tend to increase their occupancy of the interlayer midplane, interacting with tetrahedral basal oxygen atoms and adopting an orientation with their dipole moment vectors parallel to the tetrahedral sheet surface. Tunega & Lishka (2003) employed density functional theory to study the effect of the Si/Al distribution in the tetrahedral sheets on the vermiculite layer. They concluded that the dominan factor affecting the layer stacking is the formation of very strong hydrogen bonds between water molecules coordinating the interlayer Mg^{2+} cations and the basal oxygen atoms of the 2:1 layers. Furthermore the most stable vermiculite layer is observed when only Si occupies tetrahedral sites. Arab *et al.* (2004), using molecular dynamics simulation techniques, suggested that in a water-free structure, the Zn^{2+} ions are adsorbed on the surface of the clay layers. On the contrary, when H_2O molecules are present in the interlayer space, $Zn(H_2O)_6^{2+}$ complexes are built, after migration of the ions to the midplane of the interlayer space. The complexes are oriented in the interlayer space so that at least four water molecules interact by their H atoms with the O atoms of the clay surfaces.

7.5. The chlorite group

Chlorites are 2:1 layer silicates characterized by an octahedral interlayer sheet. They are usually trioctahedral with Mg^{2+}, Al^{3+} and Fe^{2+}, Fe^{3+} in both octahedral sheets. More rarely octahedra are occupied by Cr^{3+}, Mn^{2+}, Ni^{2+}, V^{3+}, Cu^{2+}, Zn^{2+} and Li^{+}. Tetrahedral cations are Si^{4+} and Al^{3+}. Si^{4+} can occasionally be substituted by Fe^{3+}, Zn^{2+}, Be^{2+} or B^{3+} (Bailey, 1988a).

Several proposals for the classification of chlorites were suggested over the years, following advances related to the definition of their composition, structure and properties. However, the difficulty in designing a fully satisfactory classification system is related to the complexity of these minerals, to the complexity of their structure and to the many

and various solid solutions being documented. The AIPEA Nomenclature Committee (Bailey, 1980) proposed that the group of chlorites be divided into four distinct subgroups according to the octahedral occupancy of both octahedral sheets (*i.e.* the octahedral sheet of the 2:1 layer and the octahedral sheet in the interlayer): (1) trioctahedral chlorites, where both octahedral sheets are trioctahedral (*e.g.* clinochlore, chamosite, pennantite, nimite, baileychlore; (2) dioctahedral chlorites, where both octahedral sheets are dioctahedral (*e.g.* dombassite); (3) di,trioctahedral chlorites characterized by a dioctahedral 2:1 octahedral sheet and by a trioctahedral interlayer (*e.g.* cookeite, sudoite); (4) tri,dioctahedral, characterized by a trioctahedral 2:1 octahedral sheet and by a dioctahedral interlayer.

Bayliss (1975) introduced a nomenclature for trioctahedral chlorites based on five end-members and discrediting all other varieties: (1) clinochlore $Mg_5^{2+}Al^{3+}(Si_3^{4+}Al^{3+})O_{10}(OH)_8$; (2) chamosite $Fe_5^{2+}Al^{3+}(Si_3^{4+}Al^{3+})O_{10}(OH)_8$; (3) pennantite $Mn_5^{2+}Al^{3+}(Si_3^{4+}Al^{3+})O_{10}(OH)_8$; (4) nimite $Ni_5^{2+}Al^{3+}(Si_3^{4+}Al^{3+})O_{10}(OH)_8$; (5) baileychlore $Zn_5^{2+}Al^{3+}(Si_3^{4+}Al^{3+})O_{10}(OH)_8$.

More recently, classification schemes for chlorites were suggested by Wiewióra & Weiss (1990), using a unified system of composition projection, and by Zane & Weiss (1996), using electron microprobe data evaluation.

The chlorite-model structure consists of negatively charged 2:1 layers and positively charged interlayer sheets, connected by long hydrogen bonds. However, different 2:1 layer and O sheet sequences are ~14 Å thick and produce a large number of polytypes (Bailey, 1988a). These different sequences are generated by the displacement of two adjacent 2:1 layers either by $+a/3$ or by $-a/3$. Furthermore, the O sheet can be oriented in two different ways with respect to the 2:1 layer, thus being referred to as type I and type II: type I shows the octahedra in both the interlayer and the 2:1 layer oriented in the same way, whereas type II is characterized by an opposed octahedral orientation (Fig. 13, after Brown & Bailey, 1963). The interlayer sheet, in either type I or type II orientation, needs to match the 2:1 layer to form H-bonds between basal oxygen atoms and OH groups of the O interlayer. This requirement is satisfied by six different geometrical arrangements which can be divided in two sets (A and B). In set A, one of the three interlayer cations, if projected on the basal plane, overlaps with the H placed at the centre of the hexagonal ring. In set B, the interlayer sheet is displaced by $a/3$ and thus the projection of the octahedral cation on the basal plane matches the H position in the adjacent 2:1 layer in the tetrahedral sheet below. The triclinic IIb-4 polytype, with symmetry $C\bar{1}$, and the monoclinic IIb-2 polytype, with symmetry $C2/m$, are the most abundant regular stacking one-layer chlorites occurring in nature. Brown & Bailey (1963) suggested that the natural abundances of chlorite polytypes is related to two main structural controls: (1) cation-cation repulsive forces between the interlayer and the tetrahedral sheet, and (2) hydrogen-bonded configurations that lead to short hydrogen bonds. The dominance of the IIb polytype results from the absence of control and from the presence of a structurally favourable hydrogen-bonding configuration. Starting from different combinations of 14 Å units, Lister & Bailey (1967) and Drits & Karavan (1969) considered the geometric relationships between the layers for a regular 28 Å stacking.

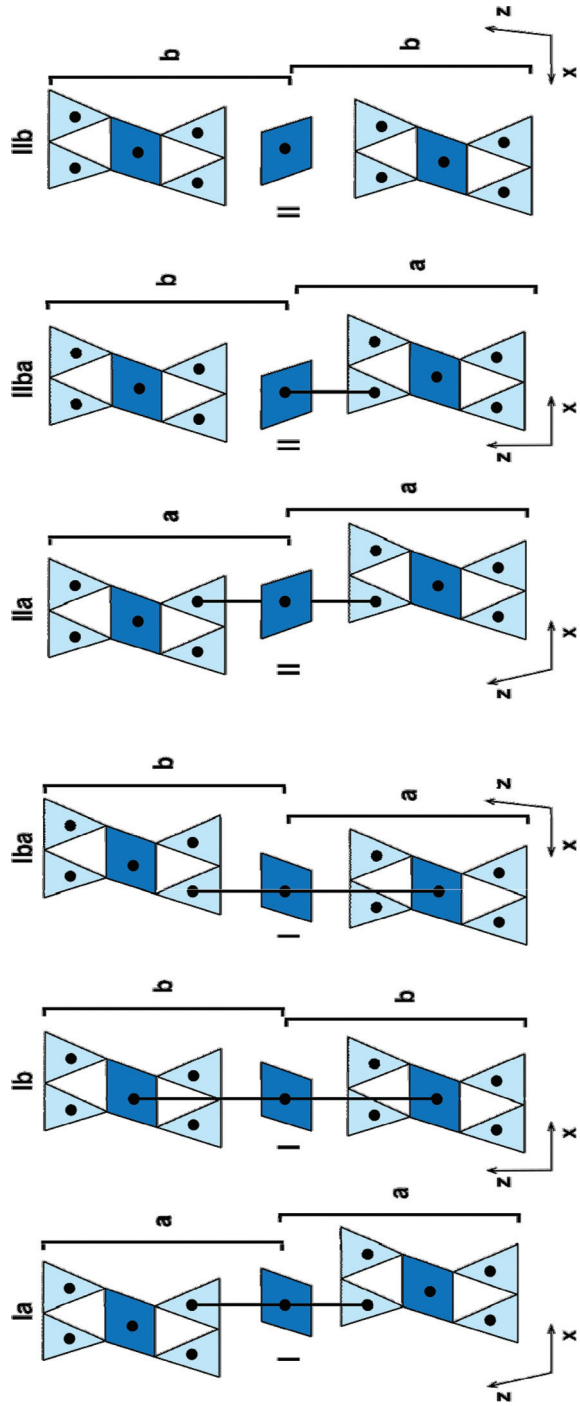

Fig. 13. Relationships between the 2:1 layer and the octahedral sheet in the I chlorite polytype (***a***) and in the II chlorite polytype (***b***).

7.5.1. Trioctahedral chlorites

The trioctahedral chlorite structure can be described as formed by 2:1 layers, negatively charged, with ideal composition $(R^{2+},R^{3+})_3(Si_{4-x}Al_x)O_{10}(OH)_2$, separated by an interlayer brucite-like octahedral sheet (O), positively charged, with composition $(R^{2+},R^{3+})_3(OH)_6$ (Bailey, 1988a). The interlayer sheet shows a positive charge, due to R^{3+}-for-R^{2+} substitution in order to balance the total negative charge of the 2:1 layer.

Large cations, such as Na^+, K^+ and Ca^{2+}, usually cannot be accommodated in the interlayer octahedral sheet. Ca^{2+} was indeed observed in franklinfurnaceite, a zinc-silicate intermediate between chlorite and mica (Peacor *et al.*, 1988) and Na^+ in glagolevite where Na atoms, sevenfold coordinated, are located between the 2:1 layers and the interlayer octahedral sheets (Krivovichev *et al.*, 2004). The main exchange vectors in trioctahedral chlorites are: (1) isovalent substitution (*e.g.* $^{[VI]}Fe^{2+}\ ^{[VI]}Mg^{2+}_{-1}$); (2) heterovalent substitutions, also known as Tschermak substitution (*e.g.* $^{[IV]}Si^{4+}_{-1}\ ^{[VI]}R^{2+}_{-1}\ ^{[IV]}Al^{3+}\ ^{[VI]}Al^{3+}$); (3) dioctahedral substitution $^{[VI]}(Mg^{2+}, Fe^{2+})_{-3}\ ^{[VI]}Al^{3+}_2\ ^{[VI]}(\square)$ leading to the generation of octahedral vacancies (Laird, 1988). Most of the structural data on trioctahedral chlorites refers to clinochlore. **Q1**

The triclinic structure (space group $C\bar{1}$, unit-cell parameters $a = 5.3301(4)$; $b = 9.2511(6)$; $c = 14.348(1)$ Å; $\alpha = 90.420(3)$; $\beta = 97.509(3)$; $\gamma = 89.996(4)^\circ$) was refined and described by several authors in IIb-4 polytype (Steinfink, 1958b; Phillips *et al.*, 1980; Zheng & Bailey, 1989; Joswig & Fuess, 1990; Nelson & Guggenheim, 1993; Smyth *et al.*, 1997; Joswig *et al.*, 1980; Zanazzi *et al.*, 2006; Valdré *et al.*, 2009). The monoclinic structure was described by Steinfink (1958a), Zheng & Bailey (1989), Rule & Bailey (1987), Joswig & Fuess (1989), and Zanazzi *et al.* (2007a) mostly in IIb-2 polytype (space group $C2/m$, $a = 5.327(2)$, $b = 9.227(2)$, $c = 14.327(5)$ Å, $\beta = 96.81(3)^\circ$).

For both polytypes, these studies generally suggested significant ordering in the interlayer octahedral sheet. The two octahedra in the interlayer differ considerably in terms of volume, distortion and mean cation–oxygen bond distance. Trivalent cations ($A1^{3+}$, Cr^{3+} and Fe^{3+}) concentrate in one of the two independent octahedral sites in the interlayer (usually called M4) creating a net positive charge to balance the net negative charge on the 2:1 layer. Bish & Giese (1981), starting from energy considerations, showed that the ordering of trivalent cations in the M4 site significantly increases the energy of the interlayer bonding and consequently the stability of the structure. A disordered Si/Al distribution was suggested for IIb-4 polytype following single crystal structure refinements (Rule & Bailey, 1987). However, Welch *et al.* (1995) on the basis of MAS-NMR spectroscopy results, indicated the existence of considerable short-range order.

Joswig *et al.* (1980) suggested that **O–H** vectors of the interlayer OH in IIb-4 polytype are tilted slightly away from the vertical towards their basal oxygen acceptors to form bent hydrogen bonds. The O–OH distances range from 2.87 to 2.91 Å. In the monoclinic polytype IIb-2, the two OH dipoles are roughly perpendicular to the interlayer sheet, forming weak to medium hydrogen bonds with O...O distances of 2.859 and 2.881 Å. The OH-dipole of the 2:1 layer is perpendicular to the (001) plane (Joswig & Fuess, 1989; Welch & Marshall, 2001; Welch *et al.*, 1995).

Valdré *et al.* (2009) studied the relationships between clinochlore cleavage characteristics, in terms of nano-morphology, and surface potential, as a function of average crystal chemistry and topology. In IIb-4 clinochlore, octahedral sites of the silicate layer are equal and equally occupied by Mg, whereas the octahedral sites in the interlayer show different sizes and are mostly completely occupied by divalent (Mg^{2+} and Fe^{2+}) or trivalent (Al^{3+}) cations. The clinochlore cleaved surface is present in two forms: (1) the stripe type, which is characterized by bands along the [100] crystal direction (4.0 Å in height, up to several μm long and ranging from a few nm to a few μm wide); (2) the triangular type (4.0 Å in height), which is characterized by triangular areas where the surface shows missing interlayer regions, with average lateral sizes ranging from a few to more than hundreds of nanometers. Both features may result either from interlayer sheets, where cleavage directions are induced by different octahedral site occupancy in the interlayer, or by weak interlayer bonding along specific directions of the connected 2:1 layer. The cleaved surface, particularly at the cleaved edges, presents high DNA affinity, which is directly related to an average positive surface and ledge potential.

Structural results on chlorites, other than clinochlore, are limited in number and could provide only a partial description. Some interesting results were presented by Rule & Radke (1988) and Walker & Bish (1992).

7.5.2. Di,trioctahedral and dioctahedral chlorites

The known di,trioctahedral chlorites are cookeite and sudoite. They present a dioctahedral 2:1 layer and a trioctahedral interlayer. *Dombassite* is a dioctahedral chlorite and presents 2:1 layer and interlayer both dioctahedral.

Cookeite, ideal composition $LiAl_4(Si_3Al)O_{10}(OH)_8$, is a di,trioctahedral chlorite in which the 2:1 layer is dioctahedral and the hydroxide interlayer is trioctahedral. Cookeite differs from other Al-, Li-rich chlorite species (*i.e.* sudoite and dombassite) due to the greater Li content (~3–4 wt.% Li_2O). Although several cookeite polytypes were reported (*i.e.* Vrublevskaja *et al.*, 1975), the structure of this mineral was detailed by Zheng & Bailey (1997) only in space group *Cc* (two-layer 'r' structure of *Iaa* polytype, $a = 5.158(1)$, $b = 8.940(2)$, $c = 28.498(6)$ Å, $\beta = 96.60(3)^\circ$). Mean T–O bond lengths indicate a partly ordered but asymmetric distribution of tetrahedral Si and Al. The two tetrahedral sheets within the 2:1 layer show different compositions and charges. The Al-rich, higher-charge tetrahedral sheet is thicker and more closely approaches the interlayer sheet than the Si-rich, lower-charged sheet. Two Al cations occupy the *cis*-octahedra in the dioctahedral 2:1 layer. Mean bond lengths in the trioctahedral interlayer sheet indicate a partly ordered distribution of octahedral Al and Li. The Li-rich, lower-charge octahedron in the interlayer is located on a vertical straight line between an Al-rich tetrahedron and a Si-rich tetrahedron. The two higher-charge interlayer Al cations are located vertically between a Si-rich tetrahedron and the centre of a six-membered ring. This pattern of ordering minimizes the cation-cation repulsion and provides the best local charge balance. The protons of the six surface OH groups tilt away from the two Al-rich interlayer sites toward the lower-charge Li site. Recently borocookeite was reported, where $^{[IV]}$Al is replaced by B (Zagorsky *et al.*, 2003).

Sudoite is a di,trioctahedral Mg-rich chlorite with ideal composition: $(Al_3Mg_2)(Si_3Al)O_{10}(OH)_8$. Natural sudoite samples are usually poorly crystalline and fine-grained, thus rendering a complete understanding of the structure of this mineral extremely complex. Eggleston & Bailey (1967) partially refined the structure of sudoite (space group $C2/m$, $a = 5.237$, $b = 9.070$, $c = 14.285$ Å, $\beta = 97.03°$) and confirmed that the mineral is composed of dioctahedral 2:1 layers separated by interlayer trioctahedral sheets with a IIb-4 stacking sequence. High-resolution TEM observations indicate that the stacking sequence is characterized by a largely uniform intralayer shift of $a/3$ in the $-\mathbf{X_1}$ direction ($\mathbf{X_i}$ represent the directions along the pseudohexagonal axes) and by an interlayer displacement of similar magnitude in either the $-\mathbf{X_2}$ or $-\mathbf{X_3}$ direction. Stacking disorder is primarily caused by the mixing of interlayer displacements in the two directions (Kameda *et al.*, 2007).

7.6. Some 2:1 layer silicates involving a discontinuous octahedral sheet and a modulated tetrahedral sheet

Structure determinations of modulated 2:1 layer silicates are limited due to a lack of suitable crystals for single-crystal XRD. As a result, numerous models were produced regarding cell dimensions and indexing of powder patterns (Christ *et al.*, 1969; Jones and Galán, 1988) and polymorphs and structure models (Bradley, 1940; Preisinger, 1963; Gard & Follet, 1968; Drits and Sokolova, 1971; Chisholm, 1992).

Sepiolite (Fig. 2b). The first structural pattern for sepiolite was introduced by Nagy & Bradley (1955), who suggested the $C2/m$ ($A2/m$) space groups as being the most appropriate. Later, Brauner & Preisinger (1956) and Preisinger (1959) proposed another structural model for sepiolite under space group *Pnan*. The difference between monoclinic and orthorhombic models is generated by the tetrahedral inversion at the edge of the ribbons, either occurring along the middle of the zigzag Si-O-Si chains (Nagy & Bradley, 1955) or along their edges (Brauner & Preisinger, 1956). In the Brauner & Preisinger (1956) model, adjacent inverted ribbons are joined by a single basal oxygen (instead of two as in the Nagy-Bradley model), and there are eight octahedral sites in a ribbon (instead of nine), four OH (instead of six), and eight water molecules (instead of six). The model of Brauner & Preisinger (1956) contains three hydrous species: (1) OH anions; (2) structural H_2O at the edges of the octahedral strips; (3) three zeolitic H_2O positions inside the channels. Electron density patterns from single sepiolite fibres obtained by Brindley (1959), Zvyagin (1967) and Gard & Follet (1968) confirmed that the systematic absences are in agreement with the space group *Pnan*. The Brauner-Preisinger model for sepiolite was also confirmed and refined by Rautureau *et al.* (1972), Rautureau & Tchoubar (1974), Yucel *et al.* (1981) and Post *et al.* (2007). Post *et al.* (2007), based on the results obtained from a Rietveld refinement, using synchrotron powder XRD data, confirmed the general structural model determined by Brauner & Preisinger (1956), suggested an additional zeolitic H_2O site inside the channels and demonstrated that two zeolitic H_2O sites are fully occupied, one half occupied and the last only one-third occupied. Sepiolite unit-cell parameters are $a = 5.2750(1)$, $b = 27.016(1)$, and $c = 13.405(1)$ Å (space group *Pnan*; Post *et al.*, 2007).

Palygorskite (Fig. 2b). Bradley (1940) suggested a model for palygorskite structure with a probable $A2/m$ space group, differing from the sepiolite model, because of a shorter b dimension following from the presence of only two tetrahedral ribbons. Like sepiolite, the palygorskite structural model (Bradley, 1940) includes three types of H_2O molecules: (1) (OH) groups bonded to some of the Mg and Al atoms; (2) H_2O molecules that complete the coordination of the Mg atoms at the edges of the octahedral strips; and (3) zeolitic H_2O molecules in the tunnels. Drits & Sokolova (1971) confirmed the Bradley model and measured a β angle of 107°. Preisinger (1963) reported an orthorhombic model for palygorskite, similarly to that previously discussed for sepiolite, except for the ribbon width. Christ *et al.* (1969) analysed powder XRD data for five palygorskite samples and concluded that palygorskite exists in structurally related orthorhombic and monoclinic forms. Chisholm (1992) compared observed and theoretical XRD powder patterns and noted that most palygorskite samples are mixtures of monoclinic and orthorhombic polymorphs. Recently, Rietveld refinements, using powder X-ray and neutron diffraction data, confirmed the basic monoclinic and orthorhombic palygorskite structure models (Artioli *et al.*, 1994; Giustetto & Chiari, 2004). Post & Heaney (2008) refined the structure of pure monoclinic palygorskite samples by Rietveld refinements on synchrotron powder XRD data. Palygorskite unit-cell parameters (monoclinic $A2/m$ space group) are $a = 5.2419(2)$, $b = 17.8476(7)$, $c = 13.2858(8)$ Å, $\beta = 107.560(5)°$ (Post & Heaney, 2008).

Galán & Carretero (1999) reviewed chemical analyses from the literature and concluded that: (1) sepiolite is a true trioctahedral mineral with eight octahedral positions filled with Mg^{2+}, and showing a formula close to $Mg_8Si_{12}O_{30}(OH)_4(OH_2)_4(H_2O)_8$; (2) palygorskite is an intermediate dioctahedral- trioctahedral mineral, showing a formula close to $(Mg_2R^{3+}_2\square_1)(Si_{8-x}Al_x)O_{20}(OH)_2{\cdot}R^{2+}_{x/2}{\cdot}(H_2O)_4$, where □ stands for vacancy, R stands primarily for Al^{3+}, Fe^{3+}, Fe^{2+} and Mn^{2+} and x ranges from 0 to 0.5. Furthermore, Post & Heaney (2008) discovered Al and Mg octahedral ordering, with Mg cations placed in octahedral sites at the edge of the channels, for monoclinic palygorskite. Q1

Sepiolite and palygorskite are commonly used in technical and mostly in sorption applications (Alvarez, 1984; Galán, 1996). The sorption capacity is controlled primarily by the fibrous mineral surface and by zeolite-like channels. Mineral-fibre surfaces include silanol groups, surface oxygen atoms and structural H_2O along with octahedral broken bonds. The zeolite-like channels allow the exchange of metal cations. Krekeler & Guggenheim (2008) observed that the different adsorption behaviour of several sepiolite and palygorskite samples can be also associated with defects, which alternatively enhance or reduce the sorption ability. A fascinating use of palygorskite is related to the manufacturing of a dye, Maya blue, long used by the ancient Maya people. The crystal structure of Maya Blue was investigated by Chiari *et al.* (2003) using the Rietveld method and synchrotron powder XRD data. Q2

Kalifersite, with ideal composition $(K,Na)_5(Fe^{3+})_7[Si_{20}O_{50}](OH)_6{\cdot}12H_2O$ (space group $P\bar{1}$, $a = 14.86$, $b = 20.54$, $c = 5.29$ Å, $\alpha = 95.6$, $\beta = 92.3$, $\gamma = 94.4°$), was described by Ferraris *et al.* (1998) after noting a modular relationship between this mineral, sepiolite and palygorskite. Kalifersite shows an alternation of one module of Q3

sepiolite (S) and palygorskite (P) along [010]. This mineral can thus be considered as the S_1P_1 term of the palysepiole polysomatic series (P_pS_S).

Tuperssuatsiaite shows a diffraction pattern similar to that of palygorskite, thus suggesting a similar crystal structure (Camara *et al.*, 2002). Tuperssuatsiaite is monoclinic, space group $C2/m$, with $a = 14.034(7)$, $b = 17.841(7)$, $c = 5.265(2)$ Å, and $\beta = 103.67(4)^\circ$. The chemical composition is $Na_{1.87}Fe_{2.14}Mn_{0.48}Ti_{0.14}Al_{0.03}Mg_{0.02}[Si_8O_{20}](OH)_2{\cdot}n(H2O)$. Like palygorskite, the tuperssuatsiaite structure consists of an octahedral sheet sandwiched between two opposing tetrahedral sheets. The octahedral sheet forms strips which are three octahedra wide and defines channels which could be occupied by H_2O. This mineral is also characterized by Na in octahedral coordination and by notable Fe^{2+} content.

8. Imogolite and allophane

Imogolite (Cradwick *et al.*, 1972) and allophane (Wada, 1967) are both nano-sized aluminosilicate minerals with a predominantly hollow structure and different Si/Al ratio. Imogolite consists of single-walled nanotubes (Fig. 3), unlike allophane, which presents a hollow spherical morphology.

Natural imogolite, mostly observed in soils originating from volcanic ashes and weathered pumice sand spodosols, is characterized by the ideal chemical formula $(OH)_3Al_2O_3SiOH$, thus meaning a Si/Al ratio of 0.5. Imogolite is commonly characterized by poor crystallinity, with short range order structures defined by hollow tubes of curved gibbsite sheets with SiO_4 tetrahedra replacing OH groups at the inner surface.

A first approach to imogolite synthesis was defined by Farmer & Fraser (1979) starting from diluted solutions of $Al(ClO_4)_3$ and silanol $(Si)(OH)_4$. Other methods include the hydrolysis of fused sodium silicates, leading to the initial formation of amorphous protoimogolite or allophane and then followed by a subsequent growth of crystalline imogolite tubes. Other methods for imogolite synthesis include tetraethoxysilane hydrolysis and hydrolysis of commercial sodium silicate.

The imogolite tube shows an inner diameter of 0.5–0.9 nm, as measured by nitrogen adsorption or by transmission electron microscopy (TEM), and an outer diameter of 2.0–2.5 nm. Tube length ranges from several hundreds of nm to 1 μm.

Solid state NMR, powder XRD and TEM allowed the definition of a structural imogolite atomic model, *i.e.* the wall of the tube consists of a single curved sheet of gibbsite, wherein the OH on one face are replaced by orthosilicate groups, with Al only occurring in octahedral coordination and Si in tetrahedral coordination. Electron diffraction measurements performed by Cradwick *et al.* (1972) suggested that the most likely structure model of natural imogolite contains ten gibbsite units (Nu) around the circumference, corresponding to a tubular diameter of 21 $\pm$ 5 Å. On the other hand, Farmer & Fraser (1979) concluded that natural imogolite consists of 12 units. Si can be partly or completely substituted by Ge. The synthesized Ge-rich products are similar to natural imogolite in their tubular morphology. However the external diameter of the tube increases with increasing Ge substitution up to ~33 Å. This evidence suggests

that Ge-for-Si substitution causes a decrease in the curvature of the gibbsite-like sheet bonding to Si or Ge polyhedra. The number of gibbsite unit cells forming the circumference of the tube is 10–12 in natural imogolite and 18 in the Ge-substituted phase (Wada & Wada, 1982). The repeat distance along the tube axis is ~8.4 Å in both Si-rich and Ge-rich imogolite. Theoretical studies (Alvarez-Ramirez, 2009) involving imogolite-like single wall nanotubes confirmed that, by increasing the Ge/(Si + Ge) ratio, the gibbsite-like units increase from 9 to 13. Maillet *et al.* (2010) suggested that the structure of Ge-substituted imogolite is a double-walled nanotube which consist of two concentric tubes of equal length and identical wall structure.

Allophane is a weathering or hydrothermal alteration product of feldspars and other primary minerals. Its ideal chemical formula is $Al_2O_3{\cdot}(SiO_2)_{1.3\text{-}2}{\cdot}2.5-3(H_2O)$. The first model describing the structural arrangement of allophane was proposed by Wada (1967). This model describes the mineral structure as consisting of a silica tetrahedral chain sharing corners with one or two chains of AlO_6 octahedra, thus giving rise to allophane with the Si/Al ratios of 1 and 0.5, respectively. Models based on kaolinite structure were introduced later (Milestone, 1971; Henmi & Wada, 1976; Okada & Ossaka, 1983; Van der Gaast *et al.*, 1985). Okada *et al.* (1975) proposed a scheme based on a two-dimensional kaolin-like structure with Si atoms in the tetrahedral sheet partially substituted by Al. The kaolin-based model was further supported by Wada *et al.* (1979), who described the synthesis process of allophane. Starting from electronic microscopy data, Kitagawa (1971) and Henmi & Wada (1976) suggested that an individual allophane is a sphere- or polyhedron-like hollow particle with external diameter ranging from 35 to 50 Å. These authors also suggested that the particles may show openings to admit water or other guest species inside the structure. Further experimental measurements, detailing the density of allophane, confirmed their hypothesis, and suggested a wall thickness ranging from 7 to 10 Å (Wada & Wada, 1977; Wada, 1995). Another model for allophane structure was proposed by Parfitt & Henmi (1980). The strong similarity between allophane and imogolite, as suggested by IR spectra, led the authors to conclude that allophane consists of imogolite structural units. Parfitt *et al.* (1980) documented a 'protoimogolite' allophane sphere with diameter of 40 Å. This latter is made up of 125 unit cells of imogolite and should present at least six openings with ~4 Å diameter. In the following paper, Parfitt *et al.* (1980) discriminated two types of allophane. The first type is characterized by Si/Al ratios of ~0.5 and is built from imogolite units. The second type of allophane shows a Si/Al ratio close to 1, contains condensed silicate units, and presents a halloysite-like structure. The two structural models of allophane were further examined in a number of studies, some of which proposed a model combining kaolin-like and imogolite-like units (Mackenzie *et al.*, 1991). This latter model was supported by the ESCA data from He *et al.* (1995).

Acknowledgements

The authors acknowledge the Italian Ministry for Education and Research for PRIN 2008 ('*Phyllosilicates of particular petrologic relevance: chemical and physical features, and their variation in different environments either natural or simulated*') and

Fondazione Cassa di Risparmio di Modena for the International grant '*The relationships of bulk structure, surface structure, chemistry and physical properties of mineral phases with six-membered silicate rings*'. A grant-in-aid by LLP-ERASMUS (2010-1-IT2-ERA-10-16274) made the organization of the school possible at which this short presentation was used as didactic support. Stephen Guggenheim kindly reviewed the chapter and suggested helpful improvements.

References

Abraham, K., Schreyer, W., Medenbach, O. & Gebert, W. (1980) Kulkeit, ein geordnetes l:1 Mixed-Layer-Mineral zwischen Klinochlor und Talk. In: *Fortschritte der Mineralogie*, *Beiheft 1*, *Abstracts*, **5E**, 4–5.

Adams, J.M. (1983) Hydrogen atom positions in kaolinite by neutron profile refinement. *Clays and Clay Minerals*, **31**, 352–356.

Adams, J.M. & Hewat, A.W. (1981) Hydrogen atom positions in dickite. *Clays and Clay Minerals*, **29**, 316–319.

Akiba, E., Hayakawa, H., Hayashi, S., Miyawaki, R., Tomura, S., Shibasaki, Y., Izumi, F., Asano, H. & Kamiyama, T. (1997) Structure refinement of synthetic deuterated kaolinite by Rietveld analysis using time-of-flight neutron powder diffraction data. *Clays and Clay Minerals*, **45**, 781–788.

Altaner, S.P. & Ylagan, R.F. (1997) Comparison of structural models of mixed-layer illite/smectite and reaction mechanisms of smectite illitization. *Clays and Clay Minerals*, **45**, 517–533.

Alvarez, A. (1984) Sepiolite: properties and uses. In: *Palygorskite–Sepiolite: Occurrences, Genesis, and Uses* (A. Singer & E. Galán, editors). Elsevier, New York, pp. 253–287.

Alvarez-Ramirez, F. (2009) Theoretical study of $(OH)_3N_2O_3MOH$, M = C, Si, Ge, Sn and N = Al, Ga, In, with imogolite-like structure. *Journal of Computational and Theoretical Nanoscience*, **6**, 1120–1124.

Anderson, C.S. & Bailey, S.W. (1981) A new cation ordering pattern in amesite-$2H_2$. *American Mineralogist*, **66**, 185–195.

Andreani, M., Grauby, O., Baronnet, A. & Munoz, M. (2008) Occurrence, composition, and growth of polyhedral serpentine. *European Journal of Mineralogy*, **20**, 159–171.

Aparicio, P. & Galán, E. (1999) Mineralogical interference on kaolinite crystallinity index measurements. *Clays and Clay Minerals*, **47**, 12–27.

Aparicio, P., Ferrell, R.E. & Galán, E. (1999) A new kaolinite crystallinity index from mathematical modelling of XRD data. In *Abstracts volume of the 9th EUROCLAY Conference, Kraków, Poland*, 57. **Q4**

Aparicio, P., Galán, E. & Ferrell, R.E. (2006) A new kaolinite order index based on XRD profile fitting. *Clay Minerals*, **41**, 811–817.

Appelo, C.A.J. (1978) Layer deformation and crystal energy of micas and related minerals. I. Structural models for 1*M* and $2M_1$ polytypes. *American Mineralogist*, **63**, 782–792.

Arab, M., Bougeard, D. & Smirnov, K.S. (2004) Structure and dynamics of interlayer species in a hydrated Zn-vermiculite. A molecular dynamics study. *Physical Chemistry Chemical Physics*, **6**, 2446–2453.

Argüelles, A., Leoni, M., Blanco, J.A. & Marcos, C. (2010) Semi-ordered crystalline structure of the Santa Olalla vermiculite inferred from X-ray powder diffraction. *American Mineralogist*, **95**, 126–134.

Árkai, P. (1991) Chlorite crystallinity: an empirical approach and correlation with illite crystallinity, coal rank and mineral facies as exemplified by Palaeozoic and Mesozoic rocks of northeast Hungary. *Journal of Metamorphic Geology*, **9**, 723–734.

Árkai, P. & Tóth, N.M. (1983) Illite crystallinity: combined effects of domain size and lattice distortion. *Acta Geologica Hungarica*, **26**, 341–358.

Árkai, P., Sassi, F.P. & Sassi, R. (1995) Simultaneous measurements of chlorite and illite crystallinity: a more reliable tool for monitoring low- to very low-grade metamorphisms in metapelites. A case study from the Southern Alps (NE Italy). *European Journal of Mineralogy*, **7**, 1115–1128.

Árkai, P., Merriman, R.J., Roberts, B., Peacor, D.R. & Tóth, M. (1996) Crystallinity, crystallite size and lattice strain of illite-muscovite and chlorite: comparison of XRD and TEM data for diagenetic and epizonal pelites. *European Journal of Mineralogy*, **8**, 1119–1137.

Artioli, G., Galli, E., Burattini, E., Cappuccio, G. & Simeoni, S. (1994) Palygorskite from Bolca, Italy: A characterization by high-resolution synchrotron radiation powder diffraction and computer modeling. *Neues Jahrbüch für Mineralogie Monatshefte*, **1994**, 271–229.

Aruja, E. (1945) An X-ray study of the crystal structure of antigorite. *Mineralogical Magazine*, **27**, 65–74.

Asimow, P.D., Stein, L.C., Mosenfelder, J.L. & Rossman, G.R. (2006) Quantitative polarized infrared analysis of trace OH in populations of randomly oriented mineral grains. *American Mineralogist*, **91**, 278–284.

Auzende, A.L., Pellenq, R.J.-M., Devouard, B., Baronnet, A. & Grauby, O. (2006) Atomistic calculations of structural and elastic properties of serpentine minerals: the case of lizardite. *Physics and Chemistry of Minerals*, **33**, 266–275.

Bailey, S.W. (1963) Polymorphism of the kaolin minerals. *American Mineralogist*, **48**, 1196–1209.

Bailey, S.W. (1969) Polytypism of trioctahedral 1:1 layer silicates. *Clays and Clay Minerals*, **17**, 355–371.

Bailey, S.W. (1980) Summary of recommendations of AIPEA nomenclature committee on clay minerals. *American Mineralogist*, **65**, 1–7.

Bailey, S.W. (1981) A system of nomenclature for regular interstratifications. *The Canadian Mineralogist*, **19**, 651–655 (reprinted in: Bailey *et al.* (1982) Report of the Clay Minerals Society Nomenclature Committee for 1980–1981: Nomenclature for regular interstratifications. *Clays and Clay Minerals*, **30**, 76–78; and in: Bailey *et al.* (1982) Report of the AIPEA Nomenclature Committee. AIPEA Newsletter No. 18, Supplement of February, 1982).

Bailey, S.W. (1988a) Structure and composition of other trioctahedral 1:1 phyllosilicates. In: *Hydrous Phyllosilicates (Exclusive of Micas)* (S.W. Bailey, editor). Reviews in Mineralogy, **19**, 169–186. Mineralogical Society of America, Washington, D.C.

Bailey, S.W. (1988b) Odinite, a new dioctahedral-trioctahedral Fe^{3+}-rich 1:1 clay mineral. *Clay Minerals*, **23**, 237–247.

Bailey, S.W. (1989a) Report of the AIPEA Nomenclature Committee. *AIPEA Newsletter*, **26**, 17–18.

Bailey, SW. (1989b) Halloysite–A critical assessment. In: *Proceedings of 9th International Clay Conference, Strasbourg, France* (V.C. Farmer & Y. Tardy, editors). Sciences Géologiques Mémoire, **86**, 89–98.

Bailey, S.W., Banfield, J.F., Barker, W.W. & Katchan, G. (1995) Dozyite, a 1:1 regular interstratification of serpentine and chlorite. *American Mineralogist*, **80**, 65–77.

Bain, D.C. & Smith, B.L.F. (1987) Chemical analysis. In: *A Handbook of Determinative Methods in Clay Mineralogy* (M.J. Wilson, editor), 248–274. Blackie, Glasgow, London.

Balan, E., Allard, T., Boizot, B., Morin, G. & Muller, J.-P. (1999) Structural Fe^{3+} in natural kaolinites: new insights from electron paramagnetic resonance spectra fitting at X and Q-band frequencies. *Clays and Clay Minerals*, **47**, 605–616.

Balan, E., Saitta, A.M., Mauri, F. & Calas, G. (2001) First-principles modeling of the infrared spectrum of kaolinite. *American Mineralogist*, **86**, 1321–1330.

Balan, E., Lazzeri, M., Saitta, A.M., Allard, T., Fuchs, Y. & Mauri, F. (2005) First-principles study of OH-stretching modes in kaolinite, dickite, and nacrite. *American Mineralogist*, **90**, 50–60.

Balan, E., Delattre, S., Guillaumet, M. & Salje, E.K.H. (2010) Low-temperature infrared spectroscopic study of OH-stretching modes in kaolinite and dickite. *American Mineralogist*, **95**, 1257–1266.

Balek, V. & Murat, M. (1996) The emanation thermal analysis of kaolinite clay minerals. *Thermochimica Acta*, **282/283**, 385–397.

Banfield, J.F. & Bailey, S.W. (1996) Formation of regularly interstratified serpentine-chlorite minerals by inversion in long-period serpentine polytypes. *American Mineralogist*, **81**, 79–91.

Baronnet, A. (1978) Some aspects of polytypism in crystals. *Progress in Crystal Growth Characterization*, **1**, 151–211.

Baronnet, A. (1992) Polytypism and stacking disorder. In: *Minerals and Reactions at the Atomic Scale: Transmission Electron Microscopy* (P.R. Buseck, editor). Reviews in Mineralogy, **27**, 231–282. Mineralogical Society of America, Washington, D.C.

Baronnet, A. & Devouard, B. (2005) Microstructures of common polygonal serpentines from axial HRTEM imaging, electron diffraction, and lattice-simulation data. *The Canadian Mineralogist*, **43**, 513–542.

Baronnet, A., Mellini, M. & Devouard, B. (1994) Sectors of polygonal serpentine. A model based on dislocations. *Physics and Chemistry of Minerals*, **21**, 330–343.

Baronnet, A., Andreani, M., Grauby, O., Devouard, B., Nitsche, S. & Chaudanson, D. (2007) Onion morphology and microstructure of polyhedral serpentine. *American Mineralogist*, **92**, 687–690.

Bates, T.F, Hildebrand, F.A. & Swineford, A. (1950) Morphology and structure of endellite and halloysite. *American Mineralogist*, **35**, 463–484.

Bayliss, P. (1975) Nomenclature of the trioctahedral chlorites. *The Canadian Mineralogist*, **13**, 178–180.

Belluso, E. & Ferraris, G. (1991) New data on balangeroite and carlosturanite from alpine serpentinites. *European Journal of Mineralogy*, **3**, 559–566.

Ben Haj Amara, A., Ben Brahim, J., Plançon, A., Ben Rhaiem, H. & Besson, G. (1997) Etude structurale d'une nacrite Tunisienne. *Journal of Applied Crystallography*, **30**, 338–344.

Ben Haj Amara, A., Ben Brahim, J., Plançon, A. & Ben Rhaiem, H. (1998) The structure of 8.4 Å hydrated and dehydrated nacrite determined by X-ray diffraction. *Journal of Applied Crystallography*, **31**, 654–662.

Benco, L. (1997) Electron densities in hydrogen bonds: Lizardite-1*T*. *European Journal of Mineralogy*, **9**, 811–819.

Benco, L. & Smrčok, L. (1998) Hartree–Fock study of pressure-induced strengthening of hydrogen bonding in lizardite-1*T*. *European Journal of Mineralogy*, **10**, 483–490.

Benco, L., Tunega, D., Hafner, J. & Lischka, H. (2001a) Orientation of OH groups in kaolinite and dickite: *ab initio* molecular dynamics study. *American Mineralogist*, **86**, 1057–1065.

Benco, L., Tunega, D., Hafner, J. & Lischka, H. (2001b) Upper limit of the O–H–O hydrogen bond. *Ab initio* study of the kaolinite structure. *Journal of Physical Chemistry*, **B105**, 10812–10817.

Beran, A. (2002) Infrared Spectroscopy of Micas. In: *Micas: crystal chemistry and metamorphic petrology* (A. Mottana, F.P. Sassi, J.B. Thompson Jr. & S. Guggenheim, editors). Reviews in Mineralogy and Geochemistry, **46**. Mineralogical Society of America, Chantilly, Virginia, USA, pp. 351–370.

Bergaya, F., Theng, B.K.G. & Lagaly, G. (editors) (2006) *Handbook of Clay Science*. Elsevier, Amsterdam, 1224 pp.

Berthier, P. (1826) Analyse de l'halloysite. *Annales de Chimie et de Physique*, **32**, 332.

Beyer, J. & Von Reichenbach, H.G. (2001) An extended revision of the interlayer structures of one- and two-layer hydrates of Na-vermiculite. *Clay Minerals*, **37**, 157–168.

Bish, D.L. (1993) Rietveld refinement of the kaolinite structure at 1.5 K. *Clays and Clay Minerals*, **41**, 738–744.

Bish, D.L. & Giese, R.F.Jr. (1981) Interlayer bonding in [Group] IIb chlorite. *American Mineralogist*, **66(11-12)**, 1216–1220.

Bish, D.L. & Johnston, C.T. (1993) Rietveld refinement and Fourier-transform infrared spectroscopy study of the dickite structure at low temperature. *Clays and Clay Minerals*, **41**, 297–304.

Bish, D.L. & Von Dreele, R.B. (1989) Rietveld refinement of non-hydrogen atom position in kaolinite. *Clays and Clay Minerals*, **37**, 289–296.

Blount, A.M., Threadgold, I.M. & Bailey, S.W. (1969) Refinement of the crystal structure of nacrite. *Clays and Clay Minerals*, **17**, 185–194.

Bonnin, D., Muller, S. & Calas, G. (1982) Iron in kaolins: EPR, Mössbauer, EXAFS spectrometric studies. *Bulletin de Mineralogie*, **105**, 467–475.

Bookin, A.S., Drits, V.A., Plançon, A. & Tchoubar, C. (1989) Stacking faults in kaolin-group minerals in the light of real structural features. *Clays and Clay Minerals*, **37**, 297–307.

Boukili, B., Holtz, F., Robert, J.L., Joriou, M., Beny, J.M. & Naji, M. (2003) Infrared spectra of annite in the OH stretching vibrational range. *Schweizerische Mineralogische und Petrographische Mitteilungen*, **83**, 331–340.

Bradley, W.F. (1940) The structural scheme of attapulgite. *American Mineralogist*, **25,** 405–410.

Brauner, K. & Preisinger, A. (1956) Struktur und Entstehung des Sepioliths. *Tschermaks Mineralogische und Petrographische Mitteilungen*, **6**, 120–140 (in German).

Breu, J., Seidl, W. & Stoll, A. (2003) Hectorite. *Zeitschrift für anorganische und allgemeine Chemie*, **629**, 503–515.

Brigatti, M.F. (1981) Hisingerite: A review of its crystal chemistry. *Proceedings of 7th International Clay Conference. Developments in Sedimentology*, **35**, 97–110.

Brigatti, M.F. & Guggenheim, S. (2002) Mica crystal chemistry and the influence of pressure, temperature, and solid solution on atomistic models. In: *Micas: Crystal Chemistry and Metamorphic Petrology* (A. Mottana, F.P. Sassi, J.B. Thompson Jr. & S. Guggenheim, editors). Reviews in Mineralogy and Geochemistry, **46**, 1–97. Mineralogical Society of America, Chantilly, Virginia, USA.

Brigatti, M.F., Galli, E., Medici, L. & Poppi, L. (1997) Crystal structure refinement of aluminian lizardite-2*H*2. *American Mineralogist*, **82**, 931–935.

Brigatti, M.F., Guggenheim, S. & Poppi, M. (2003) Crystal chemistry of the 1*M* mica polytype: The octahedral sheet. *American Mineralogist*, **88**, 667–675.

Brigatti, M.F., Colonna, S., Malferrari, D. & Medici, L. (2004) Characterization of Cu-complexes in smectite with different layer charge location: chemical, thermal and EXAFS study. *Geochimica et Cosmochimica Acta*, **68**, 781–788.

Brigatti, M.F., Malferrari, D., Poppi, M. & Poppi, L. (2005) The $2M_1$ dioctahedral mica polytype: A crystal chemical study. *Clays and Clay Minerals*, **53**, 190–197.

Brigatti, M.F., Malferrari, D., Poppi, M., Mottana, A., Cibin, G., Marcelli, A. & Cinque, G. (2008a) Interlayer potassium and its surrounding in micas: Crystal chemical modeling and XANES spectroscopy. *American Mineralogist*, **93**, 821–830.

Brigatti, M.F., Guidotti, C.V., Malferrari, D. & Sassi, F.P. (2008b) Single-crystal X-ray studies of trioctahedral micas coexisting with dioctahedral micas in metamorphic sequences from Western Maine. *American Mineralogist*, **93**, 396–408.

Brindley, G.W. (1959) X-ray and electron diffraction data for sepiolite. *American Mineralogist*, **44**, 495–500.

Brindley, G.W. (1982) Chemical compositions of berthierines – a review. *Clays and Clay Minerals*, **30**, 153–155.

Brindley, G.W. & Brown, G. (editors) (1980) *Crystal Structures of Clay Minerals and their X-ray Identification*. Mineralogical Society, Monograph **5**, London, 495 pp.

Brindley, G.W. & Nakahira, M. (1958) Further consideration of the crystal structure of kaolinite. *Mineralogical Magagazine*, **31**, 781–786.

Brindley, G.W. & Robinson, K. (1945) Structure of kaolinite. *Nature*, **156**, 661–663.

Brindley, G.W. & Robinson, K. (1946) The structure of kaolinite. *Mineralogical Magazine*, **27**, 242–253.

Brindley, G.W. & Robinson, K. (1948) X-ray studies of halloysite and metahalloysite. I. The structure of metahalloysite, an example of random layer lattice. *Mineralogical Magazine*, **28**, 393–406.

Brindley, G.W. & Wan, H.-M. (1975) Compositions, structures, and thermal behavior of Nickel-containing minerals in the lizardite-nepouite series. *American Mineralogist*, **60**, 863–871.

Brindley, G.W., Oughton, B.M. & Youell, R.F. (1951) The crystal structure of amesite and its thermal decomposition. *Acta Crystallographica*, **4**, 552–557.

Brindley, G.W., Bish, D.L., & Hsien-Ming, W. (1979) Compositions, structures, and properties of nickel-containing minerals in the kerolite-pimelite series. *American Mineralogist*, **64**, 615–625.

Brown, B.E. & Bailey, S.W. (1963) Chlorite polytypism: II. Crystal structure of a one-layer Cr chlorite. *American Mineralogist*, **48**, 42–61.

Brown, G. & Weir, A.H. (1963) The identity of rectorite and allevardite. In: *Proceedings of the International Clay Conference, Stockholm*, 27–35 (1) and 87–90 (2).

Brown, G.E., Parks, G.A. & O'Day, P.A. (1995) Sorption at mineral-water interfaces: macroscopic and microscopic perspectives. In: *Mineral Surfaces* (D.J. Vaughan & R.A.D. Pattrick, editors). Mineralogical Society Series, **5**. Chapman & Hall, London, pp. 129–183.

Bujdák, J. (2006) Effect of the layer charge of clay minerals on optical properties of organic dyes. A review. *Applied Clay Science*, **34**, 58–73.

Busigny, V., Cartigny, P., Philippot, P. & Javoy, M. (2004) Quantitative analysis of ammonium in biotite using infrared spectroscopy. *American Mineralogist*, **89**, 1625–1630.

Caillère, S., Mathieu-Sicaud, A. & Hénin, S. (1950) Nouvel essai d'identification du minéral de la Table près Allevard, l'allevardite. *Bulletin de la Société Française de Minéralogie et de Cristallographie*, **73**, 193–201 (in French).

Cámara, F, Garvie, L.A.J., Devouard, B, Groy, T.L. & Buseck, P.R. (2002) The structure of Mn-rich tupersuatsiaite: A palygorskite-related mineral. *American Mineralogist*, **87**, 1458–1463.

Capitani, G.C. & Mellini, M. (2004) The crystal structure of antigorite: the $m = 17$ polysome. *American Mineralogist*, **89**, 147–158.

Capitani, G.C. & Mellini, M. (2005) HRTEM evidence for 8-reversals in the $m = 17$ antigorite polysome. *American Mineralogist*, **90**, 991–998.

Capitani, G.C. & Mellini, M. (2006) The crystal structure of a second antigorite polysome ($m = 16$), by single-crystal synchrotron diffraction. *American Mineralogist*, **91**, 394–399.

Capitani, G.C. & Mellini, M. (2008) Rationale for the existence of four- and eight-reversals in antigorite. *American Mineralogist*, **93**, 796–799.

Capitani, G.C., Stixrude, L. & Mellini, M. (2009) First-principles energetics and structural relaxation of antigorite. *American Mineralogist*, **94**, 1271–1278.

Caruso, L.J. & Chernosky, J.V. (1979) The stability of lizardite. *The Canadian Mineralogist*, **17**, 757–769.

Cases, J.M., Lièтard, O., Yvon, J. & Delon, J.F. (1982) Étude des propriétés cristallochimiques, morphologiques, superficielles de kaolinites désordonnées. *Bulletin de Minéralogie*, **105**, 439–455 (in French).

Castro, E.A.S. & Martins, J.B.L. (2005) Theoretical study of kaolinite. *International Journal of Quantum Chemistry*, **103**, 550–556.

Chernosky, J.V. (1975) Aggregate refractive indices and unit cell parameters of synthetic serpentine in the system MgO-Al_2O_3-SiO_2-H_2O. *American Mineralogist*, **60**, 2000–2008.

Chiari, G., Giustetto, R. & Ricchiardi, G. (2003) Crystal structure refinements of palygorskite and Maya Blue from molecular modeling and powder synchrotron diffraction. *European Journal of Mineralogy*, **15**, 21–33.

Chisholm, J.E. (1992) Powder diffraction patterns and structural models for palygorskite. *The Canadian Mineralogist*, **30**, 61–73.

Chon, C.M., Lee, C.K., Song, Y. & Kim, SA. (2006) Structural changes and oxidation of ferroan phlogopite with increasing temperature: in situ neutron powder diffraction and Fourier transform infrared spectroscopy. *Physics and Chemistry of Minerals*, **33**, 289–299.

Christ, C.L., Hathaway, J.C., Hostetler, P.B. & Shepard, A.O. (1969) Palygorskite: New X-ray data. *American Mineralogist*, **54**, 198–205.

Christidis, G.E. (2001) Formation and growth of smectites in bentonites: a case study from Kimolos Island, Aegean, Greece. *Clays and Clay Minerals*, **49**, 204–215.

Christidis, G.E. (2006) Genesis and compositional heterogeneity of smectites. Part III: alteration of basic pyroclastic rocks. A case study from the Troodos ophiolite complex, Cyprus. *American Mineralogist*, **91**, 685–701.

Christidis, G.E. (2008) Validity of the structural formula method for layer charge determination of smectites: A re-evaluation of published data. *Applied Clay Science*, **42**, 1–7.

Christidis, G.E. (2011) The concept of layer charge of smectites and its implications on important smectite-water properties. In: *Layered Mineral Structures and their Application in Advanced Technologies* (M.F. Brigatti & A. Mottana, editors). EMU notes in Mineralogy, **11**, pp. xxxx–xxx.

Christidis, G. & Dunham, A.C. (1993) Compositional variations in smectites derived from intermediate volcanic rocks. A case study from Milos Island, Greece. *Clay Minerals*, **28**, 255–273.

Christidis, G. & Dunham, A.C. (1997) Compositional variations in smectites. Part II: alteration of acidic precursors. A case study from Milos Island, Greece. *Clay Minerals*, **32**, 255–273.

Christidis, G.E. & Eberl, D.D. (2003) Determination of layer charge characteristics of smectites, *Clays and Clay Minerals*, **51**, 644–655.

Christidis, G.E., Blum, A.E. & Eberl, D.D. (2006) Influence of layer charge and charge distribution of smectites on the flow behaviour and swelling of bentonites. *Applied Clay Science*, **34**, 125–138.

Chukhrov, F.V., Zvyagin, B.B., Drits, V.A., Gorshkov, A.I., Ermilova, L.P., Goilo, E.A. & Rudnitskaya, E.S. (1979) The ferric analogue of pyrophyllite and related phases. In: *Proceedings of the VI International Clay Conference, Oxford* (M.M. Mortland & V.C. Farmer, editors), 55–64. Elsevier, Amsterdam.

Churchman, G.J. & Theng, B.K.G. (1984) Interactions of halloysites with amides: Mineralogical factors affecting complex formation. *Clay Minerals*, **19**, 161–175.

Cibin, G., Mottana, A., Marcelli, A. & Brigatti, M.F. (2005) Potassium coordination in trioctahedral micas investigated by K-edge XANES spectroscopy. *Mineralogy and Petrology*, **85**, 67–87.

Cibin, G., Mottana, A., Marcelli, A. & Brigatti, M.F. (2006) Angular dependence of potassium K-edge XANES spectra of trioctahedral micas: Significance for the determination of the local structure and electronic behavior of the interlayer site. *American Mineralogist*, **91**, 1150–1162.

Cibin, G., Cinque, G., Marcelli, A., Mottana, A. & Sassi, R. (2008) The octahedral sheet of metamorphic $2M_1$-phengites: A combined EMPA and AXANES study. *American Mineralogist*, **93**, 414–425.

Coey, J.M.D., Chukhrov, F.V. & Zvyagin, B.B. (1984) Cation distribution, Mössbauer spectra, and magnetic properties of ferripyrophyllite. *Clays and Clay Minerals*, **32**, 198–204.

Comodi, P., Fumagalli, P., Montagnoli, M. & Zanazzi, P.F. (2004) A single crystal study on the pressure behavior of phlogopite and petrological implications. *American Mineralogist*, **89**, 647–653.

Comodi, P., Cera, F., Dubrovinsky, L. & Nazzareni, S. (2006) The high-pressure behavior of the 10 Å phase: A spectroscopic and diffractometric study up to 42 GPa. *Earth and Planetary Science Letters*, **246**, 444–457.

Compagnoni, R., Ferraris, G. & Mellini, M. (1985) Carlosturanite, a new asbestiform rock-forming silicate from Val Varaita, Italy. *American Mineralogist*, **70**, 767–772.

Coombes, D.S., Catlow, C., Richard, A. & Garces, J.M. (2003) Computational studies of layered silicates. *Modelling and Simulation in Materials Science and Engineering*, **11**, 301–306.

Cradwick, P.D.G., Farmer, V.C., Russell, J.D., Masson, C.R., Wada, K. & Yoshinaga, N. (1972) Imogolite, a hydrated aluminum silicate of tubular structure. *Nature Physical Science*, **240**, 187–189.

Cressey, G., Cressey, B.A., Wicks, F.J. & Yada, K. (2010) A disc with five-fold symmetry: the proposed fundamental seed structure for the formation of chrysotile asbestos fibres, polygonal serpentine fibres and polyhedral lizardite spheres. *Mineralogical Magazine*, **74**, 29–37.

Curetti, N., Levy, D., Pavese, A. & Ivaldi, G. (2006) Elastic properties and stability of coexisting $3T$ and $2M_1$ phengite polytypes. *Physics and Chemistry of Minerals*, **32**, 670–678.

Dainyak, L.G. & Drits, V.A. (2009) A model for the interpretation of Mössbauer spectra of muscovite. *European Journal of Mineralogy*, **21**, 99–106.

Dainyak, L.G., Drits, V.A. & Lindgreen, H. (2004) Computer simulation of octahedral cation distribution and interpretation of the Mössbauer Fe^{2+} components in dioctahedral trans-vacant micas. *European Journal of Mineralogy*, **16**, 451–468.

Dainyak, L.G., Rusakov, V.S., Sukhorukov, I.A., Zviagina, B.B. & Drits, V.A. (2009) An improved model for the interpretation of Mössbauer spectra of dioctahedral 2:1 *trans*-vacant Fe-rich micas: refinement of parameters. *European Journal of Mineralogy*, **21**, 995–1008.

de la Calle, C., Dubernat, J., Suquet, H., Pezerat, H., Gaulthier, J. & Mamy, J. (1975a) Crystal structure of two-layer Mg-vermiculites and Nna-, Ca-vermiculites. In: *Proceedings of the International Clay Conference, Mexico City* (S.W. Bailey, editor). Applied Publishing, Wilmette, Illinois, USA, pp. 201–209.

de la Calle, C., Suquet, H. & Pezerat, H. (1975b) Glissement de feuillets accompagnant certains echanges cationiques dans les vermiculites. *Bulletin du Groupe Français des Argiles*, **27**, 31–49 (in French).

de la Calle, C., Suquet, H., Dubernat, J. & Pezerat, H. (1978) Mode d'Empilement des feuillets dans les vermiculites hydratees a 'deux couches. *Clay Minerals*, **13**, 275–297 (in French).

de la Calle, C., Plançon, A., Pons, C.H., Dubernat, J., Suquet, H. & Pezerat, H. (1984) Mode d'empilement des feuillets dans la vermiculite sodique hydraté à une couche (Phase à 11 85 Å). *Clay Minerals*, **19**, 563–578 (in French).

de la Calle, C., Suquet, H. & Pezerat, H. (1985) Vermiculites hydratees a une couche. *Clay Minerals*, **20**, 221–230.

de la Calle, C., Suquet, H. & Pons, C.H. (1988) Stacking order in a 14.30 Å Mg-vermiculite. *Clays and Clay Minerals*, **36**, 481–490.

de Souza Santos, P., Brindley, G.W. & de Souza Santos, H. (1965) Mineralogical studies of kaolinite-halloysite clays. III. A fibrous kaolin mineral from Piedade, Sao Paulo, Brazil. *American Mineralogist*, **50**, 619–28.

De Waal, S.A. (1970) Nickel minerals from Barberton, South Africa. III. Willemseite, a nickel-rich talc. *American Mineralogist*, **55**, 31–42.

Decarreau, A., Colin, F., Herbillon, A., Manceau, A., Nahon, D., Paquet, H., Trauth-Badeaud, D. & Trescases, J.J. (1987) Domain segregation in Ni–Fe–Mg–smectites, *Clays and Clay Minerals*, **35**, 1–10.

Deer, W.A., Howie, R.A. & Zussman, J. (2009) *Rock-Forming Minerals, vol. 3B*, *Layered Silicates Excluding Micas and Clay Minerals*. 2nd edition. Geological Society, London, 314 pp.

Dera, P., Prewitt, C.T., Japel, S., Bish, D.L. & Johnston, C.T. (2003) Pressure-controlled polytypism in hydrous layered materials. *American Mineralogist*, **88**, 1429–1425.

Di Vincenzo, G., Viti, C. & Rocchi, S. (2003) The effect of chlorite interlayering on ^{40}Ar-^{39}Ar biotite dating: an ^{40}Ar-^{39}Ar laser-probe and TEM investigations of variably chloritised biotites. *Contributions to Mineralogy and Petrology*, **145**, 643–658.

Di Vincenzo, G., Tonarini, S., Lombardo, B., Castelli, D. & Ottolini, L. (2006) Comparison of ^{40}Ar-^{39}Ar and Rb-Sr data on phengites from the UHP Brossasco-Isasca Unit (Dora Maira Massif, Italy): Implications for dating white mica. *Journal of Petrology*, **47**, 1439–1465.

Dobson, D.P., De Ronde, A.A., Welch, M.D. & Meredith, P.G. (2007) The acoustic emissions signature of a pressure-induced polytypic transformation in chlorite. *American Mineralogist*, **92**, 437–440.

Dódony, I. & Buseck, P.R. (2004) Serpentines close-up and intimate: An HRTEM view. *International Geology Review*, **46**, 507–527.

Dódony, I., Pósfai, M. & Buseck, P.R. (2002) Revised structure models for antigorite: An HRTEM study. *American Mineralogist*, **87**, 1443–1457.

Dódony, I., Posfai, M. & Buseck, P.R. (2006) Does antigorite really contain 4- and 8-membered rings of tetrahedra? *American Mineralogist*, **91**, 1831–1838.

Dong, H. (2005) Interstratified illite-smectite: a review of contributions of TEM data to crystal chemical relations and reaction mechanisms. *Clay Science*, **12**, 6–12.

Dong, H., Peacor, D.R. & Freed, R.L. (1997) Phase relations among smectite, R1 illite/smectite and illite. *American Mineralogist*, **82**, 379–391.

Dong, H., Peacor, D.R., Merriman, R.J. & Kemp, S.J. (2002) Brinrobertsite: a new R1 interstratified pyrophyllite/smectite-like clay mineral: characterization and geological origin. *Mineralogical Magazine*, **66**, 605–617.

Donnay, G., Morimoto, N., Takeda, H. & Donnay, D.H. (1964) Trioctahedral one-layer micas: 1. Crystal structure of a synthetic iron mica. *Acta Crystallographica*, **17**, 1369–1373.

Drits, V.A. (1997) Mixed layer minerals. In: *Modular Aspects of Minerals* (S. Merlino, editor). EMU Notes in Mineralogy, **1**, Eötvös University Press, Budapest, pp. 153–190.

Drits, V.A. (2003) Structural and chemical heterogeneity of layer silicates and clay minerals. *Clay Minerals*, **38**, 403–432.

Drits, V.A. & Karavan, Y.V. (1969) Polytypes of the two-packet chlorites. *Acta Crystallographica, Section B: Structural Crystallography and Crystal Chemistry*, **25**, 632–639.

Drits, V.A. & Kashaev, A.A. (1960) The structure of kaolinite. *Materialy po geologii i poleznym iskopaemym vostochnoĭ Sibiri, Irkutsk*, 264–266.

Drits, V.A. & Sokolova, G.V. (1971) Structure of palygorskite. *Soviet Physics, Crystallography*, **16**, 183–185.

Drits, V.A. & Tchoubar, C. (1990) *X-ray Diffraction by Disordered Lamellar Structures: Theory and Applications to Microdivided Silicates and Carbons*. Springer-Verlag, Berlin, 371 pp.

Drits, V.A. & Zviagina, B.B. (2009) *Trans*-vacant and *cis*-vacant 2:1 layer silicates: structural features, identification, and occurrence. *Clays and Clay Minerals*, **57**, 405–415.

Drits, V.A., Plançon, A., Sakharov, B.A., Besson, G., Tsipursky, S.I. & Tchoubar, C. (1984) Diffraction effects calculated for structural models of K-saturated montmorillonite containing different types of defects. *Clay Minerals*, **19**, 541–562.

Drits, V.A. Varaxina, T.V., Sakharov, B.A. & Plançon, A. (1994) A simple technique for identification of one-dimensional powder X-ray diffraction patterns for mixed-layer illite-smectites and other interstratified minerals. *Clays and Clay Minerals*, **42**, 382–90.

Drits, V.A., Środoń, J. & Eberl, D.D. (1997a) XRD measurements of mean crystallite thickness of illite and illite/smectite: reappraisal of the Kübler index and the Scherrer equation. *Clays and Clay Minerals*, **45**, 461–475.

Drits, V.A., Lindgreen, H., Sakharov, B.A. & Salyn, A.L. (1997b) Sequential structure transformation of illite-smectite-vermiculite during diagenesis of Upper Jurassic shales, North Sea. *Clay Minerals*, **33**, 351–371.

Drits, V.A., Lindgreen, H., Salyn, A.L., Ylagan R. & McCarty, D.K. (1998) Semiquantitative determination of *trans*-vacant and *cis*-vacant 2:1 layers in illites and illite-smectites by thermal analysis and X-ray diffraction. *American Mineralogist*, **83**, 1188–1198.

Drits, V.A., McCarty, D.K. & Zviagina, B.B. (2006) Crystal-chemical factors responsible for the distribution of octahedral cations over *trans*- and *cis*-sites in dioctahedral 2:1 layer silicates. *Clays and Clay Minerals*, **54**, 131–152.

Drits, V.A., Lindgreen, H., Sakharov, B.A., Jakobsen, H.J., Fallick, A.E., Salyn, A.L., Dainyak, L.G., Zviagina, B.B. & Barfod, D.N. (2007) Formation and transformation of mixed-layer minerals by Tertiary intrusives in Cretaceous mudstones, West Greenland. *Clays and Clay Minerals*, **55**, 260–283.

Dunoyer de Segonzac, G. & Bernoulli, D. (1976) Diagenese et métamorphisme des argiles dans le Rhétien Sud-alpin et Austro-alpin (Lombardie et Grisons). *Bulletin Societé Géologique de la France*, **18**, 1283–1293 (in French).

Ďurovič, S. (1997) Fundamentals of OD theory. In: *Modular Aspects of Minerals* (S. Merlino, editor). EMU Notes in Mineralogy, **1**. Eötvös University Press, Budapest, pp. 1–28.

Ďurovič, S. (1999) Layer stacking in general polytypic structures. In: *International Tables for Crystallography, Volume C* (A.C.J. Wilson & E. Prince, editors). Kluwer Academic Publishers, Dordrecht, The Netherlands, pp. 752–765.

Ďurovič, S., Hybler, J. & Kogure, T. (2004) Parallel intergrowths in cronstedtite-1*T*: Implications for structure refinement. *Clays and Clay Minerals*, **52**, 613–622.

Dyar, M.D. (2002) Optical and Mössbauer spectroscopy of iron in micas. In: *Micas: crystal chemistry and metamorphic petrology* (A. Mottana, F.P. Sassi, J.B. Thompson Jr. & S. Guggenheim, editors). Reviews in Mineralogy and Geochemistry, **46**. Mineralogical Society of America, Chantilly, Virginia, USA, pp. 313–349.

Dyar, M.D., Gunter, M.E., Delaney, J.S., Lanzarotti, A. & Sutton, S.R. (2002a) Systematics in the structure and XANES spectra of pyroxenes, amphiboles, and micas as derived from oriented single crystals. *The Canadian Mineralogist*, **40**, 1375–1393.

Dyar, M.D., Lowe, E.W., Guidotti, C.V. & Delaney, J.S. (2002b) Fe^{3+} and Fe^{2+} partitioning among silicates in metapelites: A synchrotron micro-XANES study. *American Mineralogist*, **87**, 514–522.

Dyar, M.D., Schaefer, M.W., Sklute, E.C. & Bishop, J.L. (2008) Mössbauer spectroscopy of phyllosilicates: effects of fitting models on recoil-free fractions and redox ratios. *Clay Minerals*, **43**, 3–33.

Eberl, D.D. & Velde, B. (1989) Beyond the Kübler index. *Clay Minerals*, **24**, 571–577.

Eberl, D.D., Drits, V., Środoń, J. & Nüesch, R. (1996) *MudMaster*: *A program for calculating crystallite size distributions and strain from the shapes of X-ray diffraction peaks*. U.S. Geological Survey Open-File Report 96-171, 46 pp.

Eberl, D.D., Drits, V.A. & Środoń, J. (1998) Deducing growth mechanisms for minerals from the shapes of crystal size distributions. *American Journal of Science*, **298**, 499–533.

Eberl, D.D., Drits, V.A. & Środoń, J. (2000) *User's guide to Galoper—a program for simulating the shapes of crystal size distributions—and associated programs*. U.S. Geological Survey Open-File Report 00-505, 44 pp.

Eggleston, R.A. & Bailey, S.W. (1967) Structural aspects of dioctahedral chlorite. *American Mineralogist*, **52**, 673–689.

Eggleton, R.A. & Tilley, D.B. (1998) Hisingerite: a ferric kaolin mineral with curved morphology. *Clays and Clay Minerals*, **46**, 400–413.

Evans, B.W. & Guggenheim, S. (1988) Talc, pyrophyllite, and related minerals. In: *Hydrous Phyllosilicates (Exclusive of Micas)* (S.W. Bailey, editor). Reviews in Mineralogy, **19**, 225–294. Mineralogical Society of America, Washington, D.C.

Evans, R., James, R., Denis, G. & Grodzicki, M. (2005) Hyperfine electric field gradient tensors at Fe^{2+} sites in octahedral layers: Toward understanding oriented single crystal Mössbauer spectroscopy measurements of micas. *American Mineralogist*, **90**, 1540–1555.

Farmer, V.C. (1974) *The Infrared Spectra of Minerals*. Mineralogical Society, London, 539 pp.

Farmer, V.C. (1998) Differing effect of particle size and shape in the infrared and Raman spectra of kaolinite. *Clay Minerals*, **33**, 601–604.

Farmer, V.C. (2000) Transverse and longitudinal crystal modes associated with OH stretching vibrations in single crystals of kaolinite and dickite. *Spectrochimica Acta Part A*, **56**, 927–930.

Farmer, V.C. & Fraser, A.R. (1979) Synthetic imogolite, a tubular hydroxyaluminium silicate. In: *International Clay Conference, Oxford* (M.M. Mortland & V.C. Farmer, editors). Elsevier, Amsterdam, pp. 547–553.

Faust, G.T. (1951) Thermal analysis and X-ray studies of sauconite and of some zinc minerals of the same paragenetic association. *American Mineralogist*, **36**, 795–822.

Faust, G.T. & Murata, K.J. (1953) Stevensite, redefined as a member of the montmorillonite group. *American Mineralogist*, **38**, 973–987.

Faust, G.T., Hathway, J.C. & Millot, G. (1959) A restudy of stevensite and allied minerals. *American Mineralogist*, **44**, 343–370.

Fechtelkord, M., Behrens, H., Holtz, F., Bretherton, J.L., Fyfe, C.A., Groat, L.A. & Raudsepp, M. (2003a) Influence of F content on the composition of Al-rich synthetic phlogopite: Part II. Probing the structural arrangement of aluminum in tetrahedral and octahedral layers by ^{27}Al MQMAS and ^{1}H/^{19}F-^{27}Al HETCOR and REDOR experiments. *American Mineralogist*, **88**, 1046–1054.

Fechtelkord, M., Behrens, H., Holtz, F., Fyfe, C.A., Groat, L.A. & Raudsepp, M. (2003b) Influence of F content on the composition of Al-rich synthetic phlogopite: Part I. New information on structure and phase-formation from ^{29}Si, ^{1}H, and ^{19}F MAS NMR spectroscopies. *American Mineralogist*, **88**, 47–53.

Ferrage, E., Lanson, B., Malikova, N., Plançon, A., Sakharov, B.A. & Drits, V.A. (2005a) New insights on the distribution of interlayer water in bi-hydrated smectite from X-ray diffraction profile modeling of 00l reflections. *Chemistry of Materials*, **17**, 3499–3512.

Ferrage, E., Lanson, B., Sakharov, B.A. & Drits, V.A. (2005b) Investigation of smectite hydration properties by modeling of X-ray diffraction profiles. Part 1. Montmorillonite hydration properties. *American Mineralogist*, **90**, 1358–1374.

Ferrage, E., Seine, G., Gaillot, A.C., Petit, S., de Parseval, P., Boudet, A., Lanson, B., Ferret, J. & Martin, F. (2006) Structure of the {001} talc surface as seen by atomic force microscopy. Comparison with X-ray and electron diffraction results. *European Journal of Mineralogy*, **18**, 483–491.

Ferrage, E., Lanson, B., Sakharov, B.A., Jacquot, E., Geoffroy, N. & Drits, V.A. (2007) Investigation of smectite hydration properties by modeling of X-ray diffraction profiles. Part 2. Influence of layer charge and charge location. *American Mineralogist*, **92**, 1731–1743.

Ferrage, E., Lanson, B., Michot, L.J. & Robert, J-L. (2010) Hydration properties and interlayer organization of water and ions in synthetic Na-smectite with tetrahedral layer charge. Part 1. Results from X-ray diffraction profile modeling. *Journal of Physical Chemistry*, **114**, 4515–4526.

Ferraris, G. & Ivaldi, G. (2002) Structural features of micas. In: *Micas: Crystal Chemistry and Metamorphic Petrology* (A. Mottana, F.P. Sassi, J.B. Thompson Jr. & S. Guggenheim, editors). Reviews in Mineralogy and Geochemistry, **46**. Mineralogical Society of America, Chantilly, Virginia, USA, pp. 118–153.

Ferraris, G., Mellini, M. & Merlino, S. (1986) Polysomatism and the classification of minerals. *Rendiconti della Società Italiana di Mineralogia e Petrografia*, **41**, 181–192.

Ferraris, C., Chopin, C. & Wessicken, R. (2000) Nano to micro scale decompression products in ultrahigh pressure phengite: HRTEM and AEM study, and some petrological implications. *American Mineralogist*, **85**, 1195–1201.

Ferraris, C., Castelli, D. & Lombardo, B. (2005) SEM/TEM-AEM characterization of micro- and nano-scale zonation in phengite from a UHP Dora-Maira marble: Petrologic significance of armoured Si-rich domains. *European Journal of Mineralogy*, **17**, 453–464.

Fleet, M.E. (2003) *Rock-Forming Minerals, Volume 3A. Sheet Silicates: Micas*. 2nd edition, Geological Society, London, 758 pp.

Frank-Kamenetskii, V.A., Logvinenko, N.V. & Drits, V.A. (1965) Tosudite – a new mineral, forming the mixed-layer phase in alushtite. In: *Proceedings of the International Clay Conference, Stockholm*, pp. 181–186 (2).

Frost, R.L. (1995) Fourier transform Raman spectroscopy of kaolinite, dickite and halloysite. *Clays and Clay Minerals*, **43**, 191–195.

Frost, R.L. & Van der Gaast, S.J. (1997) Kaolinite hydroxyls; a Raman microscopy study. *Clay Minerals*, **32**, 471–484.

Galán, E. (1996) Properties and applications of palygorskite-sepiolite clays. *Clay Minerals*, **31**, 443–453.

Galán, E. & Carretero, M.I. (1999) A new approach to compositional limits for sepiolite and palygorskite. *Clays and Clay Minerals*, **47**, 399–409.

García, F.J., García Rodríguez, S., Kalytta, A. & Reller, A. (2009) Study of natural halloysite from the Dragon Mine, Utah (USA). *Zeitschrift für Anorganische und Allgemeine*, **635**, 790–795.

Gard, J.A. & Follet, E.A. (1968) A structural scheme for palygorskite. *Clay Minerals*, **7**, 367–369.

Gatta, D., Rotiroti, N., Pavese, A., Lotti, P. & Curetti, N. (2009) Structural evolution of a 3*T* phengite up to 10 GPa: an *in situ* single-crystal X-ray diffraction study. *Zeitschrift für Kristallographie*, **224**, 302–310.

Gemmi, M., Merlini, M., Pavese, A. & Curetti N. (2008) Thermal expansion and dehydroxylation of phengite micas. *Physics and Chemistry of Minerals*, **35**, 367–379.

Gianfagna, A., Scordari, F., Mazziotti-Tagliani, S., Ventruti, G. & Ottolini, L. (2007) Fluorophlogopite from Biancavilla (Mt. Etna, Sicily, Italy): crystal structure and crystal chemistry of a new F-dominant analog of phlogopite. *American Mineralogist*, **92**, 1601–1609.

Giese, R.F. & Datta, P. (1973) Hydroxyl orientation in kaolinite, dickite, and nacrite. *American Mineralogist*, **58**, 471–479.

Giese, R.F. & van Oss, C.J. (2002) *Colloid and Surface Properties of Clays and Related Minerals*. Marcel Dekker, New York, 295 pp.

Giorgetti, G., Tropper, P., Essene, E.J. & Peacor, D.R. (2000) Characterization of non equilibrium and equilibrium occurrences of paragonite/muscovite intergrowths in an eclogite from the Sesia Lanzo Zone (Western Alps, Italy). *Contributions to Mineralogy and Petrology*, **138**, 326–336.

Giustetto, R. & Chiari, G. (2004) Crystal structure refinement of palygorskite from neutron powder diffraction. *European Journal of Mineralogy*, **16**, 521–532.

Gregorkiewitz, M., Lebech, B., Mellini, M. & Viti, C. (1996) Hydrogen positions and thermal expansion in lizardite-1*T* from Elba: a low-temperature study using Rietveld refinement of neutron diffraction data. *American Mineralogist*, **81**, 1111–1116.

Grim, R.E. & Güven, N. (1978) *Bentonites*. Elsevier, New York, 256 pp.

Grobéty, B. (2003) Polytypes and higher-order structures of antigorite: A TEM study. *American Mineralogist*, **88**, 27–36.

Gruner, J.W. (1932a) The crystal structure of kaolinite. *Zeitschrift für Kristallographie, Kristallgeometrie, Kristallphysik, Kristallchemie*, **83**, 75–80.

Gruner, J.W. (1932b) The crystal structure of dickite. *Zeitschrift für Kristallographie, Kristallgeometrie, Kristallphysik, Kristallchemie*, **83**, 394–404.

Gruner, J.W. (1934a) The crystal structure of talc and pyrophyllite. *Zeitschrift für Kristallographie*, **88**, 412–419.

Gruner, J.W. (1934b) The structures of vermiculites and their collapse by dehydration. *American Mineralogist*, **19**, 557–575.

Gruner, J.W. (1935) The structural relationships of nontronite and montmorillonite. *American Mineralogist*, **20**, 475–483.

Gualtieri, A.F., Moen, A. & Nicholson, D.G. (2000) XANES study of the local environment of iron in natural kaolinites. *European Journal of Mineralogy*, **12**, 17–23.

Guggenheim, S. (2011) An overview of order/disorder in hydrous phyllosilicates. In: *Layered mineral structures and their application in advanced technologies* (M.F. Brigatti & A. Mottana, editors), EMU notes in Mineralogy, **11**, pp. xxx-xxx.

Guggenheim, S. & Eggleton, R.A. (1998) Modulated crystal structures of greenalite and caryopilite: a system with long-range, in-plane structural disorder in the tetrahedra sheet. *The Canadian Mineralogist*, **36**,163–179.

Guggenheim, S. & Zhan, W. (1998) Effect of temperature on the structures of lizardite-1*T* and lizardite-2H_1. *The Canadian Mineralogist*, **36**, 1587–1594.

Guggenheim, S., Adams, J.M., Bain, D.C., Bergaya, F., Brigatti, M.F., Drits, V.A., Formoso, M.L.L., Galán, E., Kogure, T. & Stanjek, H. (2006) Summary of recommendations of nomenclature committees relevant

to clay mineralogy: report of the Association Internationale Pour l'Etude des Argiles (AIPEA) nomenclature committee for 2006. *Clays and Clay* Minerals, **54**, 761–772.

Güven, N. (1988) Smectites. In: *Hydrous Phyllosilicates (Exclusive of Micas)* (S.W Bailey, editor). Reviews in Mineralogy, **19**. Mineralogical Society of America, Washington, D.C., pp. 497–559.

Güven, N. (1992) Molecular aspects of clay-water interactions. In: *Clay-Water Interface and its Rheological Implications* (N. Güven & R.M. Pollastro, editors). CMS Workshop Lectures**, 4**. The Clay Minerals Society, Boulder, Colorado, USA, pp. 1–80.

Hall, S.H. & Bailey, S.W. (1979) Cation ordering pattern in amesite. *Clays and Clay Minerals*, **27**, 241–247.

He, H., Barr, T.L. & Klinowski, J. (1995) ESCA and solid-state NMR studies of allophane. *Clay Minerals*, **30**, 201–209.

He, H.P., Guo, J.G., Zhu, J.X. & Hu, C. (2003) ^{29}Si and ^{27}Al MAS NMR study of the thermal transformations of kaolinite from North China. *Clay Minerals*, **38**, 551–559.

Heinrich, A.R., Eggleton, R.A. & Guggenheim, S. (1994) Structure and polytypism of bementite, a modulated layer silicate. *American Mineralogist*, **79**, 91–106.

Hendricks, S.B. (1938) The crystal structure of the clay minerals: dickite, halloysite and hydrated halloysite. *American Mineralogist*, **23**, 295–301.

Hendricks, S.B. (1939) The crystal structure of nacrite, $Al_2O_3{\cdot}2SiO_2{\cdot}2H_2O$, and the polymorphism of the kaolin minerals. *Zeitschrift für Kristallographie*, **100**, 509–518.

Hendricks, S.B. & Jefferson, M.E. (1938) Crystal structure of vermiculites and mixed vermiculite-chlorites. *American Mineralogist*, **23**, 851–862.

Henmi, T. & Wada, K. (1976) Morphology and composition of allophane. *American Mineralogist*, **61**, 379–390.

Hinckley, D.N. (1963) Variability in "crystallinity" values among the kaolin deposits of the coastal plain of Georgia and South Carolina. *Clays and Clay Minerals*, **11**, 229–235.

Hisinger, W. (1810) Undersökning af Svenska Mineralier. VI. Svart Stenart från Gillinge Jern-Grufva i Södermanland. *Afhandlingar i Fysik, Kemi, och Mineralogi*, **3**, 304–306 (in Swedish).

Hobbs, J.D., Cygan, R.T., Nagy, K.L., Schultz, P.A. & Sears, M.P. (1997) All-atom *ab initio* energy minimization of the kaolinite crystal structure. *American Mineralogist*, **82**, 657–662.

Hofmann, U., Endell, K. & Wilm, D. (1934) X-ray and colloid-chemical studies of clay. *Angewandte Chemie*, **47**, 539–547.

Honjo, G., Kitamura, N. & Mihama, K. (1954) A study of clay minerals by means of single-crystal electron-diffraction diagrams – the structure of tubular kaolin. *Clay Minerals Bulletin*, **2**, 133–141.

Hoppe, R. (1979) Effective coordination numbers (ECON) and mean fictive ionic radii (MEFIR). *Zeitschrift für Kristallographie*, **150**, 23–52.

Hybler, J. (2006) Parallel intergrowths in cronstedtite-1*T*: determination of the degree of disorder. *European Journal of Mineralogy*, **18**, 197–205.

Hybler, J., Petricek, V., Ďurovič, S. & Smrčok, L. (2000) Refinement of the crystal structure of cronstedtite-1*T*. *Clays and Clay Minerals*, **48**, 331–338.

Hybler, J., Petricek, V., Fabry, J. & Ďurovič, S. (2002) Refinement of the crystal structure of cronstedtite-2H_2. *Clays and Clay Minerals*, **50**, 601–613.

Ianovici, V., Neacsu, G., & Neacsu, V. (1990) Li-bearing stevensite from Moldova Noua, Romania. *Clays and Clay Minerals*, **38**, 171–178.

Ivanova, T.I. & Frank-Kamenetskaya, O.V. (2001) Using the statistical probability-based model of an irregular mixed-layer structure for describing the real structures of chemically nonhomogeneous single crystals. *Journal of Structural Chemistry*, **42**, 126–143.

Jiang, W.T., Peacor, D.R. & Slack, J.F. (1992) Microstructures, mixed layering, and polymorphism of chlorite and retrograde berthierine in the Kidd Creek massive sulfide deposit, Ontario. *Clays and Clay Minerals*, **40**, 501–514.

Johnston, C.T., Agnew, S.F. & Bish, D.L. (1990) Polarized single-crystal Fourier-transform infrared microscopy of Ouray dickite and Keokuk kaolinite. *Clays and Clay Minerals*, **38**, 573–583.

Johnston, C.T., Helsen, J., Schoonheydt, R.A., Bish, D.L. & Agnew, S.F. (1998) Single-crystal Raman spectroscopic study of dickite. *American Mineralogist*, **83**, 75–84.

Johnston, C.T., Wang, S.-L., Bish, D.L., Dera, P., Agnew, S.F. & Kenney III, J.W. (2002) Novel pressure-induced phase transformations in hydrous layered materials. *Geophysical Research Letters*, **29**, 1770.

Jones, B.F. & Galán, E. (1988) Sepiolite and palygorskite. In: *Hydrous Phyllosilicates* (S.W. Bailey, editor). Reviews in Mineralogy, **19**. Mineralogical Society of America, Chantilly, Virginia, USA, pp. 631–674.

Joswig, W. & Drits, V.A. (1986) The orientation of the hydroxyl groups in dickite by X-ray diffraction. *Neues Jahrbuch für Mineralogie Monatshefte*, **1**, 19–22.

Joswig, W. & Fuess, H. (1989) Neutron diffraction study of a one-layer monoclinic chlorite. *Clays and Clay Minerals*, **37**, 511–514.

Joswig, W. & Fuess, H. (1990) Refinement of a one-layer triclinic chlorite. *Clays and Clay Minerals*, **38**, 216–218.

Joswig, W., Fuess, H., Rothbauer, R., Takeuchi, Y. & Mason, S.A. (1980) A neutron diffraction study of a one-layer triclinic chlorite (penninite). *American Mineralogist*, **65**, 349–352.

Joussein, E., Petit, S., Churchman, J., Theng, B., Righi, D. & Delvaux, B. (2005) Halloysite clay minerals – a review. *Clay Minerals*, **40**, 383–426.

Kameda, J., Miyawaki, R., Kitagawa, R. & Kogure, T. (2007) XRD and HRTEM analyses of stacking structures in sudoite, di-trioctahedral chlorite. *American Mineralogist*, **92**, 1586–1592.

Kato, T. (1963) New data on the so called bementite. *Mineralogical Journal of Japan*, **6**, 93–103.

Kato, T. & Takeuchi, Y. (1980) Crystal structures and submicroscopic textures of layered manganese silicates. *Mineralogical Journal of Japan*, **14**, 165–178.

Kitagawa, Y. (1971) The unit particle of allophane. *American Mineralogist*, **56**, 465–475.

Kittrick, J.A. (1969a) Interlayer forces in montmorillonite and vermiculite. *Soil Science Society of America Journal*, **33**, 217–222.

Kittrick, J.A. (1969b) Quantitative evaluation of the strong-force model for expansion and contraction of vermiculite. *Soil Science Society of America Journal*, **33**, 222–225.

Kloprogge, J.T., Hammond, M., Hickey, L. & Frost, R.L. (2001) A new low temperature synthesis route of fraipontite $(Zn,Al)_3(Si,Al)_2O_5(OH)_4$. *Materials Research Bulletin*, **36**, 1091–1098.

Kogure, T. (2002) Investigations of micas using advanced transmission electron microscopy. In: *Micas: Crystal Chemistry and Metamorphic Petrology* (A. Mottana, F.P. Sassi, J.B. Thompson Jr. & S. Guggenheim, editors). Reviews in Mineralogy and Geochemistry, **46**. Mineralogical Society of America, Chantilly, Virginia, USA, pp. 300–380.

Kogure, T. & Kameda, J. (2008) High-resolution TEM and XRD simulation of stacking disorder in 2:1 phyllosilicates. *Zeitschrift für Kristallographie*, **223**, 69–75.

Kogure, T., Hybler, J. & Ďurovič, S. (2001) A HRTEM study of cronstedtite: determination of polytypes and layer polarity in trioctahedral 1:1 phyllosilicates. *Clays and Clay Minerals*, **49**, 310–317.

Kogure, T., Miyawaki, R. & Banno, Y. (2005) The true structure of wonesite, an interlayer deficient trioctahedral sodium mica. *American Mineralogist*, **90**, 725–731.

Kogure, T., Jige, M., Kameda, J., Yamagishi, A., Miyawaki, R. & Kitagawa, R. (2006) Stacking structures in pyrophyllite revealed by high-resolution transmission electron microscopy (HRTEM). *American Mineralogist*, **91**, 1293–1299.

Kogure, T., Elzea-Kogel, J., Johnston, C. T. & Bish, D.L. (2010) Stacking disorder in a sedimentary kaolinite. *Clays and Clay Minerals*, **58**, 62–71.

Kohyama, N. & Sudo, T. (1975) Hisingerite occurring as a weathering product of iron-rich saponite. *Clays and Clay Minerals*, **23**, 215–218.

Kohyama, N., Fukushima, K. & Fukami, A. (1978) Observation of the hydrated form of tabular halloysite by an electron microscope equipped with an environmental cell. *Clays and Clay Minerals*, **26**, 25–40.

Koshimizu, H., Higuchi, S. & Otsuka, R. (1981) Hydrothermal synthesis and some properties of talc-willemseite solid solutions. *Nendo Kagaku*, **21**, 61–71.

Krekeler, M.P.S. & Guggenheim, S. (2008) Defects in microstructure in palygorskite–sepiolite minerals: A transmission electron microscopy (TEM) study. *Applied Clay Science*, **39**, 98–195.

Krivovichev, S.V., Armbruster, T., Organova, N.I., Burns, P.C., Seredkin, M.V. & Chukanov, N.V. (2004) Incorporation of sodium into the chlorite structure: the crystal structure of glagolevite, $Na(Mg,Al)_6[Si_3AlO_{10}](OH,O)_8$. *American Mineralogist*, **89,** 1138–1141.

Kübler, B. (1964) Les argiles, indicateurs de métamorphisme. *Revue de l'Institut Francaise du Petrole*, **19**, 1093–1112 (in French).

Kübler, B. (1967) La cristallinité de l'illite et les zones tout á fait supécieures du métamorphisme. In Étages Tectoniques. *Collogue de Neuchâtel*, **1996**, 105–121 (in French).

Kübler, B. (1984) Les indicateurs des transformations physiques et chimiques dans la diagenèse, température et calorimétrie. In: *Thermométrie et barométrie géologiques* (M. Lagache, editor), 489–596. Société Française Minéralogie et de Cristallographie, Paris (in French).

Kunze, V.G. (1956) Die gewellte Struktur des Antigorits, I. *Zeitschrift fiir Kristallographie*, **108**, 82–107 (in German).

Kunze, V.G. (1958) Die gewellte Struktur des Antigorits, II. *Zeitschrift für Kristallographie*, **110**, 282–320 (in German).

Kunze, V.G. (1961) Antigorit: Struckturtheoretische Grundlagen und ihre praktische Bedeutung für die weiters Serpentinforschung. *Fortschritte der Mineralogie*, **39**, 206–324 (in German).

Lagaly, G. (1981) Characterization of clays by organic compounds. *Clay Minerals*, **16**, 1–21.

Lagaly, G. (1994) Layer charge determination by alkylammonium ions. In: *Layer Charge Characteristics of 2:1 Silicate Clay Minerals* (A.R. Mermut, editor). CMS Workshop Lectures, **6**. The Clay Minerals Society, Boulder, Colorado, USA, pp. 2–46.

Lagaly, G. & Weiss, A. (1975) The layer charge of smectitic layer silicates. In: *Proceedings of the International Clay Conference, 1975, Mexico City, Mexico*, pp. 157–172.

Laird, D.A. (1994) Evaluation of the structural formula and alkylammonium methods of determining layer charge. In: *Layer Charge Characteristics of 2:1 Silicate Clay Minerals* (A.R. Mermut, editor). CMS Workshop Lectures, **6**. The Clay Minerals Society, Boulder, Colorado, USA, pp. 80–103.

Laird, D.A. (1996) Model for crystalline swelling of 2:1 phyllosilicates. *Clays and Clay Minerals*, **44**, 553–559.

Laird, D.A. (1999) Layer charge influences on the hydration of expandable 2:1 phyllosilicates. *Clays and Clay Minerals*, **47**, 630–636.

Laird, D.A. (2006) Influence of layer charge on swelling of smectites. *Applied Clay Science*, **34**, 74–87.

Laird, J. (1988) Chlorites: Metamorphic Petrology. In: *Hydrous Phyllosilicates (exclusive of Micas)* (S. W. Bailey, editor). Reviews in Mineralogy, **19**. Mineralogical Society of America, Chantilly, Virginia, USA, pp. 405–453.

Lanson, B. (2005) Crystal structure of mixed-layer minerals and their X-ray identification: new insights from X-ray diffraction profile modeling. *Clay Science*, **12**, 1–5.

Lanson, B. (2011) Modelling of X-ray diffraction profiles: Investigation of defective lamellar structure crystal chemistry. In: *Layered Mineral Structures and their Application in Advanced Technologies* (M.F. Brigatti & A. Mottana, editors). EMU notes in Mineralogy, **11**, xxx–xxx.

Lanson, B., Sakharov, B.A., Claret, F. & Drits V.A. (2009) Diagenetic smectite to illite transition in clay-rich sediments: a reappraisal of X-ray diffraction results using the multi-specimen method. *American Journal of Science*, **300**, 476–516.

Laurora, A., Brigatti, M.F., Malferrari, D., Galli, E. & Rossi, A. (2011) Crystal chemistry of lizardite-1*T* from Northern Apennines ophiolites, near Modena, Italy. *The Canadian Mineralogist* (in press).

Lee, J.H. & Guggenheim, S. (1981) Single crystal x-ray refinement of pyrophyllite 1*Tc. American Mineralogist*, **66**, 350–357.

Lee, S.K. & Stebbins, J.F. (2003) O atom sites in natural kaolinite and muscovite: O-17 MAS and 3QMAS NMR study. *American Mineralogist*, **88**, 493–500.

Leoni, M., Gualtieri, A.F. & Roveri, N. (2004) Simultaneous refinement of structure and microstructure of layered materials. *Journal of Applied Crystallography*, **37**, 166–173.

Lièrtard, O. (1977) *Contribution à l'étude des propiétés phisicochimiques, cristallographiques et morphologiques des kaolins*. Thèse Doctoral Science Physique, Nancy, France, 345 pp. (in French).

Lim, C.H. & Jackson, M.L. (1986) Expandable phyllosilicate reactions with lithium on heating, *Clays and Clay Minerals*, **34**, 346–352.

Lin, J.-C. & Guggenheim, S. (1983) The crystal structure of a Li, Be-rich brittle mica: a dioctahedral-trioctahedral intermediate. *American Mineralogist*, **68**, 130–142.

Lindqvist, B. & Jansson, S. (1962) On the crystal chemistry of hisingerite. *American Mineralogist*, **47**, 1356–1362.

Lippmann, F. (1954) Uber einen Keuperton von Zaiserweiher bei Maulbronn. *Heidelberger Beitrdge zur Mineralogie und Petrographie*, **4**, 130–134 (in German).

Lippmann, F. (1960) Corrensit. In: *Handbuch der Mineralogie* (C. Hintze, editor). Ergänzungsband II (F. Chudoba, editor). Neue Mineralien und Neue Mineralnamen, Teil III (in German), pp. 688–691.

Lister, J.S. & Bailey, S.W. (1967) Chlorite polytypism. IV. Regular two-layer structures. *American Mineralogist*, **52**, 1614–1631.

Longchambon, H. (1937) Thermal properties of sepiolites. *Bulletin de la Société française de Minéralogie et de Cristallographie*, **60**, 232–276. **Q5**

MacEwan, D.M.C. & Wilson, M.J. (1980) Interlayer and intercalation complexes of clay minerals. In: *Crystal Structures of Clay Minerals and Their X-ray Identification* (G.W. Brindley & G. Brown, editors). Monograph **5**, Mineralogical Society, London, pp. 197–248.

Mackenzie, K.J.D. & Berezowski, R.M. (1980) Thermal and Mössbauer studies of iron-containing hydrous silicates. II. Hisingerite. *Thermochimica Acta*, **41(3)**, 335–355.

MacKenzie, K.J.D., Bowden, M.E. & Meinhold, R.H. (1991) The structure and thermal transformations of allophanes studied by ^{29}Si and ^{27}Al high resolution solid-state NMR. *Clays and Clay Minerals*, **39**, 337–346.

Maes, A. & Cremers, A. (1977) Charge density effects in ion exchange. Part 1. Heterovalent exchange equilibria. *Faraday Transactions Royal Society*, **73**, 1807–1814.

Maillet, P., Levard, C., Larquet, E., Mariet, C., Spalla, O., Menguy, N., Masion, A., Doelsch, A., Rose, J. & Thill, A. (2010) Evidence of double-walled Al-Ge imogolite-like nanotubes. A Cryo-TEM and SAXS investigation. *Journal of the American Chemical Society*, **132**, 1208–1209.

Maksimovic, Z. & Bish, D.L. (1978) Brindleyite, a nickel-rich aluminous serpentine mineral analogous to berthierine. *American Mineralogist*, **63**, 484–489.

Malikova, N., Cadene, A., Dubois, E., Marry, V., Durand-Vidal, S., Turq, P., Breu, J., Longeville, S. & Zanotti, J.-M. (2007) Water diffusion in a synthetic hectorite clay studied by quasi-elastic neutron scattering. *Journal of Physical Chemistry C*, **111**, 17603–17611.

Manceau, A. & Calas, G. (1986) Nickel-bearing clay minerals: II. Intracrystalline distribution of nickel: An X-ray absorption study. *Clay Minerals*, **21**, 341–360.

Manceau, A., Calas, G. & Petiau, J. (1984) Cation ordering in nickel-magnesium phyllosilicates of geological interest. In: *Springer Proceedings in Physics, 2 (EXAFS Near Edge Struct. 3)*, 358–361.

Manceau, A., Calas, G. & Decarreau, A. (1985) Nickel-bearing clay minerals: I. Optical spectroscopic study of nickel crystal chemistry. *Clay Minerals*, **20**, 367–387.

Manceau, A., Ildefonse, Ph., Hazemann, J.L., Flank, A.-M. & Gallup, D. (1995) Crystal chemistry of hydrous iron silicate scale deposits at the Salton Sea geothermal field. *Clays and Clay Minerals*, **43**, 304–317.

Mandarino, J.A. & Back, E.B. (2004) *Fleischer's Glossary of Mineral Species 2004*. The Mineralogical Record Inc., Tuscon, Arizona, USA, 310 pp.

Martin de Vidales, J.L., Pozo, M., Alia, J.M., Garcia-Navarro, F. & Rull, F. (1991) Kerolite–stevensite mixed-layers from the Madrid Basin, central Spain. *Clays and Clay Minerals*, **26**, 329–342.

Martin, F., Ferrage, E., Petit, S., de Parseval, P., Delmotte, L., Ferret, J., Arseguel, D. & Salvi, S. (2006) Fine-probing the crystal-chemistry of talc by MAS-NMR spectroscopy. *European Journal of Mineralogy*, **18**, 641–651.

Martynková, G.S., Valášková, M. & Šupová, M. (2007) Organo-vermiculite structure ordering after PVAc introduction. *Physica Status Solidi*, **204**, 1870–1875.

Matarrese, S., Schingaro, E., Scordari, F., Stoppa, F., Rosatelli, G., Pedrazzi, G. & Ottolini L. (2008) Crystal chemistry of phlogopite from Vulture–S. Michele Subsynthem volcanic rocks (Mt. Vulture, Italy) and volcanological implications. *American Mineralogist*, **93**, 426–437.

Mathieson, A.M. (1958) Mg-vermiculite: A refinement of the crystal structure of the 14.36 Å phase. *American Mineralogist*, **43**, 300–304.

Mathieson, A.M. & Walker, G.F. (1954) Crystal structure of magnesium-vermiculite. *American Mineralogist*, **39**, 231–255.

McAtee, J.L. & Lamkin, G. (1978) A modified freeze-drying procedure for the electron microscopy examination of hectorite. *Clays and Clay Minerals*, **27**, 293–296.

McBride, M.B. (1989) Surface chemistry of soil minerals. In: *Minerals in Soil Environments, Second edition* (J.B. Dixon & S.B. Weed, editors). Soil Science Society of America, Madison, Wisconsin, USA, pp. 35–88.

McCarty, D.K., Sakharov, B.A. & Drits, V.A. (2009) New insights into smectite illitization: a zoned K-bentonite revisited. *American Mineralogist*, **94**, 1653–1671.

Mehmel, M. (1935) Uber die Struktur von Halloysit und Metahalloysit. *Zeitschrift fur Kristallographie*, **90**, 35–43.

Mellini, M. (1982) The crystal structure of lizardite 1*T*: Hydrogen bonds and polytypism. *American Mineralogist*, **67**, 587–598.

Mellini, M. & Viti, C. (1994) Crystal structure of lizardite-1*T* from Elba, Italy. *American Mineralogist*, **79**, 1194–1198.

Mellini, M. & Zanazzi, P.F. (1987) Crystal structures of lizardite-1*T* and lizardite-2H_1 from Coli, Italy. *American Mineralogist*, **72**, 943–948.

Mellini, M. & Zanazzi, P.F. (1989) Effects of pressure on the structure of lizardite-1*T*. *European Journal of Mineralogy*, **1**, 13–19.

Mellini, M., Ferraris, G. & Compagnoni, R. (1985) Carlosturanite: HRTEM evidence of a polysomatic series including serpentine. *American Mineralogist*, **70**, 773–781.

Mellini, M., Trommsdorff, V. & Compagnoni, R. (1987) Antigorite polysomatism: behaviour during progressive metamorphism. *Contribution to Mineralogy and Petrology*, **97**, 147–155.

Mellini, M., Cressey, G., Wicks, F.J. & Cressey, B.A. (2010) The crystal structure of Mg end-member lizardite-I*T* forming polyhedral spheres from the Lizard, Cornwall. *Mineralogical Magazine*, **74**, 277–284.

Mercier, P.H.J. & Le Page, Y. (2008) Kaolin polytypes revisited *ab initio*. *Acta Crystallographica*, **B64**, 131–143.

Mercier, P.H.J. & Le Page, Y. (2009) *Ab initio* exploration of layer slipping transformations in kaolinite up to 60 GPa. *Materials Science and Technology*, **25**, 437–442.

Mercier, P.H.J., Rancourt, D.G., Redhammer, G.J., Lalonde, A.E., Robert, J.L., Berman, R.G. & Kodama, H. (2006) Upper limit of the tetrahedral rotation angle and factors affecting octahedral flattening in synthetic and natural 1*M* polytype $C2/m$ space group micas. *American Mineralogist*, **91**, 831–849.

Mercier, P.H.J., Le Page, Y. & Desgreniers, S. (2010) Kaolin polytypes revisited *ab initio* at 10 GPa. *American Mineralogist*, **95**, 1117–1120.

Méring, J. & Oberlin, A. (1971) Smectite. In: *The Electron-Optical Investigation of Clays* (J.A. Gard, editor). Monograph **2**. Mineralogical Society, London, pp. 193–229.

Merli, M., Pavese, A. & Curetti, N. (2009) Maximum entropy method: an unconventional approach to explore observables related to the electron density in phengites. *Physics and Chemistry of Minerals*, **36**, 19–28.

Mermut, A.R. (editor) (1994) *Layer Charge Characteristics of 2:1 Silicate Clay Minerals*. CMS Workshop Lectures, **6**, 134 pp.

Merriman, R.J. & Peacor, D.R. (1999) Very low-grade metapelites; mineralogy, microfabrics and measuring reaction progress. In: *Lowgrade Metamorphism* (M. Frey & D. Robinson, editors), Blackwell Sciences Ltd., Oxford, UK, pp. 10–60.

Mesto, E., Schingaro, E., Scordari, F. & Ottolini, L. (2006) An electron microprobe analysis, secondary ion mass spectrometry, and single-crystal X-ray diffraction study of phlogopites from Mt. Vulture, Potenza, Italy: Consideration of cation partitioning. *American Mineralogist*, **91**, 182–190.

Meunier, A. (2005) *Clays*. Spinger-Verlag, Berlin, 472 pp.

Michalkova, A. & Tunega, D. (2007) Kaolinite: dimethylsulfoxide intercalate – A theoretical study. *Journal of Physical Chemistry C*, **111(30)**, 11259–11266.

Middleton, A.P. & Whittaker, E.J.W. (1976) The structure of Povlen-type chrysotile. *The Canadian Mineralogist*, **14**, 301–306.

Milestone, N.B. (1971) Allophane. Its structure and possible uses. *Chemistry in New Zealand*, **35**, 191–197.

Mookherjee, M., Redfern, S.A.T., Zhang, M. & Harlov, D.E. (2002) Orientational order-disorder of ND_4^+/NH_4^+ in synthetic ND_4/NH_4-phlogopite: a low-temperature infrared study. *European Journal of Mineralogist*, **14**, 1033–1039.

Moore, D.M. & Reynolds, R.C.Jr. (1997) *X-Ray Diffraction and the Identification and Analysis of Clay Minerals*. Oxford University Press, New York, 378 pp.

Mottana, A & Aldega L. (2011) Advanced techniques to define intercalation processes. In: *Layered Mineral Structures and their Application in Advanced Technologies* (M.F. Brigatti & A. Mottana, editors). EMU notes in Mineralogy, **11**, xxx-xxx.

Mottana, A., Sassi, F.P., Thompson, J.B., Jr. & Guggenheim S. (editors) (2002a) *Micas: Crystal Chemistry and Metamorphic Petrology*. Reviews in Mineralogy and Geochemistry, **46**. Mineralogical Society of America, Chantilly, Virginia, USA.

Mottana, A., Marcelli, A., Cibin, G. & Dyar, M.D. (2002b) X-ray absorption spectroscopy of the micas. In: *Micas: Crystal Chemistry and Metamorphic Petrology* (A. Mottana, F.P. Sassi, J.B. Thompson Jr. & S. Guggenheim, editors). Reviews in Mineralogy and Geochemistry, **46**, 371–411. Mineralogical Society of America, Chantilly, Virginia, USA.

Nadeau, P.H., Wilson, M.J., McHardy, W.J. & Tait, M.J. (1985) The conversion of smectite to illite during diagenesis: Evidence from some illitic clays from bentonites and sandstones. *Mineralogical Magazine*, **49**, 393–400.

Nagy, B. & Bradley, W.F. (1955) Structure of sepiolite. *American Mineralogist*, **40**, 885–892.

Neder, R.B., Burghammer, M., Grasl, Th., Schulz, H., Bram, A. & Fiedler, S. (1999) Refinement of the kaolinite structure from single-crystal synchrotron data. *Clays and Clay Minerals*, **47**, 487–494.

Nelson, D.O. & Guggenheim, S. (1993) Inferred limitations to the oxidation of Fe in chlorite: a high-temperature single-crystal X-ray study. *American Mineralogist*, **78**, 1197–1207.

Nespolo, M. & Ďurovič, S. (2002) Crystallographic basis of polytypism and twinning in micas. In: *Micas: Crystal Chemistry and Metamorphic Petrology* (A. Mottana, F.P. Sassi, J.B. Thompson Jr. & S. Guggenheim, editors). Reviews in Mineralogy and Geochemistry, **46**. Mineralogical Society of America, Chantilly, Virginia, USA, pp. 155–272.

Nespolo, M., Takeda, H. & Ferraris, G. (1997) Crystallography of mica polytypes. In: *Modular Aspects of Minerals* (S. Merlino, editor). EMU Notes in Mineralogy, **1**. Eötvös University Press, Budapest, pp. 81–118.

Nespolo, M., Ferraris, G., Ďurovič, S. & Takeuchi, Y. (2004) Twins *vs.* modular crystal structures. *Zeitschrift für Kristallographie*, **219**, 773–778.

Newman, A.C.D. (1987) The interaction of water with clay mineral surfaces. In: *Chemistry of Clays and Clay Minerals* (A.C.D. Newman, editor). Monograph **6**, Mineralogical Society, London, pp. 237–274.

Newman, A.C.D. & Brown, G. (1987) The chemical constitution of clays. In: *Chemistry of Clays and Clay Minerals* (A.C.D. Newman, editor). Monograph **6**, Mineralogical Society, London, pp. 1–128.

Newnham, R.E. (1961) A refinement of the dickite structure and some remarks on polymorphism in kaolin minerals. *Mineralogical Magazine*, **32**, 683.

Newnham, R.E. & Brindley, G.W. (1956) The crystal structure of dickite. *Acta Crystallographica*, **9**, 759–764.

Newnham, R.E. & Brindley, G.W. (1957) The structure of dickite: correction. *Acta Crystallographica*, **10**, 88.

Norrish, K. (1954) The swelling of montmorillonite. *Discussions of the Faraday Society*, **18**, 120–133.

O'Day, P.A., Rehr, J.J., Zabinsky, S.I. & Brown, G.E. Jr. (1994) Extended X-ray absorption fine structure (EXAFS) analysis of disorder and multiple-scattering in complex crystalline solids. *Journal of American Chemical Society*, **116**, 2938–2949.

Okada, K. & Ossaka, J. (1983) Dehydration reaction of interlayer water of halloysite by heating. *Nendo Kagaku*, **23**, 27–31.

Okada, K., Morikawa, H., Iwai, S., Ohira, Y. & Ossaka, J. (1975) Structure model of allophane. *Clay Science*, **4**, 291–303.

Otten, M.T. (1993) High-resolution electron microscopy of polysomatism and stacking defects in antigorite. *American Mineralogist*, **78**, 75–84.

Ozawa, T., Takeuchi, Y., Takahata, T., Donnay, G. & Donnay, J.D.H. (1983) The pyrosmalite group of minerals. II. The layer structure of mcgillite and friedelite. *The Canadian Mineralogist*, **21**, 7–17.

Palin, E.J. & Dove, M.T. (2004) Investigation of Al/Si ordering in tetrahedral phyllosilicate sheets by Monte Carlo simulation. *American Mineralogist*, **89**, 176–184.

Palin, E.J., Dove, M.T., Hernandez Laguna, A. & Sainz Diaz, C.I. (2004) A computational investigation of the Al/Fe/Mg order disorder behavior in the dioctahedral sheet of phyllosilicates. *American Mineralogist*, **89**, 164–175.

Parfitt, R.L. & Henmi, T. (1980) Structure of some allophanes from New Zealand. *Clays and Clay Minerals*, **28**, 285–294.

Parfitt, R.L., Furkert, R.J. & Hemmi, T. (1980) Identification and structure of two types of allophane from volcanic ash soils and tephra. *Clays and Clay Minerals*, **28**, 328–334.

Pauling, L. (1930) The structures of the micas and related minerals. *Proceedings of the National Academy of Sciences of the United States of America*, **16**, 123–129.

Pavese, A., Levy, D., Curetti, N., Diella, V., Fumagalli, P. & Sani, A. (2003) Equation of state and compressibility of phlogopite by *in situ* high- pressure X-ray powder diffraction. *European Journal of Mineralogy*, **15**, 455–463.

Pavese, A., Curetti, N., Diella, V., Levy, D., Dapiaggi, M. & Russo, U. (2007) P-V and T-V equations of state of natural biotite: an *in situ* high-pressure and high-temperature powder diffraction study, combined with Mössbauer spectroscopy. *American Mineralogist*, **92**, 1158–1164.

Peacor, D.R., Essene, E.J., Simmons, W.B. Jr. & Bigelow, W.C. (1974) Kellyite, a new manganese-aluminum member of the serpentine group from Bald Knob, North Carolina, and new data on grovesite. *American Mineralogist*, **59**, 1153–1156.

Peacor, D.R., Rouse, R.C. & Bailey, S.W. (1988) Crystal structure of franklinfurnaceite: A tri-dioctahedral zincosilicate intermediate between chlorite and mica. *American Mineralogist*, **73**, 876–887.

Pearson, R.G. (1963) Hard and soft acids and bases. *Journal of the American Chemical Society*, **85**, 3533–3539.

Pearson, R.G. (1968) Hard and soft acids and bases HSAB, part 1: Fundamental principles. *Journal of Chemical Education*, **45**, 581–587.

Perdikatsis, B. & Burzlaff, H. (1981) Refinement of talc's ($Mg_3[(OH)_2Si_4O_{10}]$) structure. *Zeitschrift für Kristallographie*, **156**, 177–186.

Petit, S., Martin, F., Wiewióra, A., de Parseval, P. & Decarreau, A. (2004) Crystal-chemistry of talcs: a near infrared (NIR) spectroscopy study. *American Mineralogist*, **89** 319–326.

Petit, S., Righi, D. & Madejová, J. (2006) Infrared spectroscopy of NH_4^+-bearing and saturated clay minerals: a review of the study of layer charge. *Applied Clay Science*, **34**, 22–30.

Phillips, T.L., Loveless, J.K. & Bailey, S.W. (1980) Cr^{3+} coordination in chlorites: a structural study of ten chromian chlorites. *American Mineralogist*, **65**, 112–122.

Piccinini, M., Cibin, G., Marcelli, A., Della Ventura, G., Bellatreccia, F. & Mottana, A. (2006a) Synchrotron radiation FT-IR micro-spectroscopy of fluorophlogopite in the O–H stretching region. *Vibrational Spectroscopy*, **42**, 59–62.

Piccinini, M., Cibin, G., Marcelli, A., Mottana, A., Della Ventura, G. & Bellatreccia, F. (2006b) Synchrotron radiation FTIR micro-spectroscopy of natural layer-silicates in the O–H stretching region. *Infrared Physics and Technology*, **49**, 64–68.

Plançon, A. (2002) New modeling of X-ray diffraction by disordered lamellar structures, such as phyllosilicates. *American Mineralogist*, **87**, 1672–1677.

Plançon, A. & Zacharie, C. (1990) An expert system for the structural characterization of kaolinites. *Clay Minerals*, **25**, 249–260.

Plançon, A., Giese, R.F. Jr., Snyder, R., Drits, V.A. & Bukin, A.S. (1989) Stacking faults in the kaolin-group minerals: Defect structures of kaolinite. *Clays and Clay Minerals*, **37**, 203–210.

Post, J.E. & Heaney, P.J. (2008) Synchrotron powder X-ray diffraction study of the structure and dehydration behavior of palygorskite. *American Mineralogist*, **93**, 667–675.

Post, J.E., Bish, D.L. & Heaney, P.J. (2007) Synchrotron powder X-ray diffraction study of the structure and dehydration behaviour of sepiolite. *American Mineralogist*, **92**, 91–97.

Preisinger, A. (1959) X-ray study of the structure of sepiolite. *Clays and Clay Minerals*, **6**, 61–67.

Preisinger, A. (1963) Sepiolite and related compounds: Its stability and application. *Clays and Clay Minerals*, **10**, 365–371.

Prost, R., Dameme, A., Huard, E., Driard, J. & Leydecker, J.P. (1989) Infrared study of structural hydroxyl in kaolinite, dickite, nacrite, and poorly crystalline kaolinite at 5 to 600 K. *Clays and Clay Minerals*, **37**, 464–468.

Rancourt, D.G., Mercier, P.H.J., Cherniak, D.J., Desgreniers, S., Kodama, H., Robert, J.L. & Murad, E. (2001) Mechanisms and crystal chemistry of oxidation in annite: resolving the hydrogen loss and vacancy reactions. *Clays and Clay Minerals*, **49**, 455–491.

Range, K.J. & Weiss, A. (1969) Uber das Verhalten von kaolinitit bei hohen Drücken. *Berichte Deutsche Keramische Gesellschaft*, **46**, 231–238 (in German).

Rautureau, M. & Tchoubar, C. (1974) Precisions concernant l'analyse structurale de la sepiolite par microdiffraction electronique. *Comptes Rendues de l'Académie des Sciences, Paris*, **278**, 25–28 (in French).

Rautureau, M., Tchoubar, C. & Méring, J. (1972) Analyse structurale de la sepiolite par microdiffraction electronique. *Comptes Rendues de l'Académie des Sciences, Paris*, **274**, 269–271 (in French).

Rayner, J.H. & Brown, G. (1973) Crystal structure of talc. *Clays and Clay Minerals, Proceedings of the Conference 1973*, **21**, 103–314.

Redhammer, G.J., Amthauer, G., Lottermoser, W., Bernroider, M., Tippelt, G. & Roth, G. (2005) X-ray powder diffraction and ^{57}Fe- Mössbauer spectroscopy of synthetic trioctahedral micas $\{K\}[Me_3]O_{10}(OH)_2$, Me = Ni^{2+}, Mg^{2+}, Co^{2+}, Fe^{2+}; T = Al^{3+}, Fe^{3+}. *Mineralogy and Petrology*, **85**, 89–115.

Reynolds, R.C. Jr. (1983) Three-dimensional X-ray diffraction from disordered illite: simulation and interpretation of the diffraction pattern. In: *Computer Application in X-ray Diffraction Methods* (R.C. Reynolds & I. Walker, editors). CMS Workshop Lectures, **5**. The Clay Minerals Society, Bloomington, Indiana, USA, pp. 44–78.

Reynolds, R.C. Jr. (1985) *NEWMOD a computer program for the calculation of one-dimensional diffraction pattern of mixed layer clays*. R.C. Reynolds, 9 Brook Rd., Hanover, New Hampshire 03755, USA.

Reynolds, R.C. Jr. (1988) Mixed layer chlorite minerals. In: *Hydrous Phyllosilicates (Exclusive of Micas)* (S.W. Bailey, editor). Reviews in Mineralogy, **19**. Mineralogical Society of America, Washington, D.C., pp. 601–629.

Reynolds, R.C. Jr. & Bish, D.L. (2002) The effects of grinding on the structure of a low-defect kaolinite. *American Mineralogist*, **87**, 1626–1630.

Rinaudo, C., Roz, M., Boero, M. & Franchini, A.M. (2004) FT-Raman spectroscopy on several di- and tri-octahedral T-O-T phyllosilicates. *Neues Jahrbuch Fur Mineralogie Monatshefte*, **12**, 537–554.

Rocha, J. & Pedrosa De Jesus, J.D. (1994) ^{27}Al satellite transition MAS-NMR spectroscopy of kaolinite. *Clay Minerals*, **29**, 287–291.

Ross, C.S. (1946) Sauconite – a clay mineral of the montmorillonite group. *American Mineralogist*, **31**, 411–24.

Rule, A.C. & Bailey, S.W. (1987) Refinement of the crystal structure of a monoclinic ferroan clinochlore. *Clays and Clay Minerals*, **35**, 129–138.

Rule, A.C. & Radke, F. (1988) Baileychlore, the zinc end member of the trioctahedral chlorite series. *American Mineralogist*, **73**, 135–139.

Sainz-Diaz, C.I., Timon, V., Botella, V., Artacho, E. & Hernandez-Laguna, A. (2002) Quantum mechanical calculations of dioctahedral 2:1 phyllosilicates: Effect of octahedral cation distributions in pyrophyllite, illite, and smectite. *American Mineralogist*, **87**, 958–965.

Sakharov, B.A., Lindgreen, H., Salyn, A.L. & Drits, V.A. (1999) Determination of illite-smectite structures using multispecimen XRD profile fitting. *Clays and Clay Minerals*, **47**, 555–566.

Sanz, J., Herrero C.P. & Serratosa J.M. (2006) Arrangement and mobility of water in vermiculite hydrates followed by 1H NMR spectroscopy. *Journal of Physical Chemistry B*, **110**, 7813–7819.

Sato, H., Ono, K., Johnston, C.T. & Yamagishi, A. (2004) First-principle study of polytype structures of 1:1 dioctahedral phyllosilicates. *American Mineralogist*, **89**, 1581–1585.

Schingaro, E., Scordari, F., Mesto, E., Brigatti, M.F. & Pedrazzi, G. (2005) Cation-site partitioning in Ti-rich micas from Black Hill (Australia): A multi-technical approach. *Clays and Clay Minerals*, **53**, 179–189.

Scholtzová, E. & Smrčok, L. (2005) On local structural changes in lizardite-1*T*: $\{Si^{4+}/Al^{3+}\}$, $\{Si^{4+}/Fe^{3+}\}$, $[Mg^{2+}/Al^{3+}]$, $[Mg^{2+}/Fe^{3+}]$ substitutions. *Physics and Chemistry of Minerals*, **32**, 362–373.

Scholtzová, E., Smrčok, L., Tunega, D. & Turi Nagy, L. (2000) *Ab initio* 2-D periodic Hartree-Fock study of Fe-substituted lizardite 1*T* - a simplified cronstedtite model. *Physics and Chemistry of Minerals*, **27**, 741–746.

Schreyer, W., Medenbach, O., Abraham, K., Gebert, W. & Mueller, W.F. (1982) Kulkeite, a new metamorphic phyllosilicate mineral: ordered 1:1 chlorite/talc mixed-layer. *Contributions to Mineralogy and Petrology*, **80**, 103–109.

Schroeder, P.A. (2002) Infrared Spectroscopy in clay science. In: *Teaching Clay Science* (A. Rule & S. Guggenheim, editors). CMS Workshop Lectures, **11**. The Clay Mineral Society, Aurora, Colorado, USA, pp. 181–206.

Schroeder, P.A. & Pruett, R.J. (1996) Fe ordering in kaolinite: insights from ^{29}Si and ^{27}Al MAS NMR spectroscopy. *American Mineralogist*, **81**, 26–38.

Scordari, F., Ventruti, G., Sabato, A., Bellatreccia, F., Della Ventura, G. & Pedrazzi G. (2006) Ti-rich phlogopite from Mt. Vulture (Potenza, Italy) investigated by a multianalytical approach: substitutional mechanisms and orientation of the OH dipoles. *European Journal of Mineralogy*, **18**, 379–391.

Scordari, F., Schingaro, E., Ventruti, G., Lacalamita, M. & Ottolini, L. (2008) Red micas from basal ignimbrites of Mt. Vulture (Italy): interlayer content appraisal by a multi-methodic approach. *Physics and Chemistry of Minerals*, **35**, 163–174.

Seidl, W. & Breu, J. (2005) Single crystal structure refinement of tetramethylammonium-hectorite. *Zeitschrift für Kristallographie*, **220**, 169–176.

Sen Gupta, P.K., Schlemper, E.O., Johns, W.D. & Ross, F. (1984) Hydrogen positions in dickite. *Clays and Clay Minerals*, **32**, 483–485.

Shabani, A.A.T., Rancourt, D.G. & Lalonde, A.E. (1998) Determination of *cis* and *trans* Fe^{2+} populations in $2M_1$ muscovite by Mössbauer spectroscopy. *Hyperfine Interactions*, **117**, 117–129.

Shainberg, I., Alperovitch, N.I. & Keren, R. (1987) Charge density and Na–K–Ca exchange on smectites. *Clays and Clay Minerals*, **35**, 68–73.

Shirozu, H. & Bailey, S.W. (1966) Crystal structure of a two-layer Mg-vermiculite. *American Mineralogist*, **51**, 1124–1143.

Shoval, S., Yariv, S., Michaelian, K.H., Lapides, I., Boudeulle, M. & Panczer, G. (1999) A fifth OH-stretching band in IR spectra of kaolinites. *Journal of Colloid and Interface Science*, **212**, 523–529.

Shoval, S., Yariv, S., Michaelian, K.H., Boudeulle, M. & Panczer, G. (2001) Hydroxyl-stretching bands in curve-fitted micro-Raman, photoacoustic, and transmission infrared spectra of dickite from St. Claire, Pennsylvania. *Clays and Clay Minerals*, **49**, 347–354.

Shoval, S., Yariv, S., Michaelian, K.H., Boudeulle, M. & Panczer, G. (2002) Hydroxyl-stretching bands in polarized micro-Raman spectra of oriented single-crystal Keokuk kaolinite. *Clays and Clay Minerals*, **50**, 56–62.

Singh, B. (1996) Why does halloysite roll?–A new model. *Clays and Clay Minerals*, **44**, 191–196.

Skipper, N.T., Sposito, L.G. & Chou Chang, F.-R. (1995) Monte Carlo simulation of interlayer molecular structure in swelling clay minerals. 2. monolayer hydrates. *Clays and Clay Minerals*, **43**, 294–303.

Slade, P.G., Stone, P.A. & Radoslovich, E.W. (1985) Interlayer structures of the two-layer hydrates of Naand Ca-vermiculites. *Clays and Clay Minerals*, **33**, 51–61.

Smirnov, K.S. & Bougeard, D. (1999) A molecular dynamics study of structure and short-time dynamics of water in kaolinite. *Journal of Physical Chemistry B*, **103**, 5266–5273.

Smrčok, L., Gyepesová, D. & Chmielová, M. (1990) New X-ray Rietveld refinement of kaolinite from Keokuk, Iowa. *Crystal Research and Technology*, **25**, 105–110.

Smrčok, L., Ďurovič, S., Petricek, V. & Weiss, Z. (1994) Refinement of the crystal structure of cronstedtite-3*T*. *Clays and Clay Minerals*, **42**, 544–551.

Smyth, J.R., Dyar, M.D., May, H.M., Bricker, O.P. & Acker, J.G. (1997) Crystal structure refinement and Mössbauer spectroscopy of an ordered, triclinic clinochlore. *Clays and Clay Minerals*, **45**, 544–550.

Spinnler, G.E. (1985) *HRTEM study of antigorite, pyroxene-serpentine reactions and chlorite*. Ph.D. thesis, Arizona State University, Tempe, Arizona, USA, 248 pp.

Sposito, G. (1984) *The Surface Chemistry of Soils*. Oxford University Press, New York, 234 pp.

Sposito, G. & Prost, R. (1982) Structure of water adsorbed on smectites. *Chemical Reviews*, **82**, 553–573.

Środoń, J. & Eberl, D.D. (1984) Illite. In: *Micas* (S.W. Bailey, editor). Review in Mineralogy, **13**. Mineralogical Society of America, Washington D.C., pp. 495–544.

Steadman, R. & Nuttall, P.M. (1962) The crystal structure of amesite. *Acta Crystallographica*, **15**, 510–511.

Steinfink, H. (1958a) Crystal structure of chlorite. I. A monoclinic polymorph. *Acta Crystallographica*, **11**, 191–195.

Steinfink, H. (1958b) Crystal structure of chlorite. II. A triclinic polymorph. *Acta Crystallographica*, **11**, 195–198.

Steinfink, H. & Brunton, G. (1956) The crystal structure of amesite. *Acta Crystallographica*, **9**, 487–492.

Stoch, L. (1974) *Mineraly Ilaste ('Clay Minerals')*. Geological Publishers, Warsaw, pp. 186–193.

Sudo, T. & Nakamura, T. (1952) Hisingerite from Japan. *American Mineralogist*, **37**, 618–621.

Sugimori, H., Iwatsuki, T. & Murakami, T. (2008) Chlorite and biotite weathering, Fe^{2+}-rich corrensite formation, and Fe behaviour under low P_{O2} conditions and their implication for Precambrian weathering. *American Mineralogist*, **93**, 1080–1089.

Suitch, P.R. & Young, R.A. (1983) Atom position in highly ordered kaolinite. *Clays and Clay Minerals*, **31**, 357–366.

Sun, H., Liu, Y., Peng, T. & Yue, M. (2008) Hydrothermal synthesis and characterization of hectorite. *Rengong Jingti Xuebao*, **37**, 844-848.

Suquet, H., de la Calle, C. & Pezerat, H. (1975) Swelling and structural organization of saponite. *Clays and Clay Minerals*, **23**, 1–9.

Suquet, H., Iiyama, J.T., Kodama, H. & Pezerat, H. (1977) Synthesis and swelling properties of saponite with increasing layer charge. *Clays and Clay Minerals*, **25**, 231–242.

Takeda, H. & Ross, M. (1995) Mica polytypism: identification and origin. *American Mineralogist*, **80**, 715–724.

Tarý, G., Bobos, I., Gomes, C.S.F. & Ferriera, J.M.F. (1999) Modification of surface charge properties during kaolinite to halloysite-7Å transformation. *Journal of Colloid and Interface Science*, **210**, 360–366.

Tejedor-Tejedor, M.I., Anderson, M.A. & Herbillon, A.J. (1983) An investigation of the coordination number of Ni^{2+} in nickel bearing phyllosilicates using diffuse reflectance spectroscopy. *Journal of Solid State Chemistry*, **50**, 153–162.

Thompson, J.G. & Withers, R.L. (1987) A transmission electron microscopy contribution to the structure of kaolinite. *Clays and Clay Minerals*, **35**, 237–239.

Tien, P.L., Leavens, P.B. & Nelen, J.A. (1975) Swinefordite, a dioctahedral-trioctahedral Li-rich member of the smectite group from Kings Mountain, North Carolina. *American Mineralogist*, **60**, 540–547.

Toraya, H. (1981) Distortions of octahedra and octahedral sheets in 1*M* micas and the relation to their stability. *Zeitschrift für Kristallographie*, **157**, 173–190.

Treacy, M.M.J., Newsam, J.M. & Deem, M.W. (1991) A general recursion method for calculating diffracted intensities from crystals containing planar faults. *Proceedings: Mathematical and Physical Sciences*, **433**, 499–520.

Tsipursky, S.I. & Drits, V.A. (1984) The distribution of octahedral cations in the 2:1 layers of dioctahedral smectites studied by oblique-texture electron diffraction. *Clay Minerals*, **19**, 177–193.

Tunega, D. & Lischka, H. (2003) Effect of the Si/Al ordering on structural parameters and the energetic stabilization of vermiculites – a theoretical study. *Physics and Chemistry of Minerals*, **30**, 517–522.

Uehara, S. (1998) TEM and XRD study of antigorite superstructures. *The Canadian Mineralogist*, **36**, 1595–1606.

Uehara, S. & Kamata, K. (1994) Antigorite with a large supercell from Saganoseki, Oita Prefecture, Japan. *The Canadian Mineralogist*, **32**, 93–103.

Uehara, S. & Shirozu, H. (1985) Variations in chemical composition and structural properties of antigorite. *Mineralogical Journal*, **12**, 299–318.

Vahedi-Faridi, A. & Guggenheim, S. (1997) Crystal structure of TMA-exchanged vermiculite. *Clays and Clay Minerals*, **45**, 859–866.

Vahedi-Faridi, A. & Guggenheim, S. (1999) Structural study of tetramethylphosphonium-exchanged vermiculite. *Clays and Clay Minerals*, **47**, 219–225.

Valdrè, G., Malferrari, D. & Brigatti, M.F. (2009) Crystallographic features and cleavage nanomorphology of chlinochlore: specific applications. *Clays and Clay Minerals*, **57**, 183–193.

Van der Gaast, S.J., Wada, K., Wada, S.I. & Kakuto, Y. (1985) Small-angle X-ray powder diffraction, morphology, and structure of allophane and imogolite. *Clays and Clay Minerals*, **33**, 237–243.

Van Olphen, H. (1965) Thermodynamics of interlayer adsorption of water in clays. I Sodium vermiculite. *Journal of Colloid Science*, **20**, 822–837.

Vasconcelos, I.F., Bunker, B.A. & Cygan, R.T. (2007) Molecular dynamics modelling of ion adsorption to the basal surfaces of kaolinite. *Journal of Physical Chemistry C*, **111**, 6753–6762.

Vaughan, J.P. (1986) The iron end-member of the pyrosmalite series from the Pegmont lead-zinc deposit, Queensland. *Mineralogical Magazine*, **50**, 527–531.

Veblen, D.R. (1992) Electron microscopy applied to nonstoichiometry, polysomatism, and replacement reactions in minerals. In: *Minerals and Reactions at the Atomic Scale: Transmission Electron Microscopy* (P.R. Buseck, editor). Reviews in Mineralogy, **27**, 181–223. Mineralogical Society of America, Washington.

Veniale, F. & van der Marel, H.W. (1969) Identification of some l:l regular interstratified trioctahedral clay minerals. In: *Proceedings of the International Clay Conference, Tokyo*, 233–244.

Ventruti, G., Levy, D., Pavese, A., Scordari, F. & Suard, E. (2009) High-temperature treatment, hydrogen behaviour and cation partitioning of a Fe-Ti bearing volcanic phlogopite by in-situ neutron powder diffraction and FTIR spectroscopy. *European Journal of Mineralogy*, **21**, 385–396.

Viti, C. & Mellini, M. (1996) Vein antigorite from Elba Island, Italy. *European Journal of Mineralogy*, **8**, 423–434.

Viti, C., Di Vincenzo, G. & Mellini M. (2004) Thermal transformations in laser-heated chloritized annite. *Physics and Chemistry of Minerals*, **31**, 92–101.

Vrublevskaya, Z.V., Delitsin, I.S., Zvyagin, B.B. & Soboleva, S.V. (1975) Cookeite with a perfect regular structure, formed by bauxite alteration. *American Mineralogist*, **60**, 1041–1046.

Wada, K. (1967) A structural scheme of soil allophane. *American Mineralogist*, **52**, 690–708.

Wada, K. (1995) Structure and formation of non- and para-crystalline aluminosilicate clay minerals: a review. In: *Clays Controlling the Environment, Proceedings of the International Clay Conference, 10th, Adelaide* (G.J. Churchman, R.W. Fitzpatrick & R.A. Eggleton, editors), pp. 443–448.

Wada, S. & Wada, K. (1977) Density and structure of allophane. *Clay Minerals*, **12**, 289–298.

Wada, S. & Wada, K. (1982) Effects of substitution of germanium for silicon in imogolite. *Clays and Clay Minerals*, **30**, 123–128.

Wada, S.I., Eto, A. & Wada, K. (1979) Synthetic allophane and imogolite. *Journal of Soil Science*, **30**, 347–355.

Wahle, M.W., Bujnowski, T.J., Guggenheim, S. & Kogure, T. (2010) Guidottiite, the Mn-analogue of cronstedtite: a new serpentine-group mineral from South Africa. *Clays and Clay Minerals*, **58**, 364–376.

Walker, J.R. & Bish, D.L. (1992) Application of Rietveld refinement techniques to a disordered IIb Mg-chamosite. *Clays and Clay Minerals*, **40**, 319–322.

Weaver, C.E. & Pollard, L.D. (editors) (1973) *The Chemistry of Clay Minerals. Developments in Sedimentology*. Elsevier, Amsterdam, 221 pp.

Weber, F., Dunoyer de Segonzac, G. & Economou, C. (1976) Une nouvelle expression de la 'crystallinité' de l'illite et des micas. Notion d'epaisseur des cristallites. *Compte Rendu Sommaire de Seances de la Societé Géologique de France*, **5**, 225–227 (in French).

Weiss, Z. & Ďurovič, S. (1984) Polytypism of pyrophyllite and talc. Part II. Classification and X-ray identification of MDO polytypes. *Silikaty*, **28**, 289–309.

Weiss, Z., Rieder, M. & Chmielová, M. (1992) Deformation of coordination polyhedra and their sheets in phyllosilicates. *European Journal of Mineralogy*, **4**, 665–682.

Welch, M.D. & Crichton, W.A. (2005) A high-pressure polytypic transformation in type-I chlorite. *American Mineralogist*, **90**, 1139–1145.

Welch, M.D. & Crichton, W.A. (2010) Pressure-induced transformations in kaolinite. *American Mineralogist*, **95**, 651–654.

Welch, M.D. & Marshall, W.G. (2001) High-pressure behavior of clinochlore. *American Mineralogist*, **86**, 1380–1386.

Welch, M.D., Barras, J. & Klinowski, J. (1995) A multinuclear NMR study of clinochlore. *American Mineralogist*, **80**, 441–447.

Welch, M.D., Kleppe, A.K. & Jephcoat, A.P. (2004) Novel high pressure behaviour in chlorite: A synchrotron XRD study of clinochlore to 27 GPa. *American Mineralogist*, **89**, 1337–1340.

Whelan, J.A. & Goldich, S.S. (1961) New data for hisingerite and neotocite. *American Mineralogist*, **46**, 1412–1423.

White, C.E., Provis, J.L., Riley, D.P., Kearley, G.J. & van Deventer, J.S.J. (2009) What Is the Structure of Kaolinite? Reconciling Theory and Experiment. *Journal of Physical Chemistry B*, **113**, 6756–6765.

Whittaker, E.J.W. (1953) The structure of chrysotile. *Acta Crystallographica*, **6**, 747–748.

Whittaker, E.J.W. (1956a) The structure of chrysotile. II. Clinochrysotile. *Acta Crystallographica*, **9**, 855–862.

Whittaker, E.J.W. (1956b) The structure of chrysotile. III. Orthochrysotile. *Acta Crystallographica*, **9**, 862–864.

Whittaker, E.J.W. (1956c) The structure of chrysotile. IV. Parachrysotile. *Acta Crystallographica*, **9**, 865–867.

Wicks, F.S. & O'Hanley, D.S. (1988) Serpentine minerals; structures and petrology. In: *Hydrous Phyllosilicates (Exclusive of Micas)* (S.W. Bailey, editor). Reviews in Mineralogy, **19**. Mineralogical Society of America, Washington, D.C., pp. 91–167.

Wiewióra, A. & Weiss, Z. (1990) Crystallochemical classifications of phyllosilicates based on the unified system of projection of chemical composition: II. The chlorite group. *Clay Minerals*, **25**, 83–92.

Wiewióra, A., Rausell-Colom, J.A. & Garcia-Gonzalez, T. (1991) The crystal structure of amesite from Mount Sobotka: a nonstandard polytype. *American Mineralogist*, **76**, 647–652.

Wolters, F. & Emmerich, K. (2007) Thermal reactions of smectites – Relation of dehydroxylation temperature to octahedral structure. *Thermochimica Acta*, **462**, 80–88.

Wu, X.J., Li, F.H. & Hashimoto, H. (1989) High-resolution transmission electron microscopy study of the superstructure of Xiuyan Jade and Matterhorn serpentine. *Acta Crystallographica*, **B45**, 129–136.

Xu, S. & Harsh, J.B. (1992) Alkali cation selectivity and surface charge of 2:1 clay minerals. *Clays and Clay Minerals*, **40**, 567–574.

Yada, K. (1971) Study of the microstructure of chrysotile asbestos by high resolution electron microscopy. *Acta Crystallographica*, **27**, 659–664.

Yada, K. (1979) Microstructures of chrysotile and antigorite by high-resolution electron microscopy. *The Canadian Mineralogist*, **13**, 227–243.

Yakovenchuk, V.N., Krivovichev, S.V., Pakhomovsky, Y.A, Ivanyuk, G.Y, Selivanova, E.A., Men'shikov, Y.P. & Britvin, S.N. (2007) Armbrusterite, $K_5Na_6Mn^{3+}Mn^{2+}_{14}[Si_9O_{22}]_4(OH)_{10} \cdot 4H_2O$, a new Mn hydrous heterophyllosilicate from the Khibiny alkaline massif, Kola Peninsula, Russia. *American Mineralogist*, **92**, 416–423.

Young, R.A. & Hewat, A.W. (1988) Verification of the triclinic crystal structure of kaolinite. *Clays and Clay Minerals*, **36**, 225–232.

Yucel, A.M., Rautureau, M., Tchoubar, D. & Tchoubar, C. (1981) Calculation of the X-ray powder reflection profiles of very small needle-like crystal. II. Quantitative results on Eskischir sepiolite fibers. *Journal of Applied Crystallography*, **14**, 431–454.

Zagorsky, V.Y., Peretyazhko, I.S., Sapozhnikov, A.N., Zhukhlistov, A.P. & Zvyagin, B.B. (2003) Borocookeite, a new member of the chlorite group from the Malkhan gem tormaline deposit, Central Transbaikalia, Russia. *American Mineralogist*, **88**, 830–836.

Zanazzi, P.F. & Pavese, A. (2002) Behaviour of micas at high pressure and high temperature conditions. In: *Micas: Crystal Chemistry and Metamorphic Petrology* (A. Mottana, F.P. Sassi, J.B. Jr. Thompson &

S. Guggenheim, editors). Reviews in Mineralogy and Geochemistry, **46**, Mineralogical Society of America, Chantilly, Virginia, USA, pp. 99–116.

Zanazzi, P.F., Montagnoli, M., Nazzareni, S. & Comodi, P. (2006) Structural effects of pressure on triclinic chlorite: a single-crystal study. *American Mineralogist*, **91(11-12)**, 1871–1878.

Zanazzi, P.F., Montagnoli, M., Nazzareni, S. & Comodi, P. (2007a) Structural effects of pressure on monoclinic chlorite: A single-crystal study. *American Mineralogist*, **92**, 655–661.

Zanazzi, P.F., Comodi, P., Nazzareni, S., Rotiroti, N. & Smaalen, S. (2007b) Behavior of 10-Å phase at low temperatures. *Physics and Chemistry of Minerals*, **34**, 23–29.

Zane, A. & Weiss, Z. (1996) A procedure for classifying rock-forming chlorites based on microprobe data. *Rendiconti Lincei*, **9**, 51–56.

Zazzi, A., Hirsch, T.K., Leonova, E., Kaikkonen, A., Grins, J., Annersten, H. & Eden, M. (2006) Structural investigations of natural and synthetic chlorite minerals by X-ray diffraction, Mössbauer spectroscopy and solid-state nuclear magnetic resonance. *Clays and Clay Minerals*, **54**, 252–265.

Zheng, H. & Bailey, S.W. (1989) Structures of intergrown triclinic and monoclinic IIb chlorites from Kenya. *Clays and Clay Minerals*, **37**, 308–316.

Zheng, H. & Bailey, S.W. (1994) Refinement of the nacrite structure. *Clays and Clay Minerals*, **42**, 46–52.

Zheng, H. & Bailey, S.W. (1997) Refinement of the cookeite "r" structure. *American Mineralogist*, **82**, 1007–1013.

Zhukhlistov, A.P. (2007) Electron Diffraction Study of Lizardite 1*T* with Stacking Faults. *Crystallography Reports*, **52**, 208–214.

Zhukhlistov, A.P. (2008) Crystal Structure of Nacrite from the Electron Diffraction Data. *Crystallography Reports*, **53**, 76–82.

Zussman, J., Brindley, G.W. & Comer, J.J. (1957) Electron diffraction studies of serpentine minerals. *American Mineralogist*, **42**, 133–153.

Zviagina, B.B., Sakharov, B.A. & Drits, V.A. (2007) X-ray diffraction criteria for the identification of trans- and cis-vacant varieties of dioctahedral micas. *Clays and Clay Minerals*, **55**, 467–480.

Zvyagin, B.B. (1954) Electron diffraction of the minerals of the kaolinite group. *Doklady Akademii Nauk SSSR*, **96**, 809–812.

Zvyagin, B.B. (1960) Determination of the structure of kaolinite by electron diffraction. *Doklady Akademii Nauk SSSR*, **130**, 1023–1026.

Zvyagin, B.B. (1963) The theory of polymorphism in chlorite. *Kristallografiya*, **8**, 32–38 (in Russian, abstract in English). **Q6**

Zvyagin, B.B. (1967) *Electron Diffraction Analysis of Clay Mineral Structures*. Plenum Press, New York, 364 pp.

Zvyagin, B.B. & Drits, V.A. (1996) Interrelated features of structure and stacking of kaolin mineral layers. *Clays and Clay Minerals*, **44**, 297–303.

Zvyagin, B.B. & Mishchenko, K.S. (1965) Diagnostics of one-stacking semirandom polymorphic modifications of chlorites. *Kristallografiya*, **10**, 555–557 (in Russian, abstract in English). **Q7**

Zvyagin, B.B., Berkhin, S.I. & Gorshkov, A.I. (1966) Structural characteristics of halloysite based on X-ray and electron-diffraction patterns. *Akademii Nauk SSSR*, 69–93 (in Russian, English abstract).

Zvyagin, B.B., Soboleva, S.V. & Fedotov, A.F. (1972) Refinement of nacrite structure by a high-voltage electron-diffraction method. *Kristallografiya*, **17**, 514–520 (in Russian, abstract in English).